Modelling Physiological and Biochemical Aspects of Scalp Cooling

PROEFSCHRIFT

ter verkrijging van de graad van doctor aan de
Technische Universiteit Eindhoven, op gezag van de
Rector Magnificus, prof. dr. ir. C.J. van Duijn, voor een
commissie aangewezen door het College voor
Promoties in het openbaar te verdedigen
op dinsdag 12 juni 2007 om 16.00 uur

door

Francis–Paul Elise Maria Janssen

geboren te Geleen

Dit proefschrift is goedgekeurd door de promotoren:

prof. dr. ir. A.A. van Steenhoven
en
prof. dr. ir. F.N. van de Vosse

Copromotor:
dr. G.M.J. van Leeuwen

Copyright © 2007 by F.P.E.M. Janssen

Cover design by Jorrit van Rijt, Oranje Vormgevers

All rights reserved. No part of this publication may be reproduced, stored in a retrieval system, or transmitted, in any form, or by any means, electronic, mechanical, photocopying, recording, or otherwise, without the prior permission of the author.

Printed by the Eindhoven University Press.

This project was funded by SOBU, an administrative cooperation between Tilburg University and the Eindhoven University of Technology.

A catalogue record is available from the Library Eindhoven University of Technology

ISBN: 978-90-386-1006-1

Life is what happens to you while you're busy making other plans.
John Lennon

Voor mijn ouders Adèle en Jacques
en mijn vrouw Audrey

Contents

Samenvatting **1**

Summary **3**

1 Introduction **5**
1.1 Background . . . 5
1.2 Problem definition and thesis outline . . . 11

2 Heat transfer during scalp cooling **15**
2.1 Introduction . . . 15
2.2 Heat transfer model for the head during scalp cooling . . . 18
2.2.1 Boundary conditions . . . 21
2.2.2 Numerical methods . . . 22
2.2.3 Validation . . . 22
2.2.4 Simulations . . . 23
2.3 Results . . . 23
2.3.1 Standard model head . . . 23
2.3.2 Parameter study . . . 24
2.4 Conclusion and discussion . . . 29

3 Relationship between temperature and blood flow **31**
3.1 Introduction . . . 31
3.2 Experimental equipment . . . 33
3.2.1 Cooling the scalp . . . 33
3.2.2 Temperature measurements . . . 34
3.2.3 Blood flow measurements . . . 36
3.3 Intra–subject and inter–position variability . . . 39
3.3.1 Experimental protocol . . . 40
3.3.2 Results . . . 42
3.4 Inter–individual variability . . . 45
3.4.1 Subjects . . . 45

3.4.2 Experimental protocol . . . 45
3.4.3 Results . . . 45
3.5 Conclusion and discussion . . . 49

4 Physiologically based pharmacokinetic model for doxorubicin 51
4.1 Introduction . . . 51
4.2 Doxorubicin pharmacokinetics in a capillary . . . 53
4.2.1 Capillary flow . . . 53
4.2.2 Doxorubicin transport over the capillary membrane . . . 56
4.2.3 Doxorubicin concentration in the tissue . . . 58
4.2.4 Flow limited assumption . . . 63
4.3 A physiologically based pharmacokinetic model for doxorubicin . . . 65
4.4 Validation . . . 68
4.5 Results . . . 71
4.5.1 Standard physiologically based pharmacokinetic model . . . 71
4.5.2 Parameter study . . . 72
4.6 Conclusion and discussion . . . 73

5 Effects of temperature and doxorubicin on keratinocyte damage *in vitro* 77
5.1 Introduction . . . 77
5.2 Materials and methods . . . 79
5.2.1 Experimental protocol . . . 79
5.2.2 Cell line . . . 80
5.2.3 Viability measurement . . . 81
5.3 Pilot experiments . . . 82
5.3.1 Linearity of the MTT assay . . . 82
5.3.2 Optimal cell plating density . . . 83
5.3.3 Optimal post–exposure time . . . 83
5.3.4 Standard protocol for additional pilot experiments . . . 84
5.3.5 Doxorubicin exposure time . . . 85
5.3.6 Doxorubicin exposure temperature . . . 86
5.3.7 Doxorubicin concentration . . . 87
5.4 Final *in vitro* experiment . . . 87
5.4.1 Experimental protocol . . . 87
5.4.2 Data analysis . . . 89
5.4.3 Results . . . 90
5.5 Conclusion and discussion . . . 92

6 Computational evaluation of scalp cooling protocols 95
6.1 Introduction . . . 95
6.2 Modelling of uncertainty and variability . . . 96
6.2.1 Input parameters . . . 96

6.2.2 Determination of critical viability . . . 98
6.2.3 Optimal skin temperature and drug dose . . . 102
6.3 Evaluation of scalp cooling protocol parameters . . . 104
6.3.1 Cap temperature . . . 104
6.3.2 Duration of scalp cooling . . . 106
6.3.3 Infusion time of doxorubicin . . . 106
6.3.4 Use of conditioner . . . 107
6.3.5 Thickness of the hair layer . . . 108
6.4 Optimal scalp cooling protocol . . . 109
6.5 Conclusion and discussion . . . 110

7 Conclusions and recommendations for future work 113
7.1 Conclusions . . . 113
7.2 Recommendations for further research . . . 116

References 119

A Validation of the numerical heat transfer model 127
A.1 Introduction . . . 127
A.2 Time dependent conduction . . . 128
A.2.1 Low Biot number . . . 128
A.2.2 High Biot number . . . 129
A.3 Heat generation . . . 131
A.4 Bio–heat transfer . . . 132

Curriculum Vitae 135

Dankwoord 137

Samenvatting

Haarverlies door chemotherapie is een gevreesde bijwerking van de behandeling tegen kanker. Koelen van het hoofd tijdens de toediening van cytostatica kan dit haarverlies verminderen. Voor het koelen van het hoofd wordt veelal een cap gebruikt, die is voorgekoeld in een vriezer of die aangesloten is op een koelreservoir. De huidige hyopthese voor het beschermende effect van hoofdhuidkoeling tegen haaruitval is dat koelen zowel de bloedtoevoer (perfusie) vermindert als de chemische reactiesnelheden. Verminderde bloedtoevoer leidt tot een vermindering van de hoeveelheid cytostatica die aanwezig is voor opname, terwijl de lagere temperatuur de opname van en schade door chemotherapie vermindert. Het uiteindelijke effect is dat minder schade wordt aangericht aan de cellen in de haarfolikel, waarmee de haar behouden blijft. Het effect van hoofdhuidkoeling varieert echter sterk. Een systematische evaluatie van de huidige hypothese is noodzakelijk voor een beter inzicht in de verschillende belangrijke parameters van hoofdhuidkoeling.

Het doel van onze studie was het kwantificeren van de vermoedelijke mechanismen waarmee hoofdhuidkoeling haaruitval voorkomt, en hiermee onderzoeken hoe de effectiviteit van huidige protocollen verbeterd kan worden. Op basis van de huidige hypothese over de werking van hoofdhuidkoeling is een numeriek model ontwikkeld. Het complete numerieke model bestaat uit twee sub–modellen waarmee warmtetransport in het hoofd en transport van chemotherapie (doxorubicine) in het lichaam beschreven worden. Experimenten zijn gebruikt om de modellen te valideren en te verbeteren.

Het eerste sub–model beschrijft warmtetransport in het hoofd met behulp van de Pennes vergelijking. Parameter studies met het model tonen dat de dikte van de vetlaag en de haarlaag de belangrijkste parameters zijn die de huidtemperatuur bepalen.

In een experiment hebben we de reductie in doorbloeding als gevolg van koelen van het hoofd gemeten, voor meerdere subjecten en meerdere posities. Subjecten werden 90 minuten langzaam gekoeld met een *scalp cooling* systeem. Daarna werd elk subject opgewarmd gedurende 60 minuten, waarmee hysteresis effecten onderzocht konden worden. Huidtemperatuur en –doorbloeding werden respectievelijk gemeten met thermokoppels en Laser Doppler perfusion probes. De resultaten laten

zien dat de variatie tussen personen groter is dan de variatie binnen een enkele persoon. Tijdens koeling werd de doorbloeding van de huid langzaam gereduceerd tot een minimum niveau van 20% $\pm$ 10% bij een temperatuur reductie van 20^{o}C.

Een farmacokinetisch model, gebaseerd op fysiologische eigenschappen, is gemaakt om transport van doxorubicine in het menselijk lichaam te beschrijven. Het model bestaat uit acht compartimenten die elk individuele organen beschrijven. Verschillende processen zoals transport, uitscheiding en omzetting tussen en in deze compartimenten worden beschreven met differentiaalvergelijkingen. Parameter studies laten zien dat het lichaamsgewicht, hartslag en zowel doorbloeding als volume van de verschillende weefsels de belangrijkste eigenschappen zijn.

In vitro experimenten op haarcellen werden uitgevoerd om het effect van lokale chemoconcentratie en lokale weefseltemperatuur op schade aan haarcellen (keratinocieten) te onderzoeken. Cellen werden voor 4 uur blootgesteld aan een wijde range van chemoconcentraties. Tijdens de blootstelling werden de cellen bewaard op verschillende temperaturen. Drie dagen na blootstelling werd de viabiliteit van de cellen bepaald middels een MTT test. Controle samples werden gebruikt om een concentratie–overlevingscurve op te stellen. De resultaten laten zien dat de overleving van cellen significant hoger is voor gekoelde cellen ($T < 22^{o}$C) dan voor niet gekoelde cellen ($T = 37^{o}$C). Er waren echter geen significante verschillen zichtbaar tussen temperaturen van $T = 10^{o}$C en $T = 22^{o}$C. Een pilot–experiment laat zien dat tussen $T = 26^{o}$C en $T < 22^{o}$C geen significante verschillen in overleving zijn.

Een numeriek model voor hoofdhuidkoeling werd ontwikkeld. Doordat informatie over variabiliteit in parameters hierin werd meegenomen, is het model geschikt om de reactie van een populatie te simuleren. Een vergelijking voor viabiliteit als functie van temperatuur en doxorubicine concentratie werd gefit op resultaten van het *in vitro* experiment. Simulaties werden vergeleken met studies in literatuur over effectiviteit van hoofdhuidkoeling. Hiermee kon een kritische viabiliteit opgesteld worden, $S_{\text{crit}} = 0.88$, gedefinieerd als de minimale viabiliteitswaarde die gehaald moet worden om haaruitval tegen te gaan. Huidige protocollen voor hoofdhuidkoeling werden geanalyseerd en een geoptimaliseerd protocol werd ontwikkeld. Dit protocol kan gebruikt worden voor doxorubicine doses tot 60–70 mg, en het is erop gericht om huidtemperaturen te verlagen tot 17–18^{o}C. Om dit te bereiken, wordt gebruik gemaakt van een cap temperatuur van -10^{o}C, een infusie tijd van 2 uur en een koeltijd gelijk aan infusie tijd plus één uur. Verder wordt personen geadviseerd naar de kapper te gaan om de thermische weerstand tussen hoofd en cap te verminderen. Ons model voor hoofdhuidkoeling laat zien dat met dit protocol de effectiviteit van de hoofdhuidkoeling het hoogst is.

Summary

Chemotherapy induced hair loss is a feared side effect of cancer treatment. Scalp cooling during the administration of cytotoxic drugs can reduce this hair loss. Cooling can be achieved by means of a cap, that is pre–cooled in a freezer or that exchanges coolant with a reservoir. The current hypothesis for the hair preservative effect of scalp cooling is that cooling of the scalp skin reduces blood flow (perfusion) and chemical reaction rates. Reduced perfusion leads to less cytotoxic drugs available for uptake, while the reduced temperature decreases uptake of and damage by chemotherapy. Altogether, less damage is done to the hair cells, and the hair is preserved. However, the effect of scalp cooling varies strongly. A systematic evaluation of the current hypothesis is necessary for a better understanding of the various important parameters of scalp cooling.

In our study, we wanted to quantify the contribution of the putative mechanisms by which scalp cooling prevents hair loss, and with this investigate possible options for improving effectiveness of current day scalp cooling protocols. A computational model has been developed based on the current hypothesis of the mechanisms of scalp cooling. The full computational model consists of two sub–models that describe heat transfer in the human head and transport of doxorubicin (a specific chemotherapy agent) in the human body. Experiments have validated and improved the different computational models.

The heat transfer model uses the Pennes' equation to describe heat transfer in the human head. Parameter studies with the heat transfer model show that key parameters that determine the actual skin temperature during scalp cooling are the size of both the sub–cutaneous fat–layer and the hair–layer.

We measured the reduction in perfusion due to cooling of the head, for different subjects and for different sites. A scalp cooling system was used to slowly cool nine subjects for 90 minutes. Afterwards, subjects were re-warmed for 60 minutes to investigate hysteresis effects. Skin temperature and perfusion were monitored by thermocouples and laser Doppler perfusion probes, respectively. Results show that intra–individual variability is small compared to inter–individual variability. During cooling, perfusion was gradually reduced to a lowest level of 20% $\pm$ 10% at a skin temperature decrease of 20^{o}C.

A (physiologically based) pharmacokinetic model was created to describe doxorubicin distribution in the human body. It consists of eight compartments representing individual organs. Transport, clearance and metabolism between these compartments is described using mass balance ordinary differential equations. Parameter studies show that key parameters in the model are body mass, cardiac output, and both blood flow to and volume of the different tissues.

The effect of local drug concentration and local tissue temperature on hair cell damage was investigated using *in vitro* experiments on keratinocytes. Cells were exposed for 4 hours to a wide range of doxorubicin concentrations. During exposure, cells were kept at different temperatures. Cell viability was determined after 3 days using a modified MTT viability test. Control samples were used to establish a concentration-viability curve. Results show that cell survival is significantly higher in cooled cells ($T < 22^{\circ}$C) than in non–cooled cells ($T = 37^{\circ}$C), but no significant differences are visible between $T = 10^{\circ}$C and $T = 22^{\circ}$C. A preliminary study showed no significant differences in survival between $T = 26^{\circ}$C and $T < 22^{\circ}$C.

Information on variability was used to develop a population based computational model for scalp cooling. Results of the *in vitro* cell experiments were fitted to an equation for viability, with temperature and concentration as independent variables. Simulations were compared with studies from literature on the success of scalp cooling. With this, a critical viability could be established, $S_{\text{crit}} = 0.88$, defined as the viability value above which hair loss is prevented. Current day scalp cooling protocols were evaluated and an optimized scalp cooling protocol was developed. This protocol may be used for doxorubicin doses up to 60–70 mg, and aims to lower skin temperature to 17–18°C. To this end, a cap temperature of $T_{\text{cap}} = -10^{\circ}$C, infusion time of 2 hours and a cooling time equal to infusion time plus one hour is used. Furthermore, a haircut is advised to decrease the thermal resistance between head and cap. Our scalp cooling model shows that with this protocol, effectiveness of scalp cooling was highest.

Chapter 1

Introduction

1.1 Background

History of cancer treatment

The earliest descriptions of human cancer can be found in the Edwin Smith papyrus (3000–1500 B.C.), which is the oldest known surgical text in the history of civilization (Breasted, 1930). It is this Egyptian papyrus that provided the source of inspiration for the Greek physician Hippocrates of Kos (460–370 B.C.), the *founding father* of modern medicine (Stiefel et al., 2006). Hippocrates was the first to acknowledge that natural causes, instead of divine interventions, are the origin of disease (Daniels and Hyslop, 2003). Hippocrates also made extensive descriptions and drawings of both benign and malignant tumours. He called benign tumours *oncos*, Greek for swelling, and malignant tumours *carcinos*, Greek for crab or crayfish, probably because the swollen blood vessels around the malignant tumours reminded him of crab claws.

It was not until the late 19^{th} century, with the development of better microscopes, that significant steps in understanding cancer were made (Turk, 1993). Under these better microscopes, cancer cells proved to be markedly different in appearance from normal cells, and all cancer cells showed one characteristic: unrestrained growth and rapid cell division. Later it was found that, due to abnormalities in the genes that control proliferation, the malignant cell is prevented from going into apoptosis, a process of programmed cell–death. The better understanding of the biology of cancer cells steered the development of cures and strategies for treatment. Besides surgical removal of a tumour, these treatments include radiation therapy and chemotherapy, both based on the higher vulnerability of dividing cells.

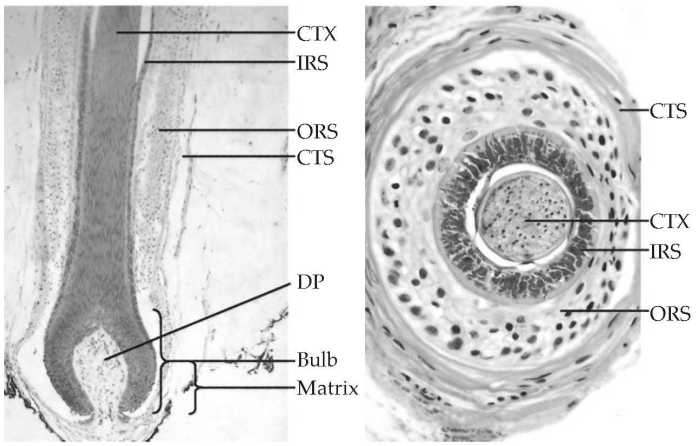

Figure 1.1: Vertical section of proximal anagen follicle (*left*) and cross section of proximal anagen follicle (*right*). CTX: cortex of the shaft; IRS: inner root sheath; ORS: outer root sheath; CTS: connective tissue sheath; DP: Dermal Papilla (Adapted from Stenn and Paus, 2001).

Chemotherapy

Chemotherapeutic agents have the ability to kill dividing cells, without affecting normal cells that are in a resting stage. Since most cells in the human body are in a resting stage at any given moment, and cancer cells are often in a dividing stage, cancer cells are more susceptible to damage than healthy cells. However, certain healthy cell types in the human body also multiply quickly, such as the blood cells forming in the bone marrow and hair follicles. These healthy cells are also affected by chemotherapy and this leads to side effects such as fatigue, nausea, and hair loss (alopecia).

Hair follicle biology

The hair follicle (figure 1.1) is a complex entity, whose growth mechanisms are now being revealed (Rogers, 2004). In the bulb at the base of the follicle, the actual hair is produced by cells in the hair matrix zone. The dermal papilla provides nutrients and growth factors to these cells (Messenger, 1993), and may therefore be viewed as a regulator of hair growth (Van Steensel et al., 1999). Initiated by the dermal papilla, keratinocytes in the hair matrix zone begin to rapidly divide (Rogers, 2004). During this process they move up the follicle and differentiate into one of six possible cell types (Hardy, 1992). As the hair cells move up they encounter the rigid inner root sheath, and subsequently they are compressed and funnelled into their final shape (Paus and Cotsarelis, 1999). Eventually a keratinized hair emerges, with a thin outer

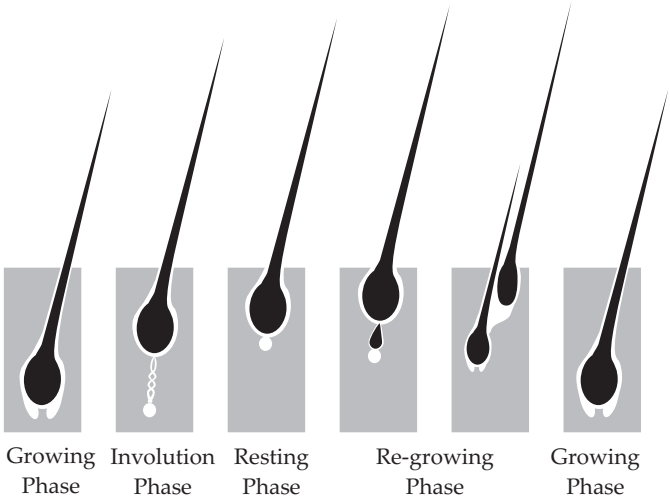

Figure 1.2: Development and cycling of hair follicles (Based on Paus and Cotsarelis, 1999).

cuticle and a thick cortex (Hardy, 1992).

During its lifetime, the hair follicle goes through three distinct growth phases (Stenn and Paus, 2001). These three stages are schematically shown in figure 1.2. During the growth phase (anagen), there is intensive growth and hair shaft production, as described earlier. For hair follicles in the human scalp, this phase may last as long as 7 years (Jones and Steinert, 1996). For reasons not yet understood this relatively long and slow cycle is suddenly interrupted, and the hair follicle enters an involution phase (catagen), in which the old hair shaft factory is broken down and a new hair follicle is formed (Stenn and Paus, 2001). In this stage, a surprisingly rapid rate of coordinated cell apoptosis is initiated, to destroy the lower two thirds of the old follicle. The remains are lifted towards the skin and remain associated with the dermal papilla, which does not migrate but remains in its position (Cotsarelis and Millar, 2001). Toward the end of the catagen stage, however, the dermal papilla condenses and moves upward towards the hair–follicle (Paus and Cotsarelis, 1999). Catagen lasts for about two to three weeks, and is followed by a relative resting phase (telogen). At the end of telogen, which lasts for about two to three months, an intermediate re–growing stage starts where a new hair follicle is produced. A new matrix is formed around the migrated dermal papilla and in time, the new follicle migrates back away from the skin. Then a new hair shaft is produced and ultimately the old hair is released from the follicle as the new shaft develops (Cotsarelis and Millar, 2001). Hair cycling in the human scalp is asynchronous, meaning that not all hair follicles have the same rhythm of cycling. Due to the long period of anagen, approximately 90% of the hair follicles are in this phase at any given time (Cotsarelis and Millar, 2001).

Chemotherapy induced hair loss

Chemotherapy affects rapidly growing keratinocytes in the hair matrix zone in anagen hair follicles (Cotsarelis and Millar, 2001). Studies have shown that a decrease in the diameter of the hair bulb and the hair matrix zone can be seen 4 to 6 days after administration of a single dose (Olsen, 2003). Excessive damage to the hair follicle may even lead to the transition of the hair follicle from an anagen stage to a regression stage (Botchkarev et al., 2000). When the damage is not excessive, the hair follicle is able to recover and the keratinocytes in the hair matrix zone begin to regrow. However, the hair shaft produced within the next 2 to 5 days shows a small constricted section, termed as a *Pohl–Pinkus* constriction (Olsen, 2003). Due to the higher levels of mechanical stress associated with these kinds of constriction, a mechanical load to the hair may easily result in a hair that breaks. This means that even when the damage to the hair follicle is not enough to force the hair follicle into catagen, hair loss through breaking may still occur. Since approximately 90% of hair follicles are in an anagen stage at any given time, the resulting hair loss may be rapid and extensive. According to Olsen (2003), chemotherapy induced hair loss begins 1 to 2 weeks after the initial chemotherapeutic dose. About 1 to 2 months after initiation, the hair loss is most apparent. The process of hair loss is reversible, meaning that in time the hairs will begin to grow again. Therefore, the effect of chemotherapy induced hair loss on patients is of minor concern to nurses and physicians. However, for patients, chemotherapy induced hair loss is one of the most feared side effects of cancer therapy (Cash, 2001). Although not highly detrimental to physical health, hair loss can be psychologically devastating and can even lead some patients to reject potentially curative treatment (Katsimbri et al., 2000).

Methods against chemotherapy induced hair loss

Since about 1970, many preventive measures have been tried to reduce chemotherapy induced alopecia: medicaments, the tourniquet and scalp cooling (Grevelman and Breed, 2005).

Recently, there have been some interesting developments in the medicamental approach of preventing chemotherapy induced hair loss. Botchkarev et al. (2000) showed that p53, a transcription factor controlling the cell cycle, is necessary in developing chemotherapy induced hair loss. In his study, p53–deficient mice treated with chemotherapeutics did not lose their hair. This suggests the use of chemical inhibitors of p53 in preventive therapy. In another study, Davis et al. (2001) showed that inhibition of another cell cycle regulator (cyclin–dependent kinase 2, CDK2) is also capable of preventing chemotherapy induced hair loss in rats. However, these studies have all been performed in rodents, and although the results are promising, it will probably take a long time before effective medicaments will have been developed, and their safety and adverse reactions have been studied.

Figure 1.3: Hospitals in the Netherlands where scalp cooling was available in 2006 (•) and hospitals where scalp cooling is planned for 2007 (○).

Tourniquets, bands applied to the head that stop blood flow by compressing blood vessels, were used in the 1970's to prevent chemotherapy induced hair loss. Their application was based on the hypothesis that a reduction in perfusion in the scalp skin can effectively reduce the amount of chemotherapeutic agent that is delivered to the hair follicle. The tourniquets' use was abandoned in the early 1980's with the introduction of the more effective scalp cooling.

Scalp cooling

In 2006, scalp cooling was available in the Netherlands in only a few hospitals, but the number of hospitals where the introduction of scalp cooling is planned is rising (figure 1.3). At the end of 2006, a total number of 17 hospitals offered scalp cooling and in 2007 this number will be increased by another 14 hospitals. This sudden increase in the number of hospitals where scalp cooling is applied may be attributed to both the attention given in the media and the success rates obtained in the last few years.

Scalp hypothermia during the administration of cytotoxic drugs can reduce hair loss (e.g. Protière et al. 2002). Since the introduction of the method, several variations have been used to cool the scalp during treatment, including crushed ice, refrigerated gel packs and cooling machines using either cold air or a cooled cap (figure 1.4). In the Netherlands, the cooling machines with cap are generally used. This system consists of a cooled reservoir connected to a cap and a pump to circulate the coolant. A system of small canals in the cap is connected via a tube to the cooling device, thus

Figure 1.4: Typical caps used for scalp cooling to prevent chemotherapy induced hair loss. From left to right: Paxman Cooler (cooled cap with cooling machine), DigniCap (cooled cap with cooling machine), Penguin cold cap (refrigerated gel cap) and Scalp Cooling System 2 (forced air cooling machine).

Table 1.1: WHO criteria for hair loss.

Grade 0	No significant hair loss.
Grade 1	Minor hair loss, not requiring a wig.
Grade 2	Moderate hair loss but not requiring a wig.
Grade 3	Severe hair loss requiring a wig.
Grade 4	Total hair loss.

forming a closed circuit. The cooling device is used to cool and transport a coolant fluid through the cap, thus extracting heat from the head.

Coolant temperature of these devices is set to -8^{o}C and with this the temperature of the skin is reduced to approximately 20^{o}C. The cap has to be applied some 15 minutes before administration of the chemotherapeutic agent begins, to ensure that the scalp skin is at the right temperature. In some hospitals, the hair is wetted using water or a conditioner to improve the thermal contact between the cap and the head. The cap remains in its position as long as the chemotherapeutic agent is administered, and during a period of post–cooling. Manufacturers of scalp cooling devices suggest a post–cooling time ranging from 1.5 to 3.5 hours. These post–cooling times depend on the specific chemotherapeutic agent and the dose administered.

The use of these cooling machines is generally very well tolerated by the patient, although extreme cooling may be painful to the patient. In clinics, satisfactory results have been obtained in terms of hair preservation (e.g. Protière et al. 2002; Ridderheim et al. 2003). One study showed that hair preservation was significantly higher when scalp cooling was applied, compared to no scalp cooling at all (Protière et al., 2002). In another study the degree of hair preservation as categorized by the World Health Organization (WHO, table 1.1) was grade 2 or better in 89% of the patients (Massey,

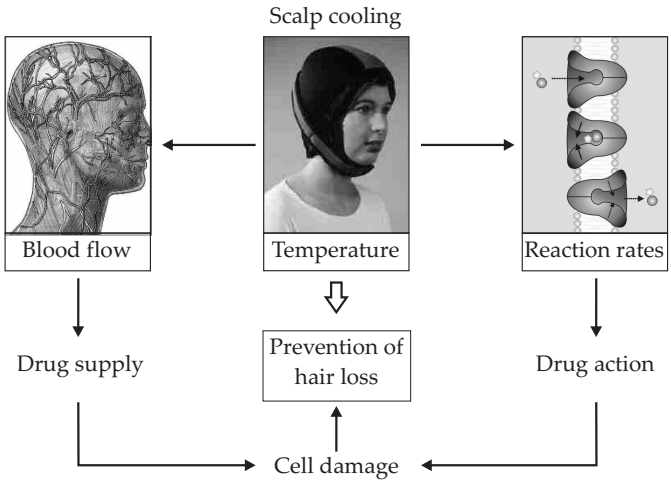

Figure 1.5: Hypothesis of scalp cooling, as proposed by Bülow et al. (1985). Cooling the scalp leads to less hair loss. The two supposed effects responsible for this are reduced blood flow by vasoconstriction and reduced cell reactions.

2004, no control group included). For specific groups of chemotherapeutic agents (taxanes and anthracyclines) the effectiveness can be as high as 100%. To put this in perspective, the chemotherapeutic agent doxorubicin (belonging to the anthracycline group) is known, without preservation measures, to cause severe and usually total hair loss in nearly all patients (Anderson et al., 1981). For other chemotherapeutic groups the efficacy of scalp cooling was 50%, compared to 19% for the control group (Grevelman and Breed, 2005).

1.2 Problem definition and thesis outline

There are large variations in the efficacy of scalp cooling. Most probably, this is largely part due to variations in cooling methods and cooling protocols such as temperature and cooling times (Breed, 2004). A better understanding of the biochemical and physiological properties playing a role in chemotherapy induced hair loss could lead to universal adoption of an optimized protocol.

Bülow et al. (1985) proposed a hypothesis for the hair preservative effect of scalp cooling, based on earlier work by Gregory et al. (1982). The latter study investigated the relationship between local tissue temperatures and the hair preservative effect of scalp cooling. It was found that the degree of hair loss was temperature dependent. Based upon their data, they concluded that scalp cooling was effective only when the subcutaneous scalp temperature was decreased below 22°C. Based upon these findings, Bülow et al. (1985) proposed that the effect of scalp cooling can be at-

tributed both to reduced supply and reduced action of drugs at a lower temperature (figure 1.5). Cooling the scalp skin induces vasoconstriction, decreasing blood flow. Because of this the total amount of cytotoxic drugs available for uptake in the hair cells is diminished. In addition, hair follicles are less susceptible to cytotoxic drug damage because of falling temperatures with subsequent lower cellular drug uptake and metabolism.

Bülow et al. (1985) investigated the effect of scalp cooling on local tissue blood flow, using a Xenon washout technique. He found that perfusion was reduced to a constant low level of about 20% when subcutaneous scalp temperature was reduced below 30°C. As stated before, however, the hair preservative effect of scalp cooling does not show until subcutaneous temperature is reduced below 22°C. Based upon this, Bülow et al. concluded that the effect of reduced metabolism probably is a more significant factor in the hair preservative effect of scalp cooling than the effect of reduced blood flow. Unfortunately, this is an analysis that no study has followed up.

In our study, we wanted to quantify the contribution of the putative mechanisms by which scalp cooling prevents hair loss, and with this investigate possible options for improving efficacy of current day scalp cooling protocols. For this, we developed a computational model of scalp cooling that encompasses all aspects in the hypothesis of scalp cooling (figure 1.6). The complete model for scalp cooling includes several sub–models to describe heat transfer, drug transport and drug effect. Several experiments were used to refine these computational models. Since there are large variations in success rates, a model with fixed subject parameters might not be able to explain observed results. Therefore, we used modelling of variability to obtain a population–based model of scalp cooling. With this model, several scalp cooling protocols were evaluated and finally, recommendations for future scalp cooling protocols were made.

The first sub–model is the heat transfer model for a human head during scalp cooling. This model will be described in chapter 2. A parameter study was performed to study the influence of variation in size and shape of the scalp and other physical parameters on scalp skin temperature and perfusion during scalp cooling.

The relationship between local scalp skin temperature and local tissue blood flow plays an important role in the hair preservative effect of scalp cooling. Therefore, we experimentally investigated the temperature–perfusion relationship during scalp cooling. To this end, laser doppler perfusion measurements were combined with simultaneous thermocouple measurements to obtain a relationship between temperature and blood flow. The results of the experiments will be described in chapter 3.

The second sub–model is the pharmacological model, and this model describes drug transport during scalp cooling. This model will be described in chapter 4. We modelled transport of the anthracycline doxorubicin, since it causes hair loss and

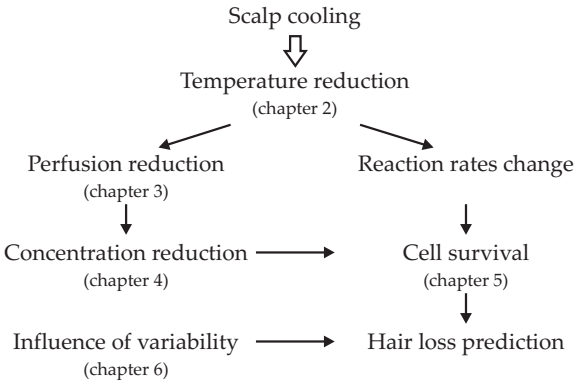

Figure 1.6: Outline of this thesis.

scalp cooling has been proven effective for this drug. A parameter study was performed to investigate the important parameters in this sub–model.

To relate local tissue concentrations to cell damage at different temperatures, we conducted a series of *in vitro* biological cell experiments. Normal Human Epidermal Keratinocytes were cultured and exposed to different concentrations of doxorubicin at several exposure temperatures. Cell damage was evaluated using a viability test. The results of these experiments will be described in chapter 5.

In chapter 6, the heat transfer model and the pharmacological model were used to develop a complete model of scalp cooling adjunct to chemotherapy administration. The results of both the experiments on the relationship between temperature and perfusion and the experiments on *in vitro* cell damage were incorporated in the model. Knowledge of variability in important parameters was used to generate a population based model for scalp cooling. The population based model was used to simulate clinical studies on the hair preservative effect of scalp cooling. The results, in combination with results of the *in vitro* experiments (chapter 5) were used to establish a hair loss criterium. This hair loss criterium was then used to evaluate various scalp cooling parameters, and finally, guidelines for future cooling protocols were derived.

Finally, conclusions of this thesis will be given in chapter 7.

Chapter 2

Heat transfer in the human head during scalp cooling*

2.1 Introduction

To gain more insight into the effect of cooling, a computer model has been developed that describes heat transfer in the human head during scalp cooling. Based on his experiments on the human forearm, Pennes (1948) was the first to establish an equation describing the relationship between the various heat processes in human tissue. He expressed this energy balance for perfused tissue in the following form (Pennes, 1948):

$$\rho c \frac{\partial T}{\partial t} = \nabla \cdot (k \nabla T) + q_{\mathrm{m}} + W_{\mathrm{b}} \tag{2.1}$$

in which ρ, c and k are the density, specific heat and thermal conductivity, respectively. T is the local tissue temperature and q_{m} and W_{b} are the metabolic heat production in the tissue and the rate of heat transfer per unit volume of tissue due to perfusion, respectively.

According to Pennes, the energy exchange between blood vessels and the surrounding tissue mainly occurs at the level of the capillaries. Therefore, he assumed that the thermal contribution of blood can be modelled by a so-called heat sink. In

*This chapter is an extended version of:
Janssen, F.E.M., Van Leeuwen, G.M.J. and Van Steenhoven, A.A. (2005). Modelling of temperature and perfusion during scalp cooling. *Physics in Medicine and Biology*, 50:4065-4073.

this approach, the blood is still at the temperature of the major supplying vessel when it reaches the capillary bed, where immediate thermal equilibration with the surrounding tissue takes place. With the blood having passed the capillaries, likewise, all heat exchange in the venous network is neglected. The thermal effect of the flowing blood is hence modelled using a heat source (or heat sink, in tissue warmer than the core), whose magnitude is proportional to the volumetric blood flow and the difference between local tissue and major supply arterial temperatures:

$$W_{\mathrm{b}} = \rho_{\mathrm{b}} c_{\mathrm{b}} w_{\mathrm{b}} (1 - \kappa)(T_{\mathrm{A}} - T) \tag{2.2}$$

Here, ρ_{b} and c_{b} are the density and specific heat of the blood, w_{b} is the volumetric blood flow per tissue volume ($\mathrm{m}^3\ \mathrm{s}^{-1}\ \mathrm{m}^{-3}$), κ is a factor that accounts for incomplete thermal equilibrium between blood and tissue, and T_{A} is the temperature of the arterial blood. Pennes assumed that $0 < \kappa < 1$, but in his final analysis, he used $\kappa = 0$ to obtain the well known *bio–heat transfer* equation:

$$\rho c \frac{\partial T}{\partial t} = \nabla \cdot (k \nabla T) + \rho_{\mathrm{b}} c_{\mathrm{b}} w_{\mathrm{b}} (T_{\mathrm{A}} - T) + q_{\mathrm{m}} \tag{2.3}$$

The physical and physiological validity of the underlying assumptions of the bio–heat transfer equation have been questioned (Arkin et al., 1994). Initiated by this criticism, several alternative models have been proposed for the blood flow term.

Chen and Holmes (1980) investigated the assumption that heat transfer mainly occurs at the level of the capillaries, by calculating the thermal equilibration length of blood vessels. This thermal equilibration length is defined as a length of blood vessel for which the temperature difference between blood and tissue is reduced to $1/e$ of its initial value. Results of these calculations showed that the premise made by Pennes was incorrect. Thermal equilibration of the blood with the tissue occurs in blood vessels with diameters in the range of 0.2–0.5 mm.

Based on these observations, Chen and Holmes proposed a new formulation of the perfusion term in the Pennes equation. Blood vessels are grouped into large vessels and small vessels. The large vessels are all treated separately and the last calculated blood temperature T_{A}^* is then used in a continuum formulation for the smaller vessels. Another two modes of heat transfer are added in this continuum formulation and with this the Chen and Holmes model becomes:

$$\rho c \frac{\partial T}{\partial t} = \nabla \cdot (k \nabla T) + \rho_{\mathrm{b}} c_{\mathrm{b}} w_{\mathrm{b}}^* (T_{\mathrm{A}}^* - T) - \rho_{\mathrm{b}} c_{\mathrm{b}} \overline{u} \cdot \nabla T + \nabla \cdot \left(k_{\mathrm{p}} \nabla T \right) + q_{\mathrm{m}} \tag{2.4}$$

This model has two additional terms compared to the Pennes equation. The first of these extra terms uses a local mean apparent blood velocity $\overline{u}$ to model the convective heat transfer attributable to the net directed flow and was originally proposed by Wulff (1974). The last extra term describes the collective effect of blood flow in small vessels with flow in opposite directions so as to have no nett flow. The qualitative effect is that of an apparent increase of conductivity of the tissue, quantitatively described by k_{p}.

Weinbaum and Jiji (1985) studied the architecture of the vasculature and identified incomplete counter–current heat exchange as the primary mechanism for blood–tissue exchange. They used an effective conductivity tensor k_{eff}, to describe the thermal effect of the blood:

$$\rho c \frac{\partial T}{\partial t} = \nabla \cdot (k_{\text{eff}} \nabla T) + q_{\text{m}} \tag{2.5}$$

The effective conductivity tensor represents both the capillary bleed off and the heat exchange between tissue and adjacent vessels. In a one dimensional situation, the effective conductivity tensor reduces to (Arkin et al., 1994):

$$k_{\text{eff}} = k \left[1 + \frac{n \pi r_{\text{v}}^2 \rho_{\text{b}} c_{\text{b}} u_{\text{b}}}{\sigma k^2} \right] \tag{2.6}$$

Here, n is the vessel pair density, k is the thermal conductivity of the tissue, r_{v} is the vessel radius, u_{b} is the blood velocity and σ is a shape factor that describes vessel–tissue heat transfer.

Since the continuum formulations are unable to predict local temperature inhomogeneities caused by the larger vessels, individual modelling of these vessels was proposed (Lagendijk, 1982). For some very simple geometries it is possible to obtain analytical solutions, but for any realistic situation it is necessary to use a numerical approach. A very sophisticated model for use in local hyperthermia treatment planning and monitoring has been developed by Kotte (1998). Separate descriptions of tissue and discrete vasculature allow for flexibility and ease of use, while the application of analytical solutions for the blood–tissue heat transfer gives sufficiently accurate results without going into detailed description of the blood flow. The patient's known (e.g., MRA derived) vasculature is discretely modelled. Final temperatures in the terminal arteries are used in a heat sink/source term in the local surrounding tissue, and the thermal conductivity of the tissue incorporates the contribution to the conductivity of the smaller vessels. The more detailed the discrete description of the vasculature, the smaller the effects (heat sink and effective conductivity) of the remaining vessels will be. However, the collective thermal effects of these small vessels are quite subtle (Van Leeuwen, 1998). It is not possible to determine an optimum effective thermal conductivity based on just the static vessel and tissue properties: it is in fact also dependent on the length scales of the temperature inhomogeneities. Therefore a more accurate description of the thermal behaviour is obtained when the known vasculature is expanded by smaller vessels with the same branching characteristics as the actual vessels. This approach was used by Van Leeuwen et al. (2000) and Stańczyk et al. (2007).

Although detailed discrete vessel models provide the best description of the thermal behaviour of perfused tissue, their use comes at a price. Firstly, obtaining a detailed description of the vasculature requires considerable efforts. After acquiring the 3D raw angiographic images, vessel data must be extracted and brought in a form that can be used. After this, the possible addition of artificial vascular detail

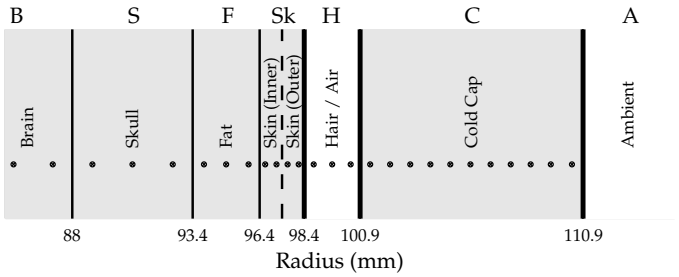

Figure 2.1: Schematic representation of the outer part of the model: head and cold cap and the placement of the nodes.

is a further time-consuming step. Having completed building the vascular network for the tissue volume, the actual running of the computer model will consume considerably more memory and CPU-time than a lumped parameter model.

Wissler (1998) investigated the criticism directed to the Pennes approach and found that this criticism is not always justified. On the contrary, temperature profiles computed with the Pennes equation agree reasonably well with the measured profiles. The heat sink model will provide sufficiently accurate results and uncover dependency relations, one of the main objects of this study. In our case, the costs of using a different approach for the blood flow term (e.g. discrete vessel approach) will not outweigh the benefits. Therefore, we used the Pennes equation to develop a heat transfer model for the head during scalp cooling. With this model, a parameter study was performed to uncover important parameters during scalp cooling.

2.2 Heat transfer model for the head during scalp cooling

The model configuration consists of a simplified head and a cooling cap system. A coolant is circulated through the cap, thus extracting heat from the patient's scalp. Heat transfer in the tissue is governed by equation 2.3, with T_A the temperature of the blood in the main arteries supplying the scalp.

The head and cold cap are both idealized with spherical elements representing brain, skull, fat, skin, hair and cold cap (figure 2.1). This idealization, and the fact that we impose boundary conditions with spherical symmetry, means that the model is essentially one dimensional, which will make it easier to identify important parameters in the heat transfer model. In addition, we assume that all tissue layers have homogeneous properties. The one-dimensional bio–heat equation in spherical

coordinates can thus be written as:

$$\rho c \frac{\partial T}{\partial t} = k\left(\frac{2}{r}\frac{\partial T}{\partial r} + \frac{\partial^2 T}{\partial r^2}\right) + \rho_{\mathrm{b}} c_{\mathrm{b}} w_{\mathrm{b}} (T_{\mathrm{A}} - T) + q_{\mathrm{m}} \tag{2.7}$$

One of the main points of interest in this study is the interplay between temperature and perfusion. The reductions in metabolism and subsequent reductions in perfusion due to falling temperatures are modelled according to a well known Q_{10} relation of thermal physiology. This rough-and-ready rule was first introduced by Van 't Hoff, and later adapted by Arrhenius, and it states that reaction rates roughly double or triple for every 10°C rise in temperature. The initial hypothesis will be that this will also hold true for lower temperatures. Due to a reduction in tissue temperature there is a corresponding reduction in cell metabolism (Dennis et al., 2003), and as a consequence the demand for nutrients (e.g. oxygen) will diminish. Subsequently it is no longer necessary to sustain the current level of blood flow and the body reacts by lowering tissue perfusion (Fiala et al., 1999). The reduction in metabolism and subsequent reduction in blood flow is by a factor Q_{10} for every 10°C. Relative metabolism (ϕ_q) and relative perfusion (ϕ_w) can now be defined as:

$$\phi_q \equiv \frac{q_{\mathrm{m}}}{q_{\mathrm{m},0}} = Q_{10}{}^{\frac{(T-T_0)}{10^{\circ}\mathrm{C}}} = e^{\frac{(T-T_0)}{T_{\mathrm{r}}}} \tag{2.8}$$

$$\phi_w \equiv \frac{w_{\mathrm{b}}}{w_{\mathrm{b},0}} = Q_{10}{}^{\frac{(T-T_0)}{10^{\circ}\mathrm{C}}} = e^{\frac{(T-T_0)}{T_{\mathrm{r}}}} \tag{2.9}$$

In which T_{r} is defined as:

$$T_{\mathrm{r}} = 10(\ln Q_{10})^{-1} \quad [^{\circ}\mathrm{C}] \tag{2.10}$$

Reported values for Q_{10} range from 2.0 to 3.0 (Dennis et al., 2003) and we use an average value of 2.5 in our standard head model. Thermoneutral metabolism, $q_{\mathrm{m},0}$ in equation 2.8, and thermoneutral perfusion, $w_{\mathrm{b},0}$ in equation 2.9, are the respective values in the thermoneutral state: at $T = T_0$. It should be noted that tissue temperatures in the thermoneutral state are spatially dependent, $T_0 = T_0(r)$, their values are obtained by calculating the steady state temperature distribution in the standard head model without scalp cooling.

Since anatomical differences in vessel densities in the skin affect heat transfer (Weinbaum et al., 1984), the skin was modelled with two layers, an inner and an outer skin layer. According to Weinbaum et al. (1984), the energy exchange due to perfusion in the outer most part of the skin is equal to zero. The perfusion term in equation 2.3 is therefore eliminated, and this is modelled by setting perfusion w_{b} for the outer skin to zero.

Coolant inflow in the cold cap is modelled with the heat sink term in equation 2.3. Density and specific heat of the coolant are assumed to be equal to those of water. The mass flow of the cap is estimated at 0.17 kg s^{-1} ($\dot{m}_{\mathrm{cap}} = 10$ kg min^{-1}) and this

Table 2.1: Thermophysical tissue parameters used in the standard head model.

	d $\left(\mathrm{mm}\right)$	k $\left(\frac{\mathrm{W}}{\mathrm{mK}}\right)$	c $\left(\frac{\mathrm{J}}{\mathrm{kg\cdot K}}\right)$	ρ $\left(\frac{\mathrm{kg}}{\mathrm{m}^3}\right)$	q_{m} $\left(\frac{\mathrm{W}}{\mathrm{m}^3}\right)$	w_{b} $\left(\frac{\mathrm{kg}}{\mathrm{m}^3\cdot\mathrm{s}}\right)$
Brain	88.0	0.5	3800	1000	8800	8.5
Skull	5.4	1.0	1700	1500	130	0.150
Fat	3.0	0.2	2390	1050	130	0.2
Inner skin	1.0	0.384	3570	1130	500	1.5
Outer skin	1.0	0.384	3570	1130	0	0.0
Hair	2.5	0.04	1000	1	0	0.0
Cold Cap	10.0	0.500	4300	1000	0	119.0

Table 2.2: Other parameters used in the standard head model.

symbol	description	dimension	value
Q_{10}	perfusion coefficient	(–)	2.5
T_{A}	arterial temperature	($^{\mathrm{o}}$C)	37
T_{cap}	cap temperature	($^{\mathrm{o}}$C)	$-$ 8
T_{amb}	ambient temperature	($^{\mathrm{o}}$C)	20
h	heat transfer coefficient	(W m^{-2} K^{-1})	4
$\dot{m}_{\mathrm{cap}}$	cap cooling mass flow	(kg min^{-1})	10

value is converted to a w_{b} of 119 kg m^{-3} s^{-1}. The default model value for the coolant temperature is $T_{\mathrm{cap}} = -8^{\mathrm{o}}$C.

To investigate the influence of variations in physiological and physical properties, a range of thermal properties, basal blood flow and basal metabolic rate values have been used. Six different studies in the literature on human head heat transfer were examined (Nelson and Nunneley, 1998; Fiala et al., 1999; Xu et al., 1999; Diao et al., 2002; Dennis et al., 2003) and mean value and range of geometry and tissue properties were determined. The mean values of these properties are used to define our standard head model (table 2.1). The range in the literature determines the lower and upper limit for the parameter study ($\bigtriangledown$ and $\bigtriangleup$, respectively, table 2.3 and 2.4). In addition, the influence of other parameters such as temperature of the blood, cap and surroundings is also investigated. Standard values and upper and lower limit of these parameters are shown in table 2.2 and table 2.5, respectively.

2.2.1 Boundary conditions

Appropriate boundary conditions for the head and cold cap before and during scalp cooling can be modelled as follows. Due to symmetry, a Neumann boundary condition ($\frac{\partial T}{\partial r} = 0$) is used for the core of the brain. At the surface, boundary conditions for both the uncovered head and the head with cold cap include convective heat transfer and radiative heat transfer. Convective heat transfer between the uncovered head or the cold cap and the surroundings is modelled as

$$q'' = h(T - T_{\text{amb}}) \tag{2.11}$$

in which h is the heat transfer coefficient for free convection. Its value can be based on appropriate Nusselt relations for natural convection for a sphere with diameter D, surrounded by a cold or warm fluid (Bejan, 1993, page 361):

$$\overline{\text{Nu}}_D = \frac{hD}{k} = 2 + \frac{0.589\text{Ra}_D^{1/4}}{\left[1 + (0.469/\text{Pr})^{9/16}\right]^{4/9}} \tag{2.12}$$

The Nusselt number depends on the Prandtl-number (Pr) and the Rayleigh number (Ra), and the appropriate ranges in this Nusselt relation are $\text{Pr} \gtrsim 0.7$ and $\text{Ra}_D < 10^{11}$. For air, the Prandtl number is equal to $\text{Pr} = 0.72$ and the Rayleigh number is equal to:

$$\text{Ra}_D = \text{Pr}\frac{g\beta\Delta T D^3}{\nu^2} \tag{2.13}$$

With ambient temperature (T_{amb}) set to 20°C, the average temperature difference between either head or cold cap and the surroundings is of order $\Delta T \sim 20$°C. With the volumetric thermal expansion coefficient of air equal to $\beta = 3.43 \cdot 10^{-3}$ K^{-1} and the kinematic viscosity of air equal to $\nu = 1.5 \cdot 10^{-5}$ m^2 s^{-1}, the Rayleigh number based on a sphere with diameter $D \sim 0.21$ m equals $\text{Ra}_D = 1.9 \cdot 10^7$. Both the Prandtl–number and the Rayleigh–number fall into the appropriate range for the Nusselt relation. The above leads to a Nusselt number of $\overline{\text{Nu}}_D = 32$, and with thermal conductivity of air equal to $k = 0.025$ W m^{-1} K, this leads to a heat transfer coefficient of $h = 4$ W m^{-2} K^{-1}. This value is used in the standard head model.

Radiative heat transfer from the surface of either the head or the cap to the surroundings is modelled as

$$q'' = \sigma\epsilon(T_1^4 - T_2^4) \tag{2.14}$$

in which σ is the Stefan Boltzmann constant ($\sigma = 5.669 \cdot 10^{-8}$ W m^{-2} K^{-4}) and ϵ the emissivity. Emissivity of both head and cold cap is taken as 1.0. In addition to radiative heat transfer to the surroundings, we assume that the density of the hair is such that it enables radiative heat transfer between the surface of the outer skin and the inner side of the cap, when the cap is on. Another mode of heat transfer between the skin and the cold cap is conductive heat transfer via the hair layer. Convective heat transfer between the skin and the cap is neglected, due to the hair forming an obstruction for convection.

2.2.2 Numerical methods

The first and second spatial derivatives in the bio–heat equation are discretized using centred difference approximations:

$$k\left(\frac{2}{r}\frac{\partial T}{\partial r}+\frac{\partial^2 T}{\partial r^2}\right)=k\left[\frac{2}{r}\frac{T_{r+1}-T_{r-1}}{2\delta r}+\frac{T_{r-1}-2T_r+T_{r+1}}{(\delta r)^2}\right] \tag{2.15}$$

This results in an ordinary differential equation (ODE) for every single node. The resulting set of ordinary differential equations is solved using a standard ODE–solver (MATLAB, the MathWorks).

Care must be taken to prevent inaccuracies due to differences in physical properties between the tissue layers (Schuh, 1957). Correct behaviour over a tissue layer transition can be obtained by formulating the equations with the help of the introduction of two virtual nodes on the interface ($r = r_{\text{ifc}}$), with one node each belonging to either side of the interface. Then, both the temperatures of the two tissue layers and the heat fluxes at the two virtual nodes are required to be equal:

$$\lim_{r\uparrow r_{\text{ifc}}} T = \lim_{r\downarrow r_{\text{ifc}}} T \tag{2.16}$$

$$\lim_{r\uparrow r_{\text{ifc}}} q'' = \lim_{r\downarrow r_{\text{ifc}}} q'' \tag{2.17}$$

Working out these requirements provides the correct equations for the actual nodes on both sides of the interface. The above procedure is also used to discretise boundary conditions at the surface of either the skin or the cold cap.

2.2.3 Validation

The model implementation has been validated by comparing the results of the model to known analytical solutions. These validations include:

- steady–state conduction in a sphere;
- unsteady conduction in a sphere;
- steady–state heat transfer in a sphere with internal heat generation;
- steady state heat transfer in a sphere with internal heat generation and perfusion (heat sink).

For each of the above cases, the error in the numerical result is determined as follows. The difference between the numerical solution (T_{num}) and the analytical solution (T_{ana}) is given by

$$\epsilon = T_{\text{num}} - T_{\text{ana}} \tag{2.18}$$

and with a typical temperature difference ΔT, the error is defined as:

$$\xi = \frac{\epsilon}{\Delta T} \tag{2.19}$$

With this, the error in the numerical solution in the simulated cases is less than 0.6% and we conclude that the model is capable of producing accurate results. A complete overview of the validations and their results is given in appendix A.

2.2.4 Simulations

Simulation of a scalp cooling procedure consisted of two steps. First, the steady–state temperature without a cold cap was calculated using the appropriate parameter set, and keeping metabolism and perfusion constant during calculations. Then, a cold cap was added to the model, and the temperature profile previously obtained provided the initial conditions for a new calculation. In addition, the temperature profile was used as reference temperature profile for temperature dependent metabolism and blood flow (equations 2.8 and 2.9), meaning that each node had its own thermoneutral temperature T_0. Simulation of this scalp cooling procedure continued until a steady state was reached.

2.3 Results

2.3.1 Standard model head

The temperature distribution in the head during cooling was first calculated for the standard configuration, using the parameter values in Tables 2.1 and 2.2.

Skin temperature during cooling drops from 34.5°C to a minimum of 19.2°C (figure 2.2). The time associated with 95% of this decline in temperature is approximately 19 minutes. Relative perfusion in the perfused skin (inner skin) is reduced to a minimum value of 27%.

Temperature profiles at steady–state in the head before cooling, and in the head and cold cap during cooling, are shown in figure 2.3. A detail of the outermost part of the head is shown in figure 2.4. In these figures, we can see that during cooling, a steep gradient is present in the outermost part of the head. At the level of the hair follicle, with part of its root fixed in the fat–layer, the temperature is reduced to less than 25°C, still some 5°C higher than the outer skin temperature. Here, perfusion is reduced to less than 40% of its original value.

From the skin inwards, only a small layer of less than 2cm is significantly influenced by the cooling of the scalp. At deeper positions, the temperature profile is very much equal to the temperature profile before cooling. The largest gradient in the head is found in the fat–layer, separating the warm brain from the cold skin. This is as expected, since the fat layer has a relatively low thermal conductivity.

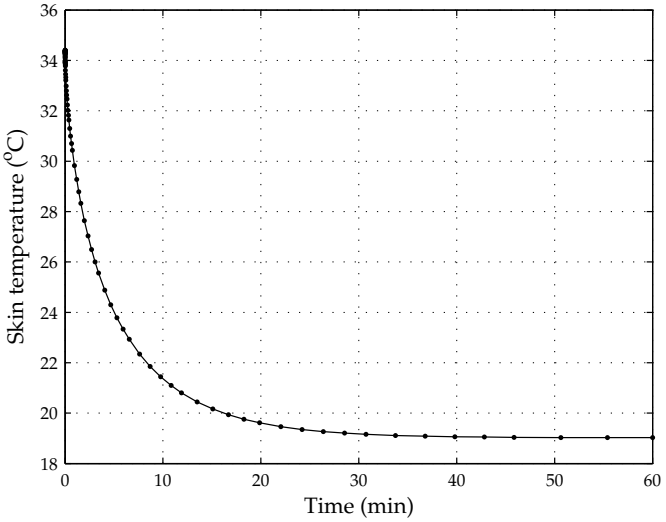

Figure 2.2: Standard model head calculations showing the time response of the skin to a cold cap at a temperature of -8^{o}C.

Another large gradient exists between the head and the cold cap. Although the cap is at -8^{o}C, the temperature of the skin does not fall below 19^{o}C, since the hair layer too has a relatively low thermal conductivity.

Based on these results, we expected that the exact properties (thickness and conductivity) of both the fat layer and the hair layer play an important role in determining the actual skin temperature and perfusion during scalp cooling. To quantify the influence of these, and all other properties, a parameter study was carried out.

2.3.2 Parameter study

In the parameter study, we investigated the influence of several parameters on the minimum skin temperature and perfusion during cooling. The values used and results for tissue layer thickness, conductivity, metabolism and perfusion are shown in table 2.3 and 2.4. Other varied parameters and results are shown in table 2.5.

Tissue layer thickness (table 2.3.I);

No significant changes are seen for variations in tissue layer thickness of either the brain, the skin or the scalp.

Greater influences are found when the thickness of the fat or hair layer are altered. The 7 mm increase in the fat layer results in a drop in minimum skin temperature of 11.5^{o}C and a further decrease in relative perfusion down to 15%. Decreasing the fat layer by 2 mm results in a 3.2^{o}C increase in skin temperature and a relative

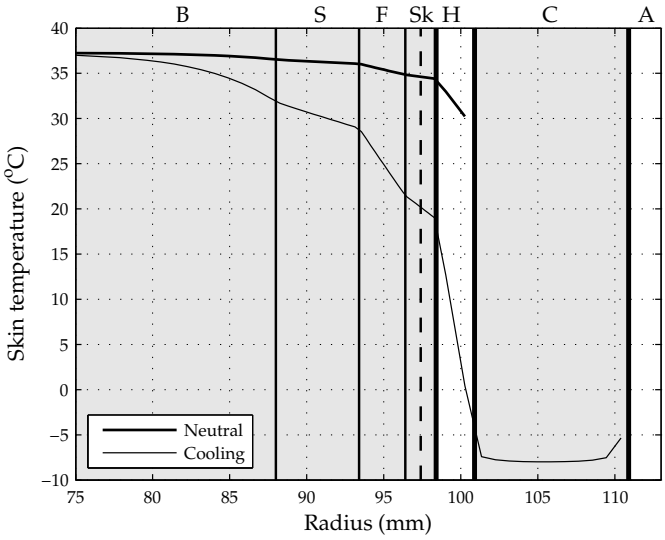

Figure 2.3: Standard model head calculations showing the temperature distribution in the head before cooling, and the temperature distribution in the head and cold cap during cooling.

perfusion of 35%. The effect of variations in the hair layer are likewise strong, but opposite in direction. Increasing the hair layer now increases both minimum skin temperature and relative perfusion. For hair layer thicknesses between 1mm and 4mm, minimum skin temperature ranges from 9.4°C to 25.1°C, and corresponding values for relative perfusion are 14% and 42%, respectively.

In the head and cold cap model, the skin is positioned right between two insulating layers (the fat layer and the hair layer), each connected to either a hot source (the brain) or a cold source (the cold cap). This means that the insulating layer at either side, determines to what extent the skin can be cooled during scalp cooling. The above results show that the influence of the insulating layer on surface skin temperature is very large.

Tissue thermal conductivity (table 2.3.II);

Variations in tissue conductivity within the range of likely values have a greater influence for all tissue layers than variations in tissue layer thicknesses. Nevertheless, changes in tissue conductivity for either brain, skull or skin show a small effect on skin temperature and perfusion compared to changes in the conductivity of both the fat and hair layer.

Reducing the conductivity of the brain, results in a minimum temperature of 17.3°C, and a minimum perfusion of 23%. This is due to the fact that reduced con-

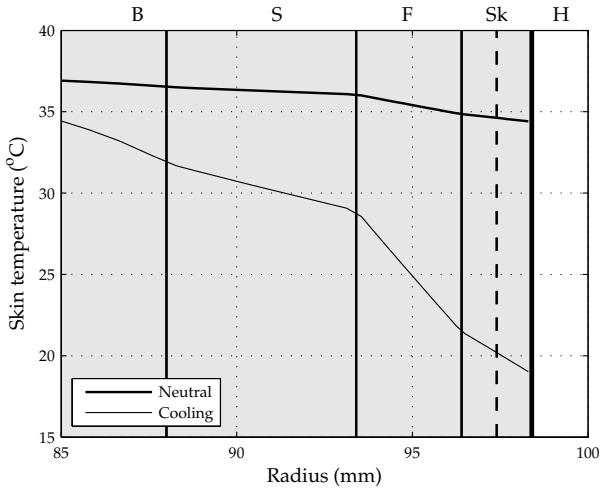

Figure 2.4: Standard model head calculations showing a detail of the temperature distribution in the outermost part of the head before and during cooling.

ductivity deteriorates the thermal contact between the warm brain and the skin. Likewise, the increase in the conductivity of the fat layer results in an increase in minimum skin temperature of 1.5°C and a relative perfusion of 30%. The simulated reduction of this parameter results in a temperature decrease of 3.6°C and a relative perfusion of 20%.

Increasing the conductivity of the hair layer, results in a further decrease in minimum skin temperature of 8.2°C and a relative perfusion of 14%. The decreased hair layer conductivity shows increased skin temperature of 6°C and a relative perfusion of 42%. Once again, this shows the effect the insulating hair layer can have on minimum skin temperature and perfusion.

Tissue basal metabolism (table 2.4.I);

The modelled variations in metabolism do not result in significant changes in either minimum skin temperature or relative perfusion. The effect on skin temperature is only noticeable for increased or decreased brain metabolism, with skin temperature being 0.1°C higher or lower, respectively. This is all too little to have a discernable effect on perfusion.

Tissue basal perfusion (table 2.4.II);

The simulations for variations in tissue basal perfusion show that the perfusion of both brain and skin are responsible for the largest changes in skin temperature.

Table 2.3: Effect of changes in I. tissue layer thickness (d) and II. thermal conductivity (k) on minimum skin temperature (T_{skin}) and relative perfusion (ϕ_w) during cooling. $\bigtriangledown$ and $\bigtriangleup$ correspond to decreasing or increasing a parameter, respectively. Responses of the standard head model (table 2.1) are $T_{\text{skin}} = 19.2$ and $\phi_w = 0.27$.

I.	d (mm)		T_{skin} (°C)		ϕ_w (–)	
	$\bigtriangledown$	$\bigtriangleup$	$\bigtriangledown$	$\bigtriangleup$	$\bigtriangledown$	$\bigtriangleup$
brain	85.0	93.0	19.1	19.3	0.27	0.27
skull	3.0	7.0	20.1	18.6	0.29	0.26
fat	1.0	10.0	22.5	11.5	0.35	0.15
skin	1.0	4.0	19.8	19.1	0.27	0.27
hair	0.85	4.0	9.4	25.1	0.14	0.42

II.	k ($\frac{\text{W}}{\text{m}\cdot\text{K}}$)		T_{skin} (°C)		ϕ_w (–)	
	$\bigtriangledown$	$\bigtriangleup$	$\bigtriangledown$	$\bigtriangleup$	$\bigtriangledown$	$\bigtriangleup$
brain	0.2	0.8	17.3	19.9	0.23	0.29
skull	0.5	1.5	18.7	19.8	0.24	0.28
fat	0.1	0.3	15.6	20.7	0.20	0.30
skin	0.174	0.594	17.9	19.9	0.27	0.27
hair	0.013	0.056	25.2	11.0	0.42	0.14

With the absence of perfusion in the brain, the primary heat source in the head is gone, and the minimum skin temperature reaches a value of 13.9°C. In this case, the minimum perfusion is reduced to 16%. For the skin, increased basal perfusion results in a 1.5°C higher skin temperature, and relative perfusion is increased to 30%. When the perfusion in the skin is absent, the minimum skin temperature drops a further 0.6°C, compared to the standard model.

Perfusion coefficient Q_{10} (table 2.5);

An important parameter in scalp cooling is the tissue perfusion coefficient Q_{10}, since it describes how perfusion is reduced by changes in skin temperature. The effect it has on temperature is small. This result is as expected, since the parameter study shows that reduced skin perfusion has a small effect on skin temperature. However, the influence on relative perfusion is considerable. A value of 3.0 reduces relative perfusion to 20%, while a weaker dependence with a value of 2.0 results in almost double the perfusion at 38%.

Table 2.4: Effect of changes in I. tissue basal metabolism (q_{m}) and II. tissue basal perfusion (w_{b}) on minimum skin temperature (T_{skin}) and relative perfusion (ϕ_w) during cooling. $\bigtriangledown$ and $\bigtriangleup$ correspond to decreasing or increasing a parameter, respectively. Responses of the standard head model (table 2.1) are $T_{\mathrm{skin}} = 19.2$ and $\phi_w = 0.27$.

I.	q_{m} $\left(\frac{\mathrm{W}}{\mathrm{m}^3}\right)$		T_{skin} $\left(^{\mathrm{o}}\mathrm{C}\right)$		ϕ_w $\left(-\right)$	
	$\bigtriangledown$	$\bigtriangleup$	$\bigtriangledown$	$\bigtriangleup$	$\bigtriangledown$	$\bigtriangleup$
brain	2800	14800	19.1	19.3	0.27	0.27
skull	0	630	19.2	19.2	0.27	0.27
fat	0	630	19.2	19.2	0.27	0.27
skin	0	1500	19.2	19.2	0.27	0.27
hair	—	—	—	—	—	—

II.	w_{b} $\left(\frac{\mathrm{kg}}{\mathrm{m}^3\cdot\mathrm{s}}\right)$		T_{skin} $\left(^{\mathrm{o}}\mathrm{C}\right)$		ϕ_w $\left(-\right)$	
	$\bigtriangledown$	$\bigtriangleup$	$\bigtriangledown$	$\bigtriangleup$	$\bigtriangledown$	$\bigtriangleup$
brain	0.85	18.5	13.9	20.3	0.16	0.30
skull	0	0.450	19.1	19.3	0.27	0.27
fat	0	0.4	19.1	19.3	0.27	0.27
skin	0	5.5	18.6	20.7	1.00	0.30
hair	—	—	—	—	—	—

Remaining parameters (table 2.5);

Of the remaining parameters, the temperature of the cold cap and the arterial blood temperature are most important.

A cold cap temperature between -12^{o}C and -4^{o}C results in skin temperatures of 17.6$^{\mathrm{o}}$C and 20.9$^{\mathrm{o}}$C, respectively. Corresponding perfusion values are 23% and 31%, respectively. The changes in arterial blood temperature show a change in skin temperature of 0.6$^{\mathrm{o}}$C. There is no significant effect on relative perfusion.

Ambient temperature, the heat transfer coefficient and the cooling mass flow rate through the cold cap have no significant effect on either temperature or perfusion. A reduced mass flow through the cap can have some influence on the skin temperature, but in the range studied, there is no effect on skin temperature or perfusion.

Table 2.5: Effect of changes in assorted parameters on minimum skin temperature (T_{skin}) and relative perfusion (ϕ_w) during cooling. $\bigtriangledown$ and $\bigtriangleup$ correspond with decreasing or increasing a parameter, respectively. Responses of the standard head model (table 2.1) are $T_{\text{skin}} = 19.2$ and $\phi_w = 0.27$.

		varied parameter		T_{skin} $\left(^{\text{o}}\text{C}\right)$		ϕ_w $\left(-\right)$	
		$\bigtriangledown$	$\bigtriangleup$	$\bigtriangledown$	$\bigtriangleup$	$\bigtriangledown$	$\bigtriangleup$
Q_{10}	(–)	2.0	3.0	19.6	18.9	0.38	0.20
T_{A}	($^{\text{o}}$C)	36	38	18.6	19.8	0.28	0.26
T_{cap}	($^{\text{o}}$C)	-12	$-$ 4	17.6	20.9	0.23	0.31
T_{amb}	($^{\text{o}}$C)	17	23	19.2	19.2	0.28	0.26
h	(W m^{-2} K^{-1})	2	6	19.2	19.2	0.26	0.28
$\dot{m}_{\text{cap}}$	(kg min^{-1})	1	20	20.0	19.2	0.29	0.27

2.4 Conclusion and discussion

We used Pennes' bio–heat equation to model a head and cold cap. The real 3-D geometry of head and cap was simplified by us, modelling spherical symmetry in 1-D simulations. Simulations in 2-D (Xu et al., 1999) and 3-D (Dennis et al., 2003) have shown that the temperature-depth profiles are pretty much identical in the upper-back part of the head. Our 1-D simulations should therefore give accurate results for most of the actual scalp surface being cooled by the cap. However, the problem of an irregular-fitting cap is one that needs to be addressed by a more sophisticated model.

Another simplification in the model is radiative heat transfer between the outer skin and the cap. In our model, we neglect absorption of the hair layer. It depends amongst other things on the thickness of the hair. In extremes, a thick head of hair will act as a radiation shield, reducing radiative heat transfer by a factor of 2. Calculations show that for this scenario, skin temperature and perfusion will be shifted towards a higher value ($\Delta T_{\text{skin}} \approx +1.5$ $^{\text{o}}$C, $\Delta\phi_w \approx +0.025$).

Based upon variations in both thermal properties and head geometries found in literature, temperature and blood perfusion were evaluated. The results of our numerical simulations show that uncertainty in predicted perfusion is dominated by uncertainty in the perfusion coefficient Q_{10}, which is used to model temperature dependent tissue blood flow. Our model computed that during a scalp cooling procedure, the temperature of the scalp skin is reduced from 34.5$^{\text{o}}$C to 19.2$^{\text{o}}$C. This reduction in temperature decreases tissue blood flow for the basal parameters down to 27%. Varying the perfusion coefficient in accordance with values found in lit-

erature resulted in tissue blood flow decreases ranging from 20% to 38% of basal level. Other important parameters are the thermal resistances of both the fat and hair layers. The thermal resistance can be increased by either decreasing the thermal conductivity k or by increasing tissue layer thickness. For fat layer, variations in the thermal resistance resulted in skin temperatures ranging from 11.5 to 22.5^{o}C and in relative perfusion values ranging from 15% to 35%. Variations in the thermal resistance of the hair layer yield skin temperatures ranging from 9.4 to 25.1^{o}C and in relative perfusion values ranging from 14% to 42%.

The results of the numerical study show that the thermal resistance of both the fat and hair layer are important parameters during scalp cooling. These parameters influence skin temperature and skin blood flow, the properties that are thought to control the reduction in chemotherapy induced hair loss. The dominance of the above parameters is predictable: fat and hair layer provide most of the thermal resistance between the hot brain and cold cap, with the skin located between them.

Chapter 3

An experimental study on the relationship between scalp skin temperature and blood flow*

3.1 Introduction

From the previous chapter, we know that the temperature–perfusion coefficient Q_{10} is a parameter that has a great influence on relative perfusion, although its effect on actual skin temperature is small. In literature, a wide range of values is given for this parameter. In this chapter, we investigated the dependence of local perfusion on local skin temperature during scalp cooling.

The initial response of skin blood flow to skin cooling is cutaneous vasoconstriction. Two different mechanisms are responsible for this vasoconstriction. The first mechanism is a response to whole–body skin cooling and is called reflex–mediated response. The second mechanism is a response to local skin cooling and is called

*Parts of this chapter have been submitted for publication as:
Janssen, F.E.M., Rajan, V., Steenbergen, W., Van Leeuwen, G.M.J. and Van Steenhoven, A.A. The relationship between local scalp skin temperature and cutaneous perfusion during scalp cooling. *Physiological Measurements.*

locally mediated response. These two mechanisms of skin blood flow control are not mutually exclusive; often, to maximize vasoconstriction, these mechanisms operate together during exposure to cold (Thompson et al., 2005).

The sympathetic nervous system is responsible for the regulation of various homeostatic mechanisms in the human body. The vasoconstrictor system is one of these mechanisms that is regulated by the sympathetic nervous system, with the transmitter appearing to be norepinephrine and one or more co–transmitters (Johnson et al., 2005). The exact mechanisms of the vasoconstrictor system are not yet known in detail, however. *In vitro* studies have shown that local cooling enhances the affinity of α_2–adrenoreceptors for norepinephrine, such that the cutaneous vascular smooth muscles contract (Pérgola et al., 1993). It is certain however, that the temperature of the blood vessels themselves plays an important role (Pérgola et al., 1993).

During scalp cooling, only the outermost part of the head experiences changes in temperature (see chapter 2). The depth of the effected region is approximately 2 cm, and is too small to have any significant effect on core temperature. Therefore, we investigated whether a local relationship between temperature and perfusion during scalp cooling can be established. As stated in chapter 2, this response has been described using the Q_{10} relation:

$$\phi_w \equiv \frac{w_{\mathrm{b}}}{w_{\mathrm{b},0}} = e^{\frac{(T-T_0)}{T_{\mathrm{r}}}} \tag{2.9}$$

with $T_{\mathrm{r}} = 10(\ln Q_{10})^{-1}$. However, insufficient data is available on the relationship between the local skin temperature and local cutaneous blood perfusion during scalp cooling. Existing data for the scalp skin during scalp cooling (Bülow et al., 1985) is brief and lacks statistical accuracy. Bülow et al. used a Xenon washout technique on 10 subjects to identify pre–cooling, cooling and post–cooling perfusion. During cooling, perfusion reduced to about 20% of the pre–cooling level. Unfortunately, standard deviations for pre–cooling and cooling perfusion were very high, leading to a high uncertainty in this minimum perfusion value. Also, no direct relationship between minimum perfusion and scalp skin temperature is given. Such information is essential for quantitative modelling of human heat transfer and for a better understanding of human thermoregulatory processes. Especially for a better understanding of the effects of scalp cooling, this information is of vital importance.

In this chapter, we will describe the results of an experimental investigation on the dependence of cutaneous blood flow on local scalp skin temperature during scalp cooling. For this, two experiments were performed (table 3.1). The first experiment investigated the reproducibility of the selected methods, the intra–subject variability and the inter–position variability. In the second experiment, the inter–subject variability was investigated.

Table 3.1: Experiments used to determine the optimal variables in the protocol of the final *in vitro* experiment.

Experiment	Variable obtained
1	Reproducibility
	Intra–subject variability
	Inter–position variability
2	Inter–subject variability

3.2 Experimental equipment

In order to investigate the relationship between local scalp skin temperature and cutaneous blood flow during scalp cooling, three different experimental devices are required: (1) the skin needs to be cooled in a controlled manner; (2) local skin temperature needs to be measured; (3) local perfusion needs to be measured. The choice of one method influences the possible choices of the other two methods. Our choices were made such as to establish an experimental protocol that is accurate and reproducible.

Based on several pilot experiments, a final experimental protocol was developed. Both the final and the pilot experiments made use of the same cooling technique, blood flow measurements and temperature measurements. The three experimental devices are described below.

3.2.1 Cooling the scalp

A commercially available scalp cooling system (Paxman coolers Ltd UK) was used to cool the scalp. This system consists of a temperature controlled reservoir of coolant connected to a cap made from silicon tubing. The use of this system was based on several considerations. First of all, with this cooling device it is possible to investigate a wide range of temperatures. Secondly, any contact cooling method induces pressure on the skin, which in turn may affect local blood flow. However, the pressure applied by the cooling system is relevant for scalp cooling in a clinical setting. In addition, the pressure is independent of the temperature of the cap. A third consideration is the unwanted effect of an induced rate of change in skin temperature. Without a doubt, a rate of change in temperature will have an influence on local blood flow. Unfortunately, the cooling temperature of this system cannot be set. To investigate a wide range of temperatures, we therefore decided to perform a cooling/re–warming experiment. At the beginning of each measurement, the reservoir of the scalp cooling system was at room temperature. Cooling was then turned on to allow the head to cool for 90 minutes. Afterwards, the cooling was switched

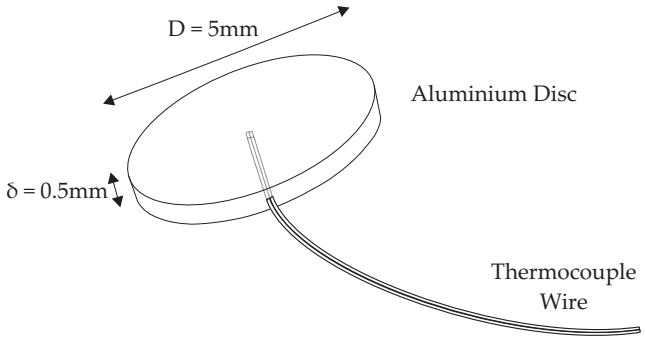

Figure 3.1: Thermocouple probe used in the experiment. A special developed shoe for the thermocouple is used to minimize measurement errors.

off to allow the head to re–warm for 60 minutes with temperature and perfusion measurement equipment still connected. This way, a quasi–stationary approach was used.

3.2.2 Temperature measurements

From chapter 2, we know that the temperature gradient between the scalp skin and the cold cap is very steep. The cold cap has a temperature of approximately -8°C, and during cooling the temperature of the skin surface is approximately 18°C. Therefore, the temperature difference between cap and skin, with a distance of only several millimetres, is very high, and this complicates temperature measurements. Care has to be taken to ensure that the measured temperature is a valid measure for the temperature of the skin.

Calibrated J type thermocouples were used in our experiments. To ensure that the registered temperature is a good measure for the skin temperature, each thermocouple end was modified with an aluminium disc of radius 2.5 mm and thickness 0.5 mm (figure 3.1). The thermocouple is attached to the skin using theatre glue with a thermal conductivity of $k = 0.15$ W m^{-1} K^{-1}. This made the attachment to the scalp skin easier and, in combination with the aluminium disc, ensured that the thermal resistance between the thermocouple and the scalp skin was much lower than the thermal resistance between the thermocouple and the cold cap. The accuracy of the developed method for temperature measurement can be estimated as follows. We assume that the thickness of the glue layer is equal to 0.1mm. We assume that the aluminium disc is homogeneous in temperature (Bi $\ll 1$). In a stationary situation, heat conduction from the skin with T_{sk} to the probe with T_{p} will be in equilibrium with radiative heat loss from the probe to the cold cap with T_{cap} and conductive heat loss to the surroundings (see figure 3.2). Convection is neglected in this calculation,

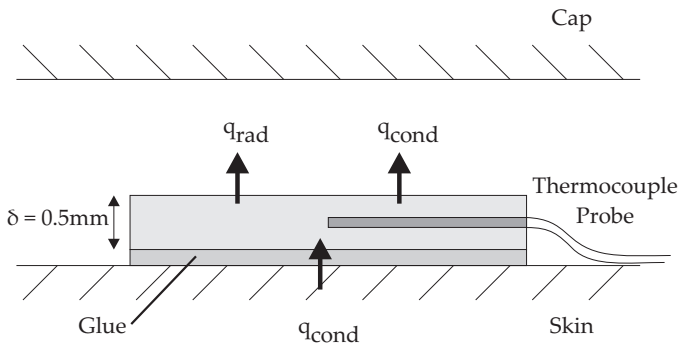

Figure 3.2: Heat balance for the thermocouple probe. The aluminium disc of the probe is connected to the skin via theatre glue. Heat loss from the probe to the surroundings is balanced by heat gained via conduction from the skin.

since the hairs between the cap and the skin will act as a barrier for this. A heat balance then states:

$$k\frac{\mathrm{d}T}{\mathrm{d}x}|_{\text{glue}} = \sigma\epsilon\Big(T_{\text{p}}^4 - T_{\text{cap}}^4\Big) + k_{\text{hair}}\frac{\mathrm{d}T}{\mathrm{d}x}|_{\text{hair}} \tag{3.1}$$

This equation can be rearranged to obtain an expression for the skin temperature as function of both the probe and cap temperature.

$$T_{\text{sk}} = T_{\text{p}} + \frac{\delta}{k}\Big[\epsilon\sigma(T_{\text{p}}^4 - T_{\text{cap}}^4) + \frac{k_{\text{hair}}}{\delta_{\text{hair}}}(T_{\text{p}} - T_{\text{cap}})\Big] \tag{3.2}$$

The emissivity coefficient for the aluminium disc of the probe is equal to $\epsilon = 0.1$ and the Stefan Boltzmann constant $\sigma = 5.669 \cdot 10^{-8}$ W m^{-2} K^{-4}. The conductivity of the hair layer is equal to $k_{\text{hair}} = 0.04$ W m^{-1} K^{-1} (see chapter 2) and the distance to the cap is equal to the thickness of the hair layer minus the thickness of the probe ($\delta_{\text{hair}} = 2.5 - 0.5 = 2$ mm). With a cap temperature of -8°C and a probe temperature of 34°C (maximum temperature difference) the actual skin temperature is equal to 34.6°C. Therefore, the systematic error in this situation is equal to 0.6°C. For a low expected skin temperature, the temperature difference between the cap and the probe is minimal (e.g. a probe temperature of 15°C), the actual skin temperature is equal to 15.4°C. Here, the systematic error is 0.4°C. In the equation for relative perfusion (equation 2.9), the temperature difference ΔT is used and thus the systematic error is largely eliminated. The difference between the maximum and the minimum systematic error is equal to 0.2°C, which is small compared to the range of temperature differences investigated. Therefore, we neglected the error as a result of measuring in a high thermal gradient.

A total of four thermocouples were used in the experiments. One thermocouple was fixed next to the perfusion probe on the scalp; another thermocouple was fixed

to the cold cap. One thermocouple measured the skin temperature at the reference site (right cheek). The last thermocouple was used to measure ambient temperature. Thermocouple measurements were taken at a sampling rate of 0.2 Hz.

3.2.3 Blood flow measurements

Until recently, non–invasive measurement of blood flow was impossible. However, with the development of lasers came novel techniques that were not possible before. One of these techniques is Laser Doppler Flowmetry.

An important property of laser radiation is its high coherence. When coherent light is scattered it produces a speckle pattern: a random intensity pattern produced by the mutual interference of coherent wavefronts with phase differences and/or intensity fluctuations. These speckles are very sensitive to temporal fluctuations in the scattering medium. Stern (1975) observed this effect in the human skin *in vivo*. He found that the speckle pattern was time dependent, with a time constant that was related to the heartbeat. This showed that the speckle variation was caused by the blood flow through the human skin. This observation showed Stern that laser light may be used as a non–invasive technique to assess the blood flow in human tissue. Ultimately, he developed an instrument with which blood flow could be measured that was based on the Doppler effect.

A Laser Doppler Flowmetry instrument consists of a light emitting part and a detector. The light emitting part sends out coherent light to the tissue. When coherent light is scattered in tissue, a part of the light will be scattered by moving red blood cells. This causes a shift in frequency Δf, called Doppler shift, which is dependent on the velocity of the moving red blood cells:

$$\Delta f = \frac{2vn}{\lambda_0} \cos\theta \tag{3.3}$$

Here, v is the velocity of the moving red blood cell, n is the refractive index of the medium, λ_0 is the wavelength of the incident light and θ is the angle between the direction of incidence and the direction of scattering.

The detector will receive a mix of both the frequency broadened light and the light scattered from static tissue. This mix will cause intensity fluctuations with Doppler frequencies. Since the light is scattered in many directions, there will be no single Doppler frequency. Instead, the detector will receive a whole spectrum. The spectral power density of the photocurrent, $S(\omega)$, can be used to relate photocurrent to blood flow. Here, the angular frequency ω is defined as $\omega = 2\pi f$.

Bonner and Nossal (1981) used the moments M_i and the weighted moments $M_{i,w}$

of the spectral power density

$$M_i = \int_a^b \omega^i S(\omega) d\omega \tag{3.4}$$

$$M_{i,w} = \frac{M_i}{M_0} \tag{3.5}$$

in which a and b are the bandwidth frequencies. Bonner and Nossal showed that the weighted first moment $M_{1,w}$ of the power density is proportional to the root–mean–square velocity of the red blood cells:

$$\sqrt{\langle v^2 \rangle} \sim M_{1,w} \tag{3.6}$$

In contrast to the weighted first moment $M_{i,w}$, the first moment M_1 is proportional to the perfusion, defined as the product of average red blood cell velocity times concentration. Currently, several Laser Doppler Flowmetry instruments are commercially available that quantify the perfusion in arbitrary units called Perfusion Units (PU). Typical measurement depth is 0.1 mm.

In our experiment, we used a commercial laser Doppler perfusion monitor with two channels (PF5000, Perimed AB, Sweden). The instrument has a semiconductor laser diode of 780 nm and a Doppler bandwidth of 20 Hz–13 kHz. The time constant of the output signals was set at 0.2 s. Perfusion measurements were taken at a sampling rate of 32 Hz.

We used two probes in the experiments (see figure 3.3). One to measure the perfusion of the cooled location, and one to monitor the perfusion at a reference location (right cheek). To obtain a good signal, the perfusion probe must be placed perpendicular to the skin. For the cooled location, this means that the probe needs to be positioned through the cap. This was realized by making a small incision between two adjacent tubes of the cap. This allowed for enough room to use a small straight perfusion probe (Probe 407, Perimed AB) at the cooled location. At the reference site, a standard probe (Probe 408, Perimed AB) could be used. For each probe, the distance between the illumination fibre and the detection fibre is equal to 250 micrometres, and each fibre has a core diameter of 125 μm and a numerical aperture of 0.37.

Two effects need to be accounted for when the results of the LDF instruments are interpreted. For one, it has to be noted that the perfusion obtained is expressed in perfusion units (PU), and these units are arbitrary. One has to be careful when comparing PU values from one body site directly to another, since values obtained depend highly on the vascular geometry of the site studied. Another effect is the so–called biological zero signal, that arises when skin perfusion is brought completely to a rest. Even though the physical perfusion is zero, the LDF instrument will still give a signal. The resulting signal is called the biological zero signal and it arises from Brownian motion of the macro molecules within the interstitium. It is additive to the flow signal (Kernick et al., 1999).

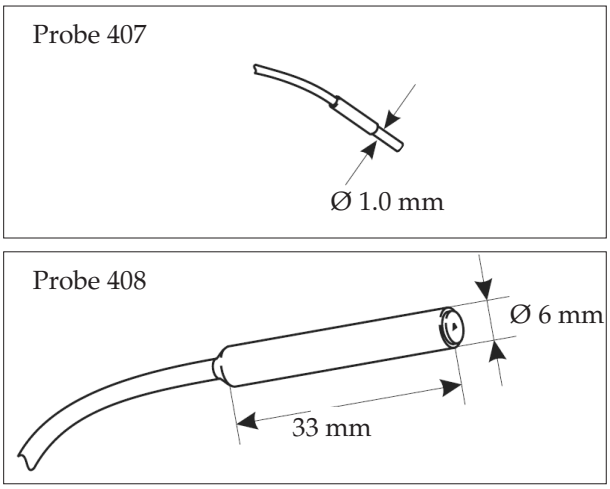

Figure 3.3: Perfusion probes used in the experiment. A small probe (407) was used to measure perfusion on the head, a standard probe (408) was used to measure perfusion at the reference location (right cheek). Figure adapted from Perimed AB, Sweden.

To correct for these two effects, we measured both the basal perfusion (w_0) and the biological zero (w_{bz}). Basal perfusion can be determined by measuring perfusion in a neutral state. The normal procedure for measuring the biological zero is to occlude the blood flow to the site that is going to be measured. Total duration of the occlusion needs to be 3 to 5 minutes (Kernick et al., 1999). This method is not suitable for measurements on the head, since it would be dangerous to the subject. Therefore, we used another procedure to find the biological zero signal to be used in corrections.

This procedure involved measurements for head and hand in 5 persons. Basal perfusion on the head (mid–front of the hairline) was measured. Subsequently, a site on the hand was sought with a similar perfusion value. At that position, another measurement was performed with the arm occluded. The average value during occlusion was taken as the biological zero signal for that person. Results are shown in table 3.2. The results show that the average basal perfusion is equal to 41.5 PU. The range in this basal perfusion is relatively high. For the persons investigated, we see that the biological zero is equal to 5.0 PU, with a standard deviation of 0.8 PU. Compared to the basal perfusion value, this standard deviation is small. Since we are not able to measure the biological zero signal directly on the head, we used the mean biological zero signal over the subjects as the biological zero signal for all measurements. Due to the difference in measurement location a systematic error in the value used is possible but this error cannot be estimated.

Using the basal perfusion (unique for each measurement) and biological zero

Table 3.2: Determination of the biological zero signal. Values are given as mean ± standard deviation.

Subject	w_0 (PU)	w_{bz} (PU)
1	34.4 ± 5	5.4 ± 0.5
2	52.7 ± 8	4.6 ± 1.6
3	34.5 ± 5	5.4 ± 0.4
4	39.7 ± 8	5.0 ± 0.7
5	46.2 ± 7	4.6 ± 0.8
mean	41.5 ± 7	5.0 ± 0.8

(same for all measurements), we define relative perfusion (ϕ_w) as:

$$\phi_w = \frac{w - \overline{w_{\text{bz}}}}{w_0 - \overline{w_{\text{bz}}}} \tag{3.7}$$

Using this transformation, the biological zero signal is accounted for and it is possible to compare individual measurements and positions to each other.

3.3 Intra–subject and inter–position variability

In our experiments, we wanted to establish a relationship between temperature and perfusion that is valid for a population. However, before experiments could be conducted to investigate the inter–subject variability, it was necessary to test whether the protocol used was reproducible. For this, we investigated the intra–subject and the inter–position variability in a pilot experiment. In this pilot experiment, a series of measurements were conducted on a single person, using two different positions.

The position where the relationship between temperature and perfusion is determined, may affect the outcome. In a preliminary experiment, we measured the temperature on the head during scalp cooling using 3 thermocouples that were positioned to the left, the centre, and the right. A pre–cooled gel cap (which is not continuously cooled) with an initial temperature of -25°C was placed on the head for approximately 20 minutes, after which the cap was removed. The results of this experiment are shown in figure 3.4. In this figure, the average temperatures of the three sites are shown. It can be seen that the temperature at the centre of the head is lowest and reaches a minimum value of 20°C after approximately 10 minutes, after which the head begins to re–warm again. The left and right sites are not cooled that far. Here, skin temperatures reach a lowest value of 25.5–27°C. Most probably, these

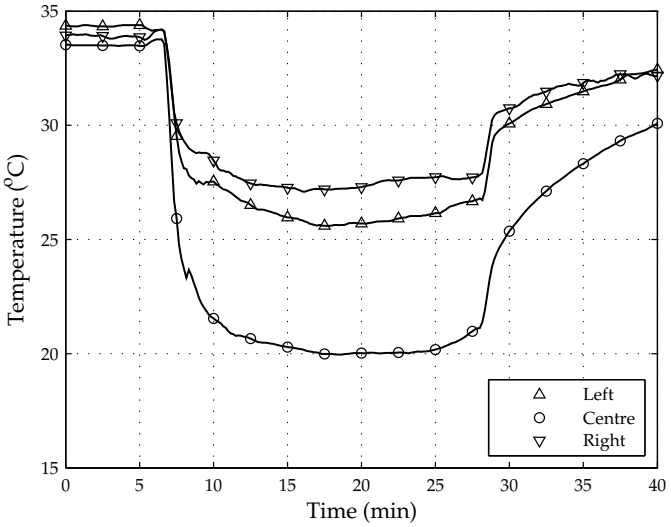

Figure 3.4: Temperature as a function of time for different positions on the head during a preliminary cooling / re–warming experiment.

higher temperatures are caused by a reduced contact between the cap and the skin. As shown in chapter 2, a small increase in the distance between the cap and the skin can lead to higher temperatures. For instance, our numerical model showed that increasing the hair layer by only 1.5 mm, resulted in a skin temperature of 25.2°C, compared to a skin temperature of 19.2°C in the standard model. The coolest and warmest position from this experiment were used to investigate the inter–position variability of the relationship between temperature and perfusion

3.3.1 Experimental protocol

The inter–experiment and inter–position variability was investigated on a single subject (male, age 26). A total of two positions were regarded (see figure 3.5), the first being the mid–front of the hairline (referred to as position 1) and the second being the top–right position of the hair–line (referred to as position 2). For each probe position, three measurements were performed.

Measurements were taken with intervals of 24 hours. Before each experiment, the laser Doppler instrument was allowed to warm up for 20 minutes. The device in combination with the two probes was calibrated using a motility standard (PF 1000, Perimed AB).

All measurements were conducted with the subject sitting upright in an environment with an ambient temperature of approximately 20°C. The subject was allowed to rest for 30 minutes before measurements to obtain a stable perfusion level. During

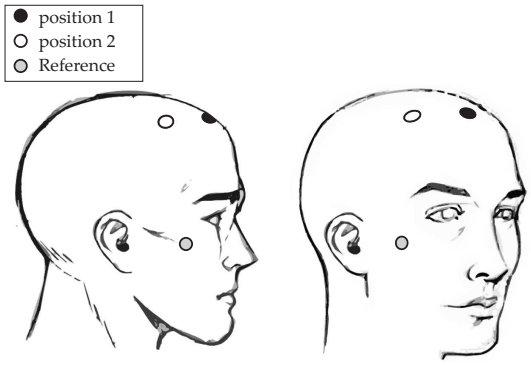

Figure 3.5: Measurement positions.

Table 3.3: Different stages during the cooling / re–warming experiment to determine the relationship between scalp skin temperature and cutaneous perfusion.

Stage	Description
1	Start the pump of the cooling system (without cooling) and measure basal perfusion (w_0) and basal temperature (T_0).
2	Turn on the cooling of the system and cool for 90 minutes.
3	Turn off the cooling system and let the head re–warm for 60 minutes.

this period, all thermocouples and perfusion probes were attached to their correct position, and the cap was placed on the head. During two minutes before the start of the cooling, temperature and perfusion of the scalp skin were measured to establish basal temperature (T_0) and basal perfusion (w_0). These basal values were used to define the temperature difference (ΔT):

$$\Delta T = T_0 - T \tag{3.8}$$

and relative perfusion (ϕ_w) according to equation 3.7. These parameters are used to compare individual measurements to each other. For the biological zero signal (w_{bz}), a value of 5 PU was used, as taken from a pilot experiment.

Each cooling/re–warming experiment consisted of three stages (table 3.3). In the first stage the pump of the scalp cooling system is switched on without cooling the reservoir. This induced both pressure changes and small temperature changes in the cap. At the start of the second stage, the cooling of the device was finally switched on. This resulted in a rate of scalp cooling that was slower than in clinical use (where

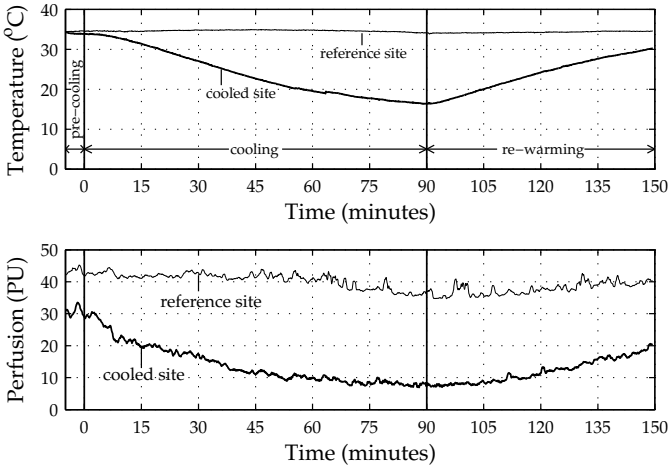

Figure 3.6: Typical time trace for temperature (top) and perfusion (bottom) of both the reference and the cooling site.

the cap and reservoir are pre–cooled). This second stage lasted 90 minutes. In the final phase, the cooler of the system was switched off to enable the scalp to re–warm. Once again, the pump of the system remained pumping to avoid pressure changes on the skin. Comparing stages 2 and 3 made it possible to see if there are hysteresis effects in the relationship between temperature and perfusion. The re–warming phase lasted 60 minutes. Skin temperature and perfusion were continuously monitored during the experiment.

3.3.2 Results

In a pilot experiment, we performed a total of 6 cooling / re–warming experiments on a single person. A typical time trace for temperature is shown in the upper panel of figure 3.6. In this measurement, skin temperature drops from 34°C to 16°C in 90 minutes. With this, the cooling rate is equal to 0.2°C min^{-1}. During re–warming, temperature increases from this 16°C to slightly above 30°C in a total of 60 minutes. The duration of this period is too short for the person to return to the basal temperature T_0, but at the end of this period the re–warming rate tends to decrease to a very low value. Therefore, and to limit the burden on subject and operators, we decided to use a re–warming stage that lasts 60 minutes. The re–warming rate can be calculated to be equal to 0.23°C min^{-1}. With this, the absolute values of the cooling and re–warming rates are of the same order.

The lower panel of figure 3.6 shows the (uncorrected) perfusion signal during the measurement. Cutaneous blood flow drops from 30 PU (perfusion units) to 8 PU. During the re–warming stage, perfusion returns to 20 PU.

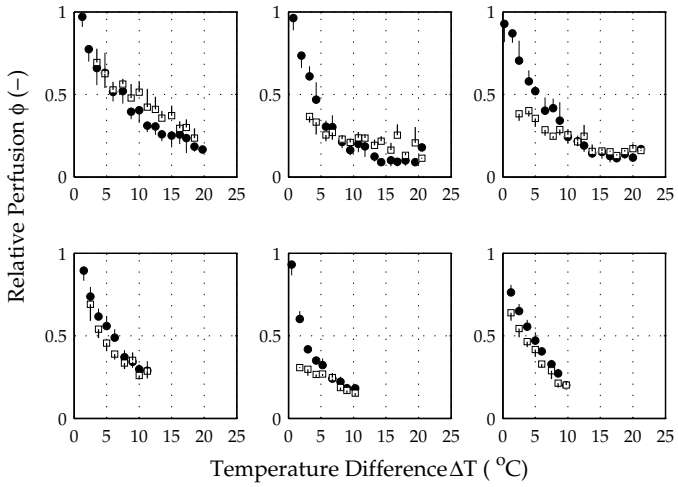

Figure 3.7: Average temperature difference and perfusion of a single subject for 6 measurements. The first three measurements (top three figures) correspond to measurements on position 1, the last three experiments (bottom three figures) are the response at the second position. (•) measurements obtained during cooling; (□) measurements obtained during re–warming. Error bars represent standard deviation of each measurement.

As can be seen in figure 3.6, the reference temperature signal is constant during the experiment. However, there is some effect of cooling visible in the perfusion signal, although the effect is small compared to the variations in perfusion for the cooled site.

In figure 3.7 the results of all measurements are shown. The top three measurements correspond to the first position, the three measurements at the bottom show the results of the second position. Each measurement shows the average relative perfusion (ϕ_w) during cooling and re–warming versus the temperature difference (ΔT).

Temperature is reduced more in the central position ($\Delta T = 20^{\circ}$C), compared to the lateral position ($\Delta T = 10^{\circ}$C). Most probably, this is the result of a tighter fit at position one. Here the cap has very good contact with the skin, as opposed to the second position, where the rigidness of the cap prevents a good fit.

There is a difference between the cooling and re–warming stage. This effect might be explained by a different reaction of the body to cooling or re–warming. The effect is small, however, and without consistent direction. Sometimes, perfusion during re–warming is higher than that in the cooling stage, and sometimes it is the other way round. What is almost consistently seen is that perfusion does not seem to return to its base value when the temperature goes back to its starting point.

The difference between individual measurements is more difficult to assess. For

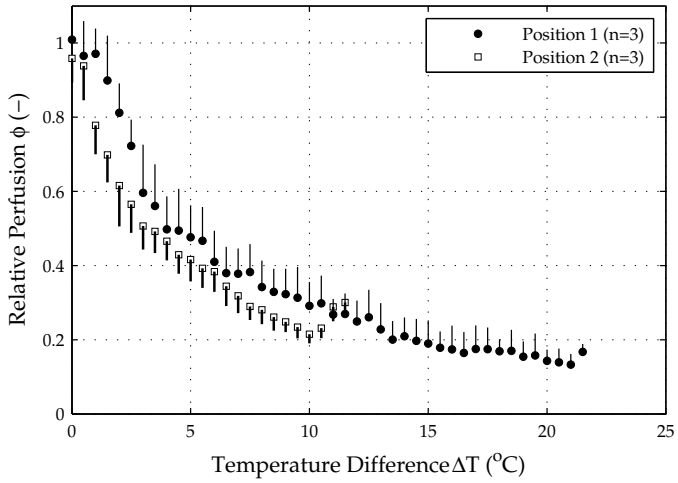

Figure 3.8: Average temperature difference and perfusion of three measurements for position 1 and position 2. (•) measurements obtained during cooling; (□) measurements obtained during re–warming. Error bars represent standard deviation of each measurement.

each position, however, it seems like the same characteristics show up: the amount of cooling applied, the value of reduced perfusion during cooling and the trajectory between an uncooled state and a cooled state are roughly the same for repeated experiments for the same location. Based on this, we expect that a single measurement for a subject gives a representative response of perfusion to cooling for a particular site. Moreover, the inter–measurement variability in perfusion (three experiments) has an average standard deviation of 0.08. In our view, considering the range of ϕ_w is from 0.18 to 1.0, and since we obtain many T, ϕ_w points per experiment, this value is usable.

We averaged the three measurements of each position to obtain a single response for each position (figure 3.8). We also investigated the effect of the two positions on the response. An analysis of variance (ANOVA) was performed using statistical software (SPSS version 15.0, SPSS inc.), using a general linear model. The influence of position is modelled as:

$$\phi_w = \mu + \alpha T + \beta X \begin{cases} X = \ 1, \text{ for position 1} \\ \\ X = -1, \text{ for position 2} \end{cases} + \epsilon \tag{3.9}$$

Here, the error ϵ is assumed to be normally distributed. The model investigates whether the position is significantly relevant for describing our data. A significance level of $p < 0.05$ was used in these statistical tests. The results of the ANOVA analysis show that there is a significant difference between the two positions in the relationship between temperature and perfusion [F(1,712) = 65.737, p<0.001]. The effect

size (η_p^2) is defined as the proportion of the effect variance to the sum of the effect variance and the error variance.

$$\eta_p^2 = SS_{factor}/(SS_{factor} + SS_{error}) \tag{3.10}$$

The effect size of position was $\eta_p^2 = 0.09$, which means that 9% of the variance can be explained by including position in the model. This value is considered to be a moderate effect.

3.4 Inter–individual variability

3.4.1 Subjects

Experiments were performed on nine healthy subjects (7 male, 2 female; age 24-43) after informed consent. Subjects were not screened for any cardiovascular or neurological disorder. Based on the outcomes of the previous section, we used only one position in our inter–individual experiment. This position was position 1, where the greatest effect was found in our inter–position experiment. For each subject, we performed a single measurement. Both the cooling and re–warming stage were measured.

3.4.2 Experimental protocol

The experimental protocol is the same as described earlier for the intra–individual experiment. Here a short overview of the protocol will be given.

Measurements were conducted with subjects sitting in an upright position. Ambient temperature was approximately 20°C. Subjects were subdued to a resting period of 30 minutes to allow perfusion to come to a stable level. At the start of each experiment, basal temperature and basal perfusion of the scalp skin were measured.

The experiment consisted of three stages: (1) a pre–cooling stage, (2) a cooling stage and (3) a re–warming stage (see table 3.3). In the first stage, the cap is applied to the head. In the second stage the head was cooled for 90 minutes. Then, the re–warming stage began, which lasted for 60 minutes. Skin temperature and perfusion were continuously monitored during the experiment.

3.4.3 Results

We investigated the relationship between skin perfusion and skin temperature on nine subjects. For cooling, a scalp cooling device was used, and perfusion and temperature were continuously monitored using Laser Doppler Flowmetry probes and thermocouples, respectively.

The results for each individual are shown in figure 3.9. For each subject, the

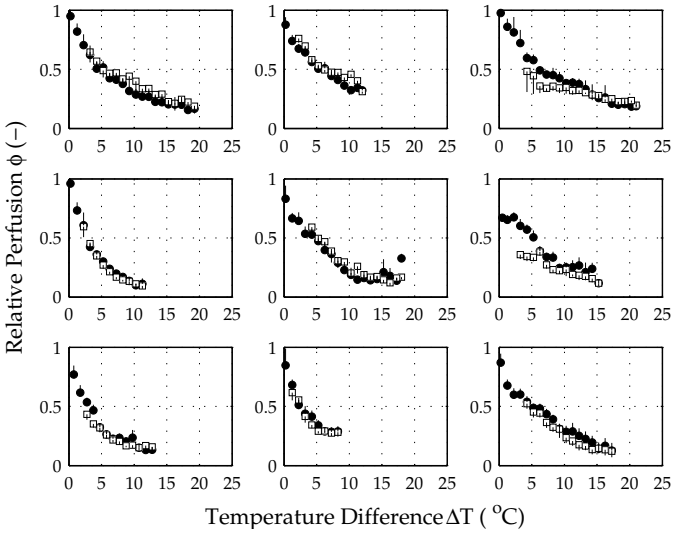

Figure 3.9: Average temperature difference and perfusion of each individual subject. Error bars represent standard deviation.

relationship between temperature difference and relative perfusion shows a smooth curve. Relative perfusion starts at a value of 1.0 and gradually reduces to a lower value for increased temperature differences. For one person, however, perfusion did not start at a value of 1, but instead at a value of approximately 0.7 (mid–right panel in figure 3.9). There are no clear differences between the cooling and re–warming stage, although in the re–warming stage the temperature–perfusion graph does not return to the starting point of the experiment ($\Delta T = 0$, $\phi_w = 1$). This is due to the fact that we used a re–warming time of 60 minutes, as opposed to a cooling stage that lasted 90 minutes. However, the perfusion during the re–warming stage roughly equals the perfusion during cooling. The achieved temperature difference for the nine subjects ranged from 7°C to 22°C. Lowest relative perfusion for the nine subjects ranged from 21% to 44%. The results indicate that inter–subject variability is high.

For each individual subject, we fitted the data to the Q_{10} relation (equation 2.9). Another Q_{10} fit was made to the averaged data of all 9 subjects. The results are shown in table 3.4. We can see that a large variation exists in the fitted Q_{10} value for each individual. Minimum Q_{10} value is 2.6, and the maximum value is 10. The mean value of the 9 individual fits is 5.2, with a standard deviation of 3.0. The fit on the average data shows a Q_{10} value of 3.6 with an R–squared value of 0.86. The average fit and the range in the individual fits is higher than was expected based on literature, where values for Q_{10} range from 2 to 3. We experienced that a good fit to the Q_{10} equation is impossible due to the observed behaviour in our experiments

Table 3.4: Results of the individual fits of 9 subjects to the Q_{10} relation. The average Q_{10} value is based on a fit on the averaged data of the 9 individual responses.

Subject	1	2	3	4	5	6	7	8	9	average
Q_{10}	3.0	2.9	2.6	10	4.0	4.8	8.6	9.1	3.7	3.6
R^2	0.84	0.80	0.78	0.96	0.88	0.73	0.89	0.79	0.87	0.86

Table 3.5: Results of the individual fits of 9 subjects to the minimum perfusion criterium ($\phi_{\min}$). The average $\phi_{\min}$ and Θ values are based on a fit on the averaged data of the 9 individual responses.

Subject	1	2	3	4	5	6	7	8	9	average
$\phi_{\min}$	0.15	0.29	0.20	0.05	0.09	0.17	0.14	0.26	0.10	0.18
Θ	6.3	4.8	5.9	3.7	5.6	3.8	3.0	2.0	5.9	4.3
R^2	0.88	0.86	0.84	0.96	0.89	0.81	0.94	0.92	0.89	0.98

that perfusion levels off at a value larger than zero instead of continuing towards zero. This is something that the Q_{10} equation does not describe.

To provide a better description of our data, we introduced a new equation for relative perfusion as a function of temperature difference. As described in chapter 1, Bülow et al. found that perfusion during scalp cooling decreases exponentially to a minimum value of about 20%. This observation can be described as:

$$\phi_w = \phi_{\min} + \big(1 - \phi_{\min}\big) e^{\left(-\frac{\Delta T}{\Theta}\right)} \tag{3.11}$$

where $\phi_{\min}$ is the minimum relative perfusion value, and Θ is a constant that determines the rate at which perfusion drops with temperature. This equation was fitted for each individual. The results are shown in table 3.5. In the table, we can see that individual differences exist in fitted values for the minimum perfusion equation. The lowest fit for $\phi_{\min}$ is 0.05, whilst the highest fit is equal to $\phi_{\min} = 0.26$. The average value of the 9 persons is $\phi_{\min} = 0.16$, with a standard deviation of 0.07. The fit based on the average response of all the 9 individuals shows a minimum perfusion value of 0.18.

The rate of response is defined by Θ. The individual fits show a range in Θ of 2 to 6.3°C. The mean value is 4.5°C, with a standard deviation of 1.4°C. The fit on the averaged data shows a value of 4.3°C. The value of Θ defines how quickly the minimum perfusion value is reached. When the temperature difference reaches a value of 3Θ, 95% of the maximal drop in perfusion is reached. This means that the minimum perfusion value in our experiment is reached for $\Delta T \approx 12$°C, with

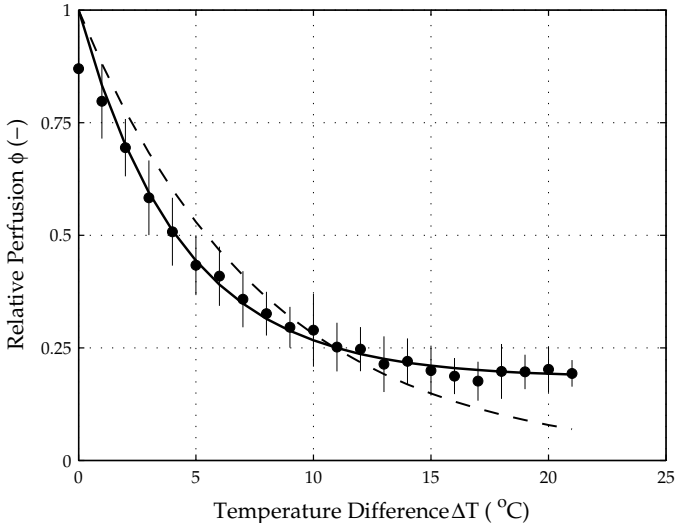

Figure 3.10: Average temperature difference and perfusion and best fits for minimum perfusion, $\phi_{\min}$(—) and Q_{10} (- -). Error bars represent standard error.

extremes of $\Delta T = 6$°C and $\Delta T = 19$°C, for $\Theta = 2$°C and $\Theta = 6.3$°C, respectively. This indicates that the variations between individuals are large.

The minimum perfusion function introduced above provides a much better fit than the Q_{10} equation. The coefficient of determination (R^2) of all subjects is higher for the minimum perfusion function than for the Q_{10} equation (see tables 3.4 and 3.5). Therefore, we decided to use the minimum perfusion function in our final scalp cooling model (chapter 6).

The average response over the nine individuals was calculated. In this response, no distinction was made between the cooling and re–warming stage. The response is shown in figure 3.10. The averaged measured perfusion starts at a value of approximately 0.87, and gradually continues with increasing temperature difference towards a minimum value of approximately 0.2. The cause why perfusion does not start at unity, is that for one person, perfusion was immediately reduced to approximately 0.70 (see figure 3.9, mid–right panel). This lowers the perfusion in the first section slightly. In the figure, to the right a plateau is reached for a temperature difference of approximately 14°C. The same figure also shows the best fits using the Q_{10} equation and using the minimum perfusion equation. The dashed line shows the Q_{10} equation, whilst the solid line shows the minimum perfusion equation. From this figure it is clear why the coefficient of determination is relatively low for the Q_{10} equation. A good fit is impossible due to the fact that perfusion reaches a minimum value during cooling. Hence the fit function for Q_{10} underestimates relative perfusion for strong cooling, while overestimating perfusion for low and mild cooling.

The minimum perfusion function with $\phi_{\min} = 0.18$ and $\Theta = 4.3$ describes the data well. This function gives a much better fit to the data over the entire cooling range than Q_{10}, and individual fit results are also better.

3.5 Conclusion and discussion

We have investigated the relationship between temperature and perfusion on the human scalp skin with thermocouples and Laser Doppler Perfusion probes. The single–subject repetitive experiments showed that the measurements are reproducible, and that the differences between the two different positions are small. We were not able to cool the position on the right–hand side as much as the central position. This can be attributed to better contact between the skin and the cap at the central position for this head/cap combination, since computations in chapter 2 have shown a high sensitivity of skin temperature to the gap thickness between the skin and the cap. The experiments on the nine subjects showed that cooling the scalp reduced perfusion down to 10–34%.

Re–warming resulted in a return of perfusion. In a previous study (Bülow et al., 1985), blood flow remained significantly lower than the pre–cooling level during the re–warming phase. However, in our study there were no significant differences between the cooling phase and the re–warming phase, which suggests that this kind of hysteresis effect does not play a role in this experiment.

We experienced that we were not able to cool each person to the same degree. This is probably caused by anatomical differences such as head shape and thickness of the insulating fat layer, two factors that were previously shown to have a strong influence on scalp skin temperature during scalp cooling (see chapter 2).

The data was used to establish a relationship between scalp skin temperature and cutaneous perfusion. The Q_{10} relationship, often used in literature, was not able to describe the data well. It overestimates perfusion during low and mild cooling, and underestimates perfusion during strong cooling. This is due to the fact that the Q_{10} relationship assumes that perfusion exponentially goes to zero. Our experiments indicate, however, that perfusion reaches a plateau. Instead, a minimum perfusion equation, that describes an exponential decrease with Θ = 4.3°C to a relative perfusion level of 0.18 described the data well.

The value of rate constant Θ implies that cooling beyond $\Delta T \approx 3\Theta$ = 13°C does not significantly reduce the supply of the drug to the skin any further. The effect of this will be studied using a pharmacological model in chapter 4.

Chapter 4

Physiologically based pharmacokinetic model for doxorubicin*

4.1 Introduction

To study the effect of reduced perfusion on local tissue concentrations during scalp cooling, a mass transfer model for chemotherapy was developed. Pharmacokinetics is defined as the study of the time course of a drug and its metabolite levels in different fluids, tissues, and excreta of the body, and of the mathematical relationships required to develop models to interpret such data (Chen and Gross, 1979). Pharmacokinetic models can provide basic information regarding drug distribution and resulting toxicity in the tissues. Consequently, pharmacokinetic models can be used to investigate the effect scalp cooling has on local cytostatic concentrations in the hair follicle and with this, provide a first insight into the relationship between scalp cooling and prevention of chemotherapy induced hair loss.

Pharmacokinetic models can be classified in order of increasing complexity. At the lowest level, empirical models have been used to describe time–concentration relationships by a sum of exponential terms. These models have proved to be useful for data description and interpolation, but they do not explain anything and are very poor at extrapolation due to the lack of physiological parameters. This prob-

*Parts of this chapter, together with parts of chapter 6 have been submitted for publication as:
Janssen, F.E.M., Van Leeuwen, G.M.J. and Van Steenhoven, A.A. A computational model for scalp cooling to prevent chemotherapy induced hair loss incorporating modelling of variability. *Physics in Medicine and Biology.*

lem has somewhat been resolved by using a compartmental approach, where every compartment is parameterized using a physiological interpretation. In total, 2 or 3 compartments are used in these models. Although some physiological data is present in these models, the compartments do not represent real physical spaces, and these models should be viewed as semi–mechanistic models (Aaron, 2005). This is a major difficulty of these models, since compartments, and their associated volumes and transfer rate constants have no anatomic or physiologic significance (Chen and Gross, 1979). Therefore it is very hard to predict how model properties change with changing physiology. Moreover, the choice of parameters largely depends on the specific characteristics of the drug being modelled.

At the upper level of complexity is the physiologically based pharmacokinetic model. A physiologically based pharmacokinetic model consists of several compartments, representing real organs or anatomic tissue regions in the body where the drug is distributed or metabolized. As a starting point, compartments can be subdivided into a vascular, an interstitial and an intracellular space. Use of the compartments to represent anatomical elements of the body allows inclusion of the actual blood flow rates and physiological volumes. Because of the physiologically based nature, mechanistic questions with regard to the pharmacokinetic properties, as well as the concentration–effect relationships may be studied. Physiologically based pharmacokinetic models are therefore routinely applied in chemical risk assessment and can be considered as an established methodology in toxicology (Theil et al., 2003).

For each tissue compartment in the physiologically based pharmacokinetic model, a generic tissue mass balance needs to be formulated to describe drug uptake in that particular tissue. Because of the complexities of the biological system, many assumptions are necessarily imposed, either to simplify the model or because of the paucity of data (Chen and Gross, 1979).

There are two assumptions that are commonly used in these models (Hoang, 1995). The first assumption is that distribution can be homogeneous (both on large and small scale). Therefore a lumped–parameter approach may be used, and a system of ODEs is developed for the set of sub–compartments. This assumption is usually the case for well–perfused organs, but for poorly perfused organs this is only a first–order approximation (Chen and Gross, 1979). If this assumption is not valid it is necessary to use a distributed–parameter approach, which is very complex and requires pharmacokinetic data and parameters well beyond the realm of currently available procedures (Hoang, 1995).

The second assumption is that the transport of the chemical to the organs is flow–limited. In a flow limited model, drug concentrations in the arterial blood rapidly reach equilibrium with the drug levels in the tissue space of each compartment. Instead of several sub–compartments, a single compartment to represent the tissue space may be used. For a flow–limited approach to be valid, the transport over the

capillary wall has to be relatively fast compared to both the transport of doxorubicin in the capillary, and the residence time of the blood in the capillary.

Only a few physiologically based pharmacokinetic models for doxorubicin have been developed before (Harris and Gross, 1975; Chan et al., 1975; Gustafson et al., 2002). All of these models made the assumption that drug uptake in each compartment can be described using a flow–limited model in a lumped–parameter approach. Although these assumptions may be necessary, especially when data is lacking, their validity has not been researched. With approximate properties of doxorubicin we evaluated the validity of this approach for doxorubicin and typical administration parameters/conditions, using a theoretical analysis.

In this chapter, a pharmacological model for doxorubicin during scalp cooling was developed. First of all however, we evaluated the validity of the flow–limited and lumped parameter approach for doxorubicin. To this end, we investigated the flow characteristics of the blood and doxorubicin transport in a human capillary. With this, the transport of doxorubicin over the capillary wall to the surrounding tissue was investigated. Finally, transport of doxorubicin in the tissue space was regarded. With this, estimates of the concentration profiles in the tissue were given to check the validity of both the lumped parameter approach and the flow–limited assumption. In § 4.3 a pharmacological model for doxorubicin will be described. A parameter study was performed with the model to identify important parameters in doxorubicin transport during scalp cooling.

4.2 Doxorubicin pharmacokinetics in a capillary

4.2.1 Capillary flow

We used established theory to analyse the flow characteristics in a capillary. A schematic overview of the capillary is shown in figure 4.1 and typical characteristics are shown in table 4.1. Transport in the capillary with velocity vector $\mathbf{v} = (v_r, v_\theta, v_z)$ and doxorubicin concentration C can be described in cylindrical coordinates using the dimensionless Navier–Stokes equation, with incompressibility and the dimensionless convection-diffusion equation:

$$\begin{aligned} &\mathrm{Sr}\frac{\partial \mathbf{v}}{\partial t} + (\mathbf{v}\cdot\nabla)\mathbf{v} = -\nabla p + \frac{1}{\mathrm{Re}}\nabla^2\mathbf{v} \\ &\nabla\cdot\mathbf{v} = \mathbf{0} \\ &\mathrm{Sr}\frac{\partial C}{\partial t} + (\mathbf{v}\cdot\nabla)C = \frac{1}{\mathrm{Pe}}\nabla^2 C \end{aligned} \tag{4.1}$$

In these equations, $\mathrm{Sr} = \frac{R}{\tau U}$ is the Strouhal number and $\mathrm{Pe} = \frac{UR}{D}$ the Peclet number. The Reynolds number is the ratio of inertia force to viscous force and is defined as:

$$\mathrm{Re} = \frac{UR}{\nu} \tag{4.2}$$

Table 4.1: Characteristics of a capillary.

Property	Symbol	Value
Inside radius	R	5μm
Length	L_z	$0.1 \cdot 10^{-2}$m
Wall thickness	t_{m}	0.5μm
Blood velocity	U	$0.05 \cdot 10^{-2}$m s^{-1}
Pore fraction	ϵ	0.01
Wall pore diameter	r	4nm
Intercapillary Distance	R_{tis}	17–85μm
Womersley number	α	0.01

For a tube flow, the transition from laminar flow to turbulent flow occurs at a critical Reynolds number of $\mathrm{Re}_{\mathrm{crit}} \sim 2300$. For a capillary, the Reynolds number can be estimated using an average velocity $U = 0.05 \cdot 10^{-2}$ m s^{-1}, an average capillary diameter $R = 5$ microns and a kinematic viscosity $\nu \sim 10^{-6}$. This results in a Reynolds number $\mathrm{Re} \sim 1 \cdot 10^{-2}$, which means that the flow in the capillary is laminar. The relative importance of the instationary forces can now be calculated from:

$$\mathrm{Sr} = \frac{\alpha^2}{\mathrm{Re}} \tag{4.3}$$

Here, α is the Womersley number, which for the capillaries has a value of 0.01. This means that the Strouhal number is of the order of $\mathrm{Sr} \sim 0.01^2/0.01 = 0.01$. Therefore, instationary effects can be neglected.

The flow in the capillary needs some distance before the hydrodynamic boundary layer and the concentration boundary layer are fully developed. The hydrodynamic inlet length can be determined from the hydrodynamic boundary layer $\delta(z)$:

$$\delta(z) \sim \sqrt{\frac{\nu z}{U}} \tag{4.4}$$

At the inlet length ($z = L_{\mathrm{h}}$), the boundary layer is equal to the radius of the capillary R. Therefore, the hydrodynamic inlet length is given by (Van Steenhoven, 1993):

$$\frac{L_{\mathrm{h}}}{2R} = 0.056\mathrm{Re} \tag{4.5}$$

and this means that with the Reynolds number in the capillary ($\mathrm{Re} \sim 10^{-2}$), the inlet length is $L_{\mathrm{h}} = 0.001R$. This inlet length is very small compared to the diameter and the length of the capillary ($L_z = 0.1 \cdot 10^{-2}$ m) and we may therefore assume that the flow is fully developed in the entire capillary.

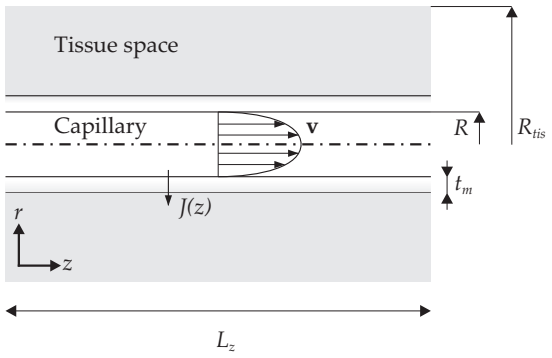

Figure 4.1: Schematic overview of the flow in a capillary. The flow moves with velocity $\mathbf{v}$ and concentration C through the capillary with radius R. The transport over the capillary wall with thickness t_m to the tissue with concentration C_T is given by the flux $J(z)$.

In order to calculate the inlet length for the concentration boundary layer, we first need the Schmidt number. It is defined as the ratio of momentum diffusivity (kinematic viscosity) to mass diffusivity and is given by:

$$\mathrm{Sc} \equiv \frac{\nu}{D} \tag{4.6}$$

with D the diffusion coefficient of the species regarded. We can estimate the diffusion coefficient of doxorubicin using the Stokes-Einstein equation:

$$D = \frac{k_\mathrm{b} T}{6\pi\mu a} \tag{4.7}$$

With k_b Boltzmann's constant ($k_\mathrm{b} = 1.38 \cdot 10^{-23}$ J K^{-1} mol^{-1}, T the temperature of the medium, μ the dynamic viscosity of the medium, and a is the radius of the solute regarded. To calculate the diffusion coefficient using the Stokes-Einstein equation, a first estimate for the radius of doxorubicin is needed. We assume that the shape of doxorubicin (see figure 4.2) can be approximated by a sphere with radius:

$$a_\mathrm{DOX} = \left(\frac{3M_\mathrm{w}}{4\pi\rho N_\mathrm{A}}\right)^{1/3} \tag{4.8}$$

Here, N_A is avogadro's number ($N_\mathrm{A} = 6.022 \cdot 10^{23}$ mol^{-1}).

For doxorubicin, the molecular mass is equal to $M_\mathrm{w} = 544$ g mol^{-1}, and we assume that the density of doxorubicin is equal to that of water. The radius of doxorubicin can then be estimated as 0.60 nm, and the diffusion coefficient at 300 K in

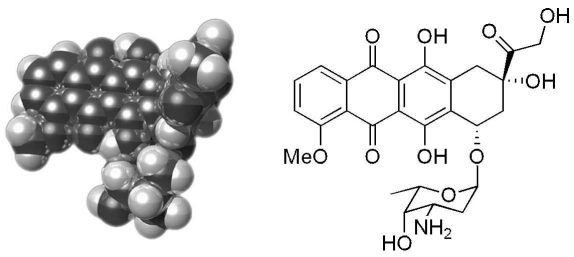

Figure 4.2: 3-Dimensional view of doxorubicin (left) and molecular structure of doxorubicin (right).

blood plasma ($\mu = 1.2 \cdot 10^{-3}$kg m^{-1} s^{-1}) is determined to be $D = 3 \cdot 10^{-10}$ m^2 s^{-1}. With this, the Schmidt number can be estimated to be $\mathrm{Sc} = 4000$.

For $\mathrm{Sc} \gg 1$, the ratio between the hydrodynamic boundary layer thickness and the concentration boundary layer thickness is given by

$$\frac{\delta_\mathrm{c}}{\delta} = \mathrm{Sc}^{-1/3} \tag{4.9}$$

which gives a ratio of 0.06 and leads to the conclusion that the concentration boundary layer develops more slowly than the hydrodynamic boundary layer. The thickness of the concentration boundary layer is given by:

$$\delta_\mathrm{c} \sim \mathrm{Sc}^{-1/3}{\mathrm{Re}_z}^{-1/2} z \tag{4.10}$$

At $z = L_\mathrm{c}$ the concentration boundary layer is fully developed and equal to $\delta_\mathrm{c}(L_\mathrm{c}) = R$, and thus the inlet length can be estimated as $L_\mathrm{c} \approx 1.5R$ which, compared to the total length of the capillary ($L_z = 200 \cdot R$), is negligible.

The above calculations show that the hydrodynamic boundary layer and the concentration boundary layer are fully developed in a capillary. This asset will be used to derive mass transfer characteristics over the capillary membrane and to calculate the concentration profile in the tissue.

4.2.2 Doxorubicin transport over the capillary membrane

Diffusion of the solute from the blood over the capillary to the tissue space (figure 4.1) is proportional to the concentration difference of the solute and is represented by an overall mass transfer coefficient (K_0):

$$J(z) = K_0\Big(C(z) - C_\mathrm{T}(z, R + t_\mathrm{m})\Big) \tag{4.11}$$

In this equation $C(z)$ and $C_\mathrm{T}(z, R + t_\mathrm{m})$ are the mixing–cup concentration in the capillary and the concentration at the outer capillary wall (tissue domain), respectively.

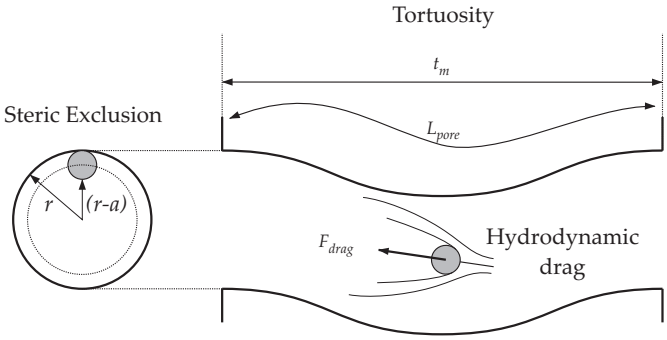

Figure 4.3: Schematic overview of the solute transport through a capillary pore and the effects of tortuosity, steric exclusion and hydrodynamic drag.

The overall mass transfer coefficient is dependent on both the mass transfer coefficient for diffusion in the capillary (h_m) and the permeability of the capillary wall for solute (P_m):

$$K_0 = \frac{1}{\frac{1}{h_\mathrm{m}} + \frac{1}{P_\mathrm{m}}} \tag{4.12}$$

The mass transfer coefficient h_m is related to the Sherwood number through:

$$\mathrm{Sh} = \frac{2h_\mathrm{m}R}{D} \tag{4.13}$$

For constant wall concentration and a fully developed flow, the Sherwood number is equal to $\mathrm{Sh} = 3.66$. The mass transfer coefficient h_m can now be calculated, and it follows that $h_\mathrm{m} \sim 2.0 \cdot 10^{-4}$ m s^{-1}.

The permeability of the capillary with wall thickness t_m is dependent on the solute and given by Fournier (1999):

$$P_\mathrm{m} = \frac{D}{t_\mathrm{m}} \left(\frac{A_\mathrm{p}}{S} \right) \left(\frac{K\omega_\mathrm{r}}{\tau} \right) \tag{4.14}$$

The permeability is a function of several properties of the capillary wall, specifically the porosity of the capillary wall (defined as the area of the pores to the total surface area of the capillary $\epsilon = \frac{A_\mathrm{p}}{S}$), the solute dependent effect of steric exclusion (K) and increase of hydrodynamic drag (ω_r), and the effect of increased path length through the membrane (tortuosity, τ). The definitions and effects of steric exclusion, hydrodynamic drag and tortuosity will be considered in more detail (see also figure 4.3).

The solute with radius a needs to be transported through small pores in the capillary. The size of these pores (radius r) is often of the same order as that of the solute.

The solute can only enter the capillary pore, if the distance of its centre to the pore edge is larger than the radius of the solute. Therefore, the effective pore area available to the solute molecule is reduced. The fraction of pore volume available to the solute is given by the following ratio: $K = \pi(r-a)^2/\pi r^2 = (1-a/r)^2$.

When the solute diffuses through the capillary pore, the flow over the surface of the solute causes hydrodynamic drag. Due to this hydrodynamic drag, diffusion through the pore is reduced. Experimental investigations have shown that this increased drag can have a considerable result on the effective diffusion. The effect of steric exclusion and increase of dynamic drag is given by the Renkin equation (Renkin, 1954):

$$K\omega_{\mathrm{r}} = \left(1-\frac{a}{r}\right)^2\left[1-2.1\left(\frac{a}{r}\right)+2.09\left(\frac{a}{r}\right)^3-0.95\left(\frac{a}{r}\right)^5\right] \tag{4.15}$$

With a/r the ratio between doxorubicin radius and the pore radius in the capillary membrane. With a pore radius of $r = 4$ nm and a doxorubicin radius of $a = 0.6$ nm, the ratio a/r is equal to 0.15, and the effect of steric exclusion and dynamic drag can be calculated as $K\omega_{\mathrm{r}} = 0.5$. Consequently, these effects reduce the effective diffusivity of the solute by 50%.

Finally, the last effect that reduces the effective diffusivity is the increased path length through the membrane, or the tortuosity. This effect comes into play because the pores in the capillary exhibit curved cylindrical geometries ($t_{\mathrm{m}} < L_{\mathrm{pore}}$). In this way, the path length that a solute needs to travel is not equal to the thickness of the membrane, but slightly higher. In our study, we assume a tortuosity of $\tau = 1.1$.

With the above, and the porosity of the capillary assumed to be $\epsilon = 0.01$, the permeability of the capillary wall can then be calculated to be equal to $P_{\mathrm{m}} = 2.8{\cdot}10^{-6}$ m s^{-1}. It can be seen that the vessel wall permeability for doxorubicin is almost 3 orders of magnitude smaller than the lumen mass transfer coefficient h_{m} and it follows that the resistance of the membrane determines the diffusion, $K_0 \approx P_{\mathrm{m}}$. The flux over the membrane is now equal to:

$$J(z) = P_{\mathrm{m}}(C(z) - C_{\mathrm{T}}(z, R+t_{\mathrm{m}})) \tag{4.16}$$

Since the flux $J(z)$ over the membrane can be determined, it is possible to analyze the mass transfer across the capillary membrane and with this, the tissue concentration can be determined.

4.2.3 Doxorubicin concentration in the tissue

In order to test the hypothesis that the tissue concentration may be regarded to be homogeneous, we used a mass balance for the capillary and the convection–equation to derive the concentration profile of doxorubicin in the tissue.

Doxorubicin transport in the tissue is governed by the diffusion equation:

$$\frac{\partial C_{\mathrm{T}}}{\partial t} = \nabla \cdot \left(D_{\mathrm{T}} \nabla C_{\mathrm{T}}\right) - M\left(C_{\mathrm{T}}\right) \tag{4.17}$$

with C_{T} the tissue concentration, D_{T} the diffusion coefficient in the tissue space and M denoting the nett effect of conversion (metabolism) of doxorubicin to harmless substances in moles per litre per second (mol l^{-1} $\mathrm{s}^{-1} \equiv \mathrm{M\ s}^{-1}$). Next, we will solve this equation in a cylindrical coordinate system for which the concentration in the tissue space is $C_{\mathrm{T}} = C_{\mathrm{T}}(r, z)$, see figure 4.1. First we will introduce dimensionless variables to identify the important parameters and to find out whether a stationary approach is valid. We introduce parameters for concentration ($C^*_{\mathrm{T}} = C_{\mathrm{T}}/C_0$), time ($t^* = t/\tau$), radius ($r^* = r/R_{\mathrm{tis}}$) and vessel length ($z^* = z/L_z$). These variables are substituted into equation 4.17, and after dividing by $D_{\mathrm{T}}C_0/R^2_{\mathrm{tis}}$ we can obtain the dimensionless diffusion equation:

$$\frac{1}{\mathrm{Fo_m}} \frac{\partial C^*_{\mathrm{T}}}{\partial t^*} = \frac{1}{r^*} \frac{\partial}{\partial r^*}\left(r^* \frac{\partial C^*_{\mathrm{T}}}{\partial r^*}\right) + \frac{R^2_{\mathrm{tis}}}{L^2_{\mathrm{c}}} \frac{\partial^2 C^*_{\mathrm{T}}}{\partial {z^*}^2} - \frac{M R^2_{\mathrm{tis}}}{C_0 D_{\mathrm{T}}} \tag{4.18}$$

in which the Fourier number for mass transfer is defined by:

$$\mathrm{Fo_m} = \frac{D_{\mathrm{T}}}{R^2_{\mathrm{tis}}}\tau \tag{4.19}$$

We will estimate a typical time scale for diffusion in the tissue cylinder using this Fourier number with $\mathrm{Fo_m} = 1$. First we need to have an estimate for R_{tis}. A typical scale for the tissue radius is given by the intercapillary distance, which is between 17 and 85 μm (Hsieh et al., 2006). The diffusion coefficient for doxorubicin in tissue (D_{T}) is a bit smaller than the diffusion coefficient of doxorubicin in blood ($D = 3 \cdot 10^{-10}$), but due to the relatively small size of doxorubicin it will still be of the same order. Therefore, we can calculate a typical time scale for the transport of doxorubicin in the tissue. With the diffusion coefficient of doxorubicin in tissue of the order of $D_{\mathrm{T}} = 1 \cdot 10^{-10}$ m^2 s^{-1} and an average intercapillary distance of $R_{\mathrm{tis}} = 50$ μm, we find for the time scale: $\tau_{\mathrm{s}} = (50 \cdot 10^{-6})^2/1 \cdot 10^{-10} = 25$ s.

We need to compare this time–scale to a relevant time scale of the boundary conditions to see whether a stationary approach is valid. Therefore, we compare this time scale to the temporal changes of the doxorubicin concentration in the arterial blood. In figure 4.4 a typical time–concentration profile is shown. During chemotherapy, arterial doxorubicin concentrations range from 10–10,000 nM. From this figure it is possible to determine the rate of change in doxorubicin concentration and to compare this with the mean concentration at that point. A typical time–scale for changes in arterial concentration is then taken to be the time that it takes for the serum concentration to change by 1%. This time–scale is defined as:

$$\tau_{\mathrm{wb}} = \frac{\overline{C}}{100}\left(\frac{\mathrm{d}C}{\mathrm{d}t}\right)^{-1} \tag{4.20}$$

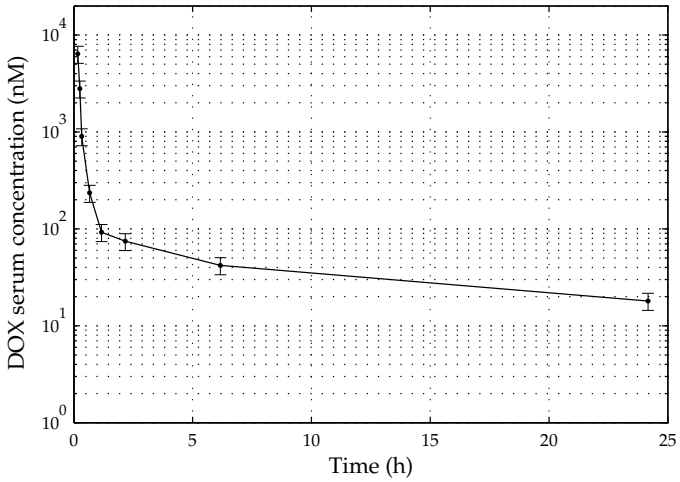

Figure 4.4: Average blood serum concentration (mean $\pm$ SD) of 24 human patients receiving a dose of 50 mg m^{-2} (Andersen et al., 1999).

A few hours after administration, the rate of change is equal to $5 \cdot 10^{-4}$ nM s^{-1} with an average concentration of 50 nM. This gives a typical time–scale of 1000 seconds. In the first two hours of the treatment, the rate of change is equal to 12nM s^{-1} and the mean concentration is equal to $\overline{C} = 6400$ nM. With this, the typical time–scale is equal to 5 seconds. During administration, the serum concentration rapidly rises from zero to a maximum level in only a few minutes. Except for the beginning of the administration, the typical time–scale is one to two orders larger than the time scale of diffusion into the tissue. Therefore, we will use a stationary approach. Furthermore, we will neglect axial diffusion since the intercapillary distance is small compared to the length of the capillary, $R_{\text{tis}}^2 \ll L_z^2$. Finally, we will assume that the metabolic term is constant: $M(C_{\text{T}}) = M_0$. With these assumptions, the diffusion equation (in dimensional form) for the tissue becomes:

$$\frac{D_{\text{T}}}{r}\frac{\partial}{\partial r}\left(r\frac{\partial C_{\text{T}}}{\partial r}\right) - M_0 = 0 \tag{4.21}$$

We solved equation 4.21 following the approach by Fournier (1999) to obtain an expression for the tissue concentration. We used as boundary conditions that the concentration at the boundary of the capillary membrane ($r = R + t_{\text{m}}$) is equal to $C_{\text{T}}|_{R+t_{\text{m}}}$ and that the radial flux at the intercapillary distance ($r = R_{\text{tis}}$) is equal to zero. Mathematically, these boundary conditions are written as:

$$\begin{aligned} C_{\text{T}} &= C_{\text{T}}|_{R+t_{\text{m}}} \qquad \text{at} \quad r = R + t_{\text{m}} \\ \frac{\partial C_{\text{T}}}{\partial r} &= 0 \qquad\qquad\quad \text{at} \quad r = R_{\text{tis}} \end{aligned}$$

The tissue concentration in the tissue space can then be solved to be:

$$C_{\mathrm{T}}(r,z) = C_{\mathrm{T}}(z)|_{R+t_{\mathrm{m}}} + \frac{M_0}{4D_{\mathrm{T}}}\left[r^2 - (R+t_{\mathrm{m}})^2\right] - \frac{M_0 R_{\mathrm{tis}}^2}{2D_{\mathrm{T}}}\ln\left(\frac{r}{R+t_{\mathrm{m}}}\right) \tag{4.22}$$

The concentration at the tissue membrane, $C(z)|_{R+t_{\mathrm{m}}}$ can be obtained by formulating the mass balance for the tissue cylinder. In steady state, the total amount of solute metabolized in the tissue is equal to the total amount of doxorubicin that enters the tissue over the capillary membrane:

$$2\pi R z P_{\mathrm{m}}\big(C(z) - C_{\mathrm{T}}(z)|_{R+t_{\mathrm{m}}}\big) = \pi\left[R_{\mathrm{tis}}^2 - (R+t_{\mathrm{m}})^2\right] z M_0 \tag{4.23}$$

which results in an expression for the tissue concentration at the capillary membrane. It is differing by a constant from the concentration in the capillary, with the latter still to be determined:

$$C_{\mathrm{T}}(z)|_{R+t_{\mathrm{m}}} = C(z) - \frac{M_0}{2RP_{\mathrm{m}}}\left[R_{\mathrm{tis}}^2 - (R+t_{\mathrm{m}})^2\right] \tag{4.24}$$

To obtain the concentration in the capillary $C(z)$, we will state another mass balance, this time for the capillary. For fully developed flow, the velocity in the capillary may be assumed to be dependent only on the radial coordinate: $v_z = v_z(r)$. Let the average velocity in the capillary be equal to U. In a stationary situation, the total solute mass entering the capillary is equal to the solute mass leaving the capillary and we may state:

$$\pi R^2 U C(z) - \pi R^2 U C(z+\Delta z) = 2\pi R \int_z^{z+\Delta z} J(z)dz \tag{4.25}$$

which may be written in differential form as:

$$-U\frac{dC}{dz} = \frac{2}{R}P_{\mathrm{m}}\Big(C(z) - C_{\mathrm{T}}(z, R+t_{\mathrm{m}})\Big) \tag{4.26}$$

With the boundary condition that at $z = 0$ the tissue concentration is equal to C_0, and the tissue concentration at the membrane given by equation 4.24, we can easily solve this equation for the concentration in the capillary:

$$C(z) = C_0 - \frac{M_0}{UR^2}\left[R_{\mathrm{tis}}^2 - (R+t_{\mathrm{m}})^2\right] z \tag{4.27}$$

Now with this, the stationary concentration profile in the tissue space can be determined as:

$$\begin{aligned} C_{\mathrm{T}}(r,z) \;=\; & C_0 - \frac{M_0}{UR^2}\left[R_{\mathrm{tis}}^2 - (R+t_{\mathrm{m}})^2\right] z - \frac{M_0}{2RP_{\mathrm{m}}}\left[R_{\mathrm{tis}}^2 - (R+t_{\mathrm{m}})^2\right] \\ & + \frac{M_0}{4D_{\mathrm{T}}}\left[r^2 - (R+t_{\mathrm{m}})^2\right] - \frac{M_0 R_{\mathrm{tis}}^2}{2D_{\mathrm{T}}}\ln\Big(\frac{r}{R+t_{\mathrm{m}}}\Big) \end{aligned} \tag{4.28}$$

Now we only need an estimate for the metabolism of doxorubicin in the tissue to assess the homogeneity of the concentration in the tissue. In a more sophisticated description, the metabolic term M is concentration dependent and can be described by either linear reaction kinetics, or saturable reaction kinetics. The latter is usually described by a Michaelis–Menten equation:

$$M = \frac{V_{\text{max}} C_{\text{T}}}{K_{\text{M}} + C_{\text{T}}} \tag{4.29}$$

When $C_{\text{T}} \ll K_{\text{M}}$, then $M = \frac{V_{\text{max}}}{K_{\text{M}}} C_{\text{T}}$ and metabolism exhibits a linear behaviour in C_{T}. For liver, where metabolism is naturally high, $V_{\text{max}} = 1.8$ mmol h^{-1} kg tissue^{-1} and $K_{\text{M}} = 275$ μM. With a tissue density of approximately 1 kg per litre, the value of V_{max} is about 0.50 μM s^{-1}. Since the arterial concentration is in the range of 10–100nM, we will assume that tissue concentrations are in the same range. Therefore, tissue concentrations are much lower than the Michaelis constant and in that case the metabolic term is is in good approximation $\frac{V_{\text{max}}}{K_{\text{M}}} C_{\text{T}}$, which is equal to 0.18 nM s^{-1} for a tissue concentration of 100 nM. We can now use this value to evaluate the doxorubicin concentrations and gradients in the tissue. Since the metabolism for the liver is naturally high, we may view this calculation as a *worst–case* scenario.

We numerically evaluated equation 4.28 for the situations of high arterial concentration. In this situation, an arterial concentration of $C_0 = 100$ nM and an initial metabolism of 0.18 nM s^{-1} was used. Values for other parameters (including tissue geometry) are taken as described earlier. The distribution of doxorubicin was then calculated and the mean concentration of doxorubicin was used to adjust the metabolism in the tissue. This iterative process was repeated until the mean concentration was equal to the concentration that was used to calculate the metabolism. Calculations were repeated for the scalp skin, with metabolism set to zero. The results of these calculations are shown in figure 4.5.

We found that the average tissue space concentration for the liver equals 73 nM, with 80% of tissue having a concentration between 66nM and 80nM. Maximum and minimum concentrations are found at $(r, z) = (R, 0)$ and $(r, z) = (R_{\text{tis}}, L_z)$, respectively. Values for these concentrations are 88 nM and 59 nM, respectively. These calculations show that the variations in the tissue concentration are quite high, with a standard deviation of about 10%. In general, we expect that these variations are lower when concentration dependent metabolism is used. This way, positions where the concentration is higher than that used to calculate metabolism, will also show higher metabolism which reduces the local solute concentration. On the other hand, positions where the concentration is lower than that used to calculate metabolism, will show less metabolism which will result in higher solute concentrations. Therefore, the concentration differences will level out a bit.

There are only three organs in the human body capable of metabolizing doxorubicin, namely the liver, the kidney and the heart. This means that only these tissues

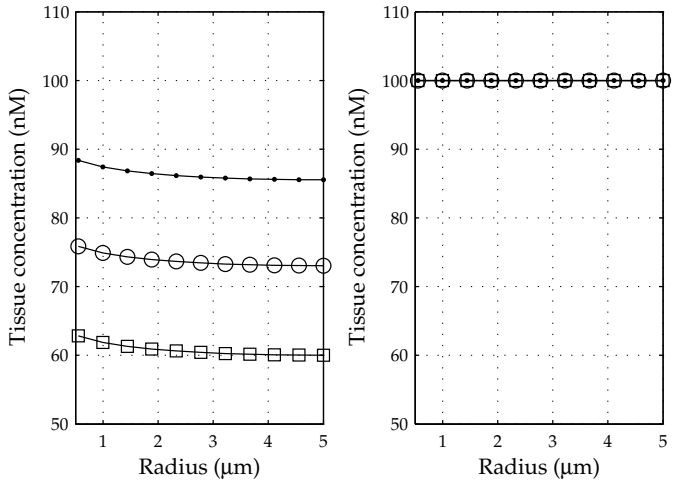

Figure 4.5: Doxorubicin concentrations in the tissue space surrounding a capillary for the liver (left) and the scalp skin (right) at different positions in the capillary. The different positions are $z = 0$ (•); $z = 0.5L_z$ (○) and $z = L_z$ (□).

will show inhomogeneities in tissue concentration. Moreover, the metabolism for the kidney and the heart is lower than that for liver, and thus these tissues will show more homogeneity. Other tissues in the human body, such as the scalp skin, cannot metabolize doxorubicin. In these tissues, doxorubicin remains intact, even when it kills a cell. Doxorubicin remains in the tissue space until the arterial concentration is lower than the tissue concentration. Calculations for the scalp skin show that the concentration in the tissue space surrounding the capillary is homogeneous, and thus the concentration in all tissues without metabolism will be homogeneous. Since the concentration in these tissues is homogeneous, and the heterogeneity in tissues with metabolism is fairly small, we will use a lumped–parameter approach in the pharmacological model.

4.2.4 Flow limited assumption

For the validity of the flow limited assumption, it is necessary that the transport of solute over the tissue membrane can keep up with the solute delivery in the capillary.

To investigate the magnitude of these two transport mechanisms we will consider a special case in which the solute concentration in the tissue space is equal to zero, $C_{\mathrm{T}}(z, R + t_{\mathrm{m}}) = 0$. Then, the flux over the capillary membrane is equal to

$$J(z) = P_{\mathrm{m}} C(z)$$

and the mass balance (equation 4.26) for the capillary becomes:

$$-U\frac{\mathrm{d}C}{\mathrm{d}z} = \frac{2P_\mathrm{m}}{R}C(z) \tag{4.30}$$

This equation can be integrated using that the concentration at $z = 0$ is equal to C_0. The result is the so called Renkin–Crone equation, describing how the solute concentration varies along the length of the capillary for the special case where the solute concentration in the tissue space is zero:

$$C(z) = C_0 \exp\left(-\frac{2P_\mathrm{m}z}{UR}\right) \tag{4.31}$$

We can now define the dimensionless extraction coefficient Φ, based on the given concentration at the inlet C_0 and the calculated concentration at the outlet $C_\mathrm{V} = C(L_z)$.

$$\Phi = \frac{C_0 - C_\mathrm{V}}{C_0} = 1 - \exp\left(-\frac{2P_\mathrm{m}L_z}{UR}\right) \tag{4.32}$$

The value of the dimensionless extraction coefficient Φ depends on the ratio of the permeability of the capillary wall $2\pi RL_zP_\mathrm{m}$ to the blood flow rate $U\pi R^2$. We can see that there are two limiting cases, namely $\Phi \downarrow 0$ and $\Phi \uparrow 1$.

For $\Phi \downarrow 0$, the concentration at the end of the capillary is more or less the same as the concentration at the inlet. Almost no mass transfer has occurred over the capillary membrane and the transport is considered to be diffusion limited. When $\Phi \uparrow 1$, the venous concentration approaches zero. All doxorubicin in the arterial blood flow is transported over the capillary membrane into the tissue space. Therefore the transfer of doxorubicin to the tissue is limited by the supply, rather than by diffusion over the capillary.

For doxorubicin, the ratio between $2P_\mathrm{m}L_z$ and UR can be calculated. With a permeability of $P_\mathrm{m} = 2.8 \cdot 10^{-6}$ m s^{-1}, a capillary length of $L_z = 0.1 \cdot 10^{-2}$ m, an average velocity of $U = 0.05 \cdot 10^{-2}$ m s^{-1} and a vessel radius of $R = 5$ microns, this ratio is approximately 2.24. With this, the dimensionless extraction coefficient is equal to 0.89 which means that almost 90% of the drug is taken up into the tissue.

The above calculation shows that at the start of doxorubicin administration, the solute transport over the capillary membrane is large enough to extract almost 90% of the total arterial concentration. This means that the doxorubicin transport in the tissue is close to being flow–limited. Still care has to be maintained when this flow–limited approach is being used for the pharmacological model, especially when concentrations following bolus administrations (i.e. step responses in the capillary inlet concentration) need to be predicted (Olsen, 2003). In that case, a more appropriate model would be a model that incorporates dispersion concepts, but this also means that information regarding doxorubicin transport is needed that currently is unavailable. Therefore, a flow–limited approach will be used as a first estimate to develop a physiologically based pharmacokinetic model for doxorubicin during scalp cooling.

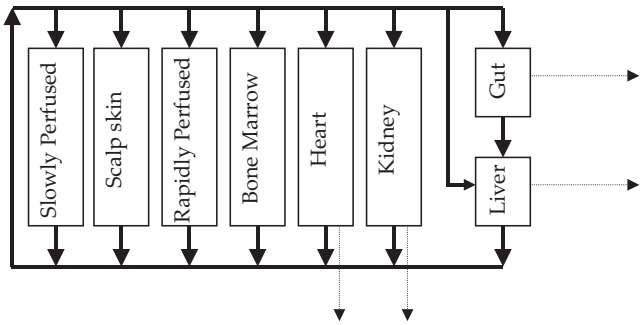

Figure 4.6: Schematic representation of the PBPK model for doxorubicin. Solid lines represent the blood circulation, dashed lines represent the metabolic and excretory pathways that eliminate doxorubicin from the body.

4.3 A physiologically based pharmacokinetic model for doxorubicin

From the previous section, we know that a flow–limited, lumped–parameter approach is a first approximation for describing the distribution of doxorubicin in the human body. A physiologically based pharmacokinetic model for doxorubicin was developed using an eight-compartment model. The model is largely based on a previous model for doxorubicin (Gustafson et al., 2002), with some modifications. A schematic of this model is shown in figure 4.6. The standard model represents a female with a body mass of 70kg and a body height of 1.67 m, which is in agreement with the mean of the Dutch female population in 2002 (CBS, 2002). For each compartment, a generic tissue mass balance for doxorubicin is formulated:

$$\frac{\mathrm{d}A_{\mathrm{T}}}{\mathrm{d}t} = W_{\mathrm{B}}\Big(C_{\mathrm{A}} - C_{\mathrm{V}}\Big) - M \tag{4.33}$$

in which A_{T} (mol) is the amount of doxorubicin in the tissue, W_{B} ($\mathrm{m}^3\ \mathrm{s}^{-1}$) is the volumetric blood flow rate through the tissue, C_{A} and C_{V} ($\mathrm{mol\ m}^{-3}$) are the arterial concentration entering the tissue and the venous concentration leaving the tissue, respectively, and M ($\mathrm{mol\ s}^{-1}$) is the rate of metabolism and/or excretion of doxorubicin in the tissue. Values for blood flow and tissue volume used in the standard model are shown in table 4.2.

Doxorubicin exhibits a strong binding to various proteins, such as cardiolipin (a specific lipid on the cell membrane) and DNA in the tissue, and plasma proteins in the blood. The concentrations of cardiolipin and DNA molecules in the tissue have been shown to correlate with doxorubicin partitioning from blood to tissues (Terasaki et al., 1982). To account for this saturable chemical-specific binding, a partitioning coefficient K_{p} was introduced by Gustafson et al. (2002), which relates the

Table 4.2: Physiological properties and doxorubicin dependent parameters used in the standard model: Tissue properties. Values for perfusion and volume are obtained from Brown et al. (1997), values for binding capacity are taken from Gustafson et al. (2002). Values are shown as mean ± standard deviation.

	W_B $\left(\frac{l}{min}\right)$	V_T (l)	T_{DNA} (μM)	T_{CAL} (μM)
Liver	0.35 ± 0.05	1.82 ± 0.28	23.7 ± 2.3	44.6
Heart	0.26 ± 0.04	0.35 ± 0.04	8.3 ± 4.0	43.8
Kidney	1.05 ± 0.08	0.28 ± 0.03	16.2 ± 2.2	52.3
Bone Marrow	0.29 ± 0.02	1.47 ± 0.14	19.1 ± 13.7	25
Gut	1.17 ± 0.11	1.19 ± 0.13	25.2 ± 2.3	25
Slowly Perfused	1.57 ± 0.15	51.2 ± 5	4.5	15
Scalp Skin	0.29 ± 0.03	2.89 ± 0.28	4.5	15
Rapidly Perfused	0.85	5.25	15	30
Blood	5.84	5.53	–	–

venous concentration to the tissue concentration.

$$C_V = \frac{1}{K_p} C_T \tag{4.34}$$

with the partitioning coefficient mathematically represented by (Leung et al., 1990):

$$K_p = \left(1 + \frac{T_{DNA}}{K_{DNA} + C_T} + \frac{T_{CAL}}{K_{CAL} + C_T}\right) \tag{4.35}$$

with T_{DNA} and T_{CAL} the DNA and cardiolipin binding capacity available and K_{DNA} and K_{CAL} the binding affinities of doxorubicin to DNA and cardiolipin, respectively (see table 4.2), and C_T the doxorubicin tissue concentration $C_T = A_T/V_T$. The affinity constants for DNA and cardiolipin are set to $K_{DNA} = 200$ nM and $K_{DNA} = 400$ nM, respectively (see table 4.3).

There are two limiting cases for the venous concentration. Either the venous concentration is equal to zero or the venous concentration is equal to the tissue concentration. When tissue concentrations are high, the value for K_p approaches a value of 1, and with this the venous concentration will be equal to the tissue concentrations. For low tissue concentrations, K_p will reach its minimum value and the venous concentration will be a factor K_p smaller than the tissue concentration.

Binding to proteins in the blood is also accounted for. It is assumed that only unbound drug concentration in the blood C_A is available for uptake in the tissue – except for the liver, where total drugs C_{BL} is available for uptake. The fraction of

Table 4.3: Physiological properties and doxorubicin dependent parameters used in the standard model: Body properties.

parameter	symbol	standard model
Body Mass[1]	m_{b}	70 kg
Height[1]	h_{b}	1.69 ± 0.2 m
BMI[1]	-	24.5 ± 1.7 kg m^{-2}
Surface Area	-	1.8 m^2
Cardiac Output[2]	W_{CO}	5.8 l min^{-1}
Dox fraction bound to blood[3]	F_{B}	0.7
Affinity constant for DNA[3]	K_{DNA}	200 nM
Affinity constant for cardiolipin[3]	K_{CAL}	400 nM
Fraction renal blood flow cleared[3]	F_{f}	0.1

[1] Based on data obtained from Statistics Netherlands (Centraal Bureau voor de Statistiek, CBS)
[2] Value obtained from Brown et al. (1997).
[3] Based on data from Gustafson et al. (2002).

doxorubicin that is bound to plasma proteins is equal to $F_{\mathrm{B}} = 0.7$ (Gustafson et al., 2002). The blood compartment mass balance may now be specified as:

$$\frac{\mathrm{d}A_{\mathrm{B}}}{\mathrm{d}t} = \sum_i W_{\mathrm{B},i} C_{\mathrm{V},i} - C_{\mathrm{A}} W_{\mathrm{CO}} - W_{\mathrm{B,L}} \Big(C_{\mathrm{BL}} - C_{\mathrm{A}} \Big) \tag{4.36}$$

with $W_{\mathrm{CO}} = \sum W_{\mathrm{B},i}$ the total cardiac output and the total arterial concentration C_{BL} and unbound arterial concentration C_{A} defined as:

$$C_{\mathrm{BL}} = \frac{A_{\mathrm{B}}}{V_{\mathrm{B}}} \tag{4.37}$$

$$C_{\mathrm{A}} = C_{\mathrm{BL}} \Big(1 - F_{\mathrm{B}} \Big) \tag{4.38}$$

In some tissues doxorubicin is metabolized to non–harmful products. In the liver, kidney and the heart, doxorubicin is metabolized to doxorubicin aglycone (AG), which can be described by a linear process:

$$M_{\mathrm{AG}} = K_{\mathrm{AG}} C_{\mathrm{T}} V_{\mathrm{T}} \tag{4.39}$$

Other metabolic processes include the metabolism by aldo–keto reductase (AKR) to doxorubicinol in the liver and the kidney, and excretion in the faeces by P–glycoprotein (PGP) in the liver and the gut. Michaelis–Menten kinetics may be used to describe these processes:

$$M_{\mathrm{AKR,PGP}} = \frac{V_{\text{max-AKR,PGP}} C_{\mathrm{T}}}{K_{\text{M-AKR,PGP}} + C_{\mathrm{T}}} \tag{4.40}$$

Table 4.4: Doxorubicin specific metabolic and excretory parameters used in the standard model. The first order rate constant K_{m} for metabolism to aglycone (AG) is expressed in $\left(\mathrm{h}^{-1}\ \mathrm{kg\ tissue}^{-1}\right)$. The activities for aldo–keto reductase (AKR) and P–glycoprotein (PGP) are expressed as K_{m} $\left(\mu\mathrm{M}\right)$ and V_{m} $\left(\mu\mathrm{mol\ h}^{-1}\ \mathrm{kg\ tissue}^{-1}\right)$.

	AG	AKR		PGP	
	K_{m}	K_{m}	V_{m}	K_{m}	V_{m}
Liver	12104	275	1804	10	300
Kidney	484	539	3161	10	100
Heart	760	–	–	–	–
Gut	–	–	–	0.2	80

Finally, excretion of doxorubicin by filtration in the urine in the kidney compartment is modelled by:

$$M_{\mathrm{f}} = F_{\mathrm{f}} W_{\mathrm{B}} C_{\mathrm{A}} \tag{4.41}$$

Values for metabolic activity that are used in the standard model are shown in table 4.4.

For each tissue compartment, a single ordinary differential equation (ODE) is obtained. The complete set of ODEs is solved using a ODE solver (MATLAB, The MathWorks).

4.4 Validation

For validation purposes, we would like to compare some results from our model to available data. Unfortunately, there is hardly any data available describing the doxorubicin concentration in time for individual organs in humans. Currently, only blood serum levels in time are available in literature. This means that the results of the model can only be compared to these blood serum levels, and that the model cannot be validated on the scale of individual organs. This puts a serious question mark, but it does not mean that the model results for organs are without merit. The concentration in the blood serum is a direct result of the distribution, metabolism and excretion of doxorubicin in individual organs, which, in a physiologically based pharmacokinetic model are based on physiological fundamentals. Therefore, when the model accurately predicts blood serum levels, it is very likely that the concentration levels in each individual organ are of the correct order. This means that the complete validated model may still be used –with some restraint– to make predictions for tissue concentrations.

Results from the complete model are compared to data from literature to gain understanding of the validity of the physiologically based pharmacokinetic model

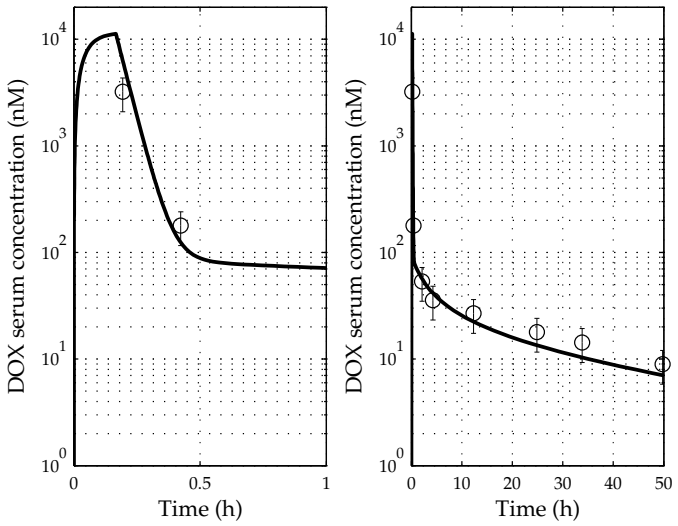

Figure 4.7: Validation of the computational model. Blood plasma concentrations obtained by the computational model (–) are compared to blood plasma concentration levels (○ , mean ± range) following the administration of six independent doses of 75 mg doxorubicin to a single individual (Jacquet et al., 1990). The left figure shows a time range of 50 hours, the right figure shows the first hour only.

for doxorubicin. For this, we have compared our model to two independent data sets describing the time course of doxorubicin levels in blood serum after a specific dose, and to characteristic pharmacokinetic properties reported in literature. Results of these validations are shown in figure 4.7 and 4.8 and table 4.5.

We compared blood serum levels from two independent studies with results from our model. The first study (Jacquet et al., 1990, figure 4.7) shows the blood plasma concentration (mean ± range) of six independent administrations of 75 mg m^{-2} doxorubicin as a 15 minute infusion to a single person. The results of our model describe the measured data well; peak concentration, first half–life time and final half–life time are predicted within the range of intra–individual variation.
The second study (Andersen et al., 1999, figure 4.8) shows the blood plasma concentration (mean ± SD) of 24 patients receiving a dose of 50 mg m^{-2} as a 10 minute infusion. Once again, peak concentration, first half–life time and final half–life time are accurately predicted by the model.

As a further validation, we compared several pharmacokinetic properties obtained from the model to data available in literature. For this, we used a modelling of variability and uncertainties approach (Nestorov, 1999), as described in more detail in chapter 6. In brief, this procedure is as follows. The available uncertainties and variations in model parameters (e.g. body weight, cardiac output) are used in a series of simulations. For each simulation, model properties are randomly assigned, based

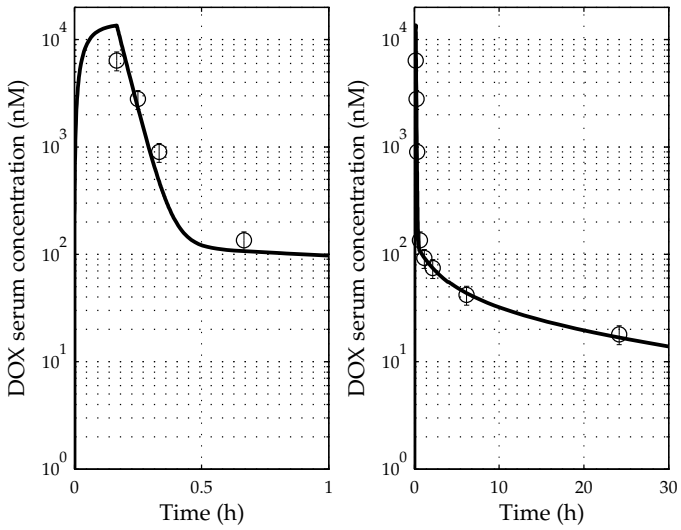

Figure 4.8: Validation of the computational model. Blood plasma concentrations obtained by the computational model (–) are compared to the average blood plasma concentration (○ , mean ± SD) of 24 patients receiving a dose of 50 mg m^{-2} (Andersen et al., 1999). The left figure shows a time range of 30 hours, the right figure shows the first hour only.

on the known variations, thus modelling a random sample from a population. For each sample, pharmacokinetic parameters are determined. In this validation, a total of 100 samples were used, and average pharmacokinetic and standard deviations were determined. In this way, the variability in the determined pharmacokinetic parameters not only reflects the uncertainties and variabilities in the model, but also the variability in the population.

The results of the pharmacokinetic analysis are shown in table 4.5. The pharmacokinetic parameters that were investigated are the first half–life time ($t_{1/2}\,\alpha$), the second half–life time ($t_{1/2}\,\beta$), the final half–life time ($t_{1/2}\,\gamma$), the area under the curve (AUC) and the clearance of doxorubicin (CL). The half–time analysis is based on the first pharmacokinetic models, that used a series of exponentials to describe the decay of blood serum levels in time. It was found that a combination of three or two exponentials, or even one exponential, was capable of describing these plasma levels. For doxorubicin, a series of three exponentials is used, with half–life times α, β and γ.

The simulated distributions of characteristics for the population are comparable to pharmacokinetic properties to those described in literature. The first half–life time is accurately predicted, while the second and third half–life time are a bit over– and underpredicted, respectively. Also the area under the curve and the clearance, as well as their standard deviations, are comparable to results from literature. There-

Table 4.5: Doxorubicin pharmacokinetic parameters in human patients and PBPK model simulations.

PK Parameters	Literature[a]	Literature[b]	Simulated Data[c]
$t_{1/2}\,\alpha$ (h)	0.034 ± 0.014	–	0.033 ± 0.009
$t_{1/2}\,\beta$ (h)	0.64 ± 0.46	–	1.7 ± 0.4
$t_{1/2}\,\gamma$ (h)	23.0 ± 5.6	28.5 ± 10.7	18 ± 2
AUC (nM x h)	63.4 ± 13.1	43.2 ± 16.2	69.4 ± 16
CL (l/h)	46.5 ± 28.5	44.5 ± 18.1	52.1 ± 16

[a] Data shows mean $\pm$ standard deviation from five patient data sets from a previously published study (Gustafson et al., 2002)
[b] Data shows mean $\pm$ standard deviation from 18 patient data sets from a previously published study (Andersen et al., 1999).
[c] Derived parameters show average $\pm$ standard deviation of 100 simulations using randomly selected physiological parameters.

fore, we assume that the model may be used for further simulations. First, we will use the standard model to study the influence of scalp cooling on local tissue concentrations in the scalp skin. Then, a parameter study will be performed with the standard model to investigate important parameters in scalp cooling.

4.5 Results

4.5.1 Standard physiologically based pharmacokinetic model

The model was used for a first investigation of the effects of scalp cooling on local scalp skin concentrations. A standard chemotherapy procedure was modelled, in which the patient receives a total dose of 75 mg m^{-2} doxorubicin, intra–venously administered in a period of 2 hours. The effect of scalp cooling was compared to no cooling. In the scalp cooling case, perfusion to the scalp skin was reduced to 20% during administration of chemotherapy and the subsequent 2 hours, for a total period of 4 hours. The results of these simulations are shown in figure 4.9. Blood serum levels are continuously high during the 2 hours of administration, after which they show a rapid fall. The concentration in the scalp skin is a little higher than the blood serum concentration and it stays relatively high for the complete simulation period. Doxorubicin concentration in the scalp is significantly lower when scalp cooling is applied, compared to no scalp cooling. After a certain period, no distinction in scalp skin concentration can be made between the two cases. When no cooling is applied, the maximum concentration in the scalp is equal to 1.66 μg ml^{-1} and the average concentration during the first 24 hours is 0.61 μg ml^{-1}. With scalp cooling, the maximum concentration is 0.48 μg ml^{-1} and the average concentration equals 0.38 μg

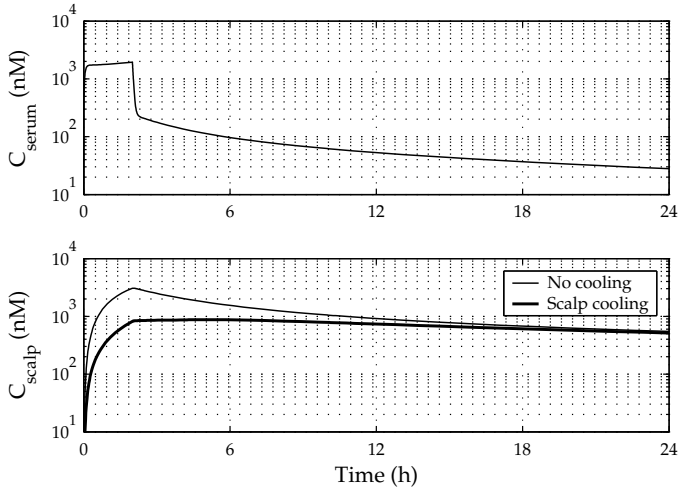

Figure 4.9: Results of the standard model showing doxorubicin serum levels C_{serum} (top) and scalp skin concentration C_{scalp} (bottom) after a 2 hour intravenous administration of a total dose of 75 mg m^{-2} doxorubicin. The bottom figure shows the effect of cooling the scalp to 19.2°C for 4 hours during administration on scalp skin concentration, compared to no cooling at all.

ml^{-1}. Thus, reducing the perfusion by a factor of 5, reduces the maximum concentration by a factor of 3.5 and the average concentration by a factor of 1.6. In toxicology, such a reduction can have a notable effect on cell survival.

4.5.2 Parameter study

In a parameter study we investigated important parameters in the physiologically based pharmacokinetic model for doxorubicin. The effect of these parameters on maximum and average scalp skin concentration during scalp cooling will be evaluated. In the simulations, we used a skin temperature of $T = 19.2$°C and a minimum perfusion value of $\phi_{\min} = 0.20$. Values used and results for tissue perfusion and tissue volume are shown in table 4.6. Changes in these parameters are compensated by changing perfusion or volume of the rapidly perfused compartment, such that cardiac output and total body volume of the model remain the same. Other varied parameters and results are shown in table 4.7. Some of these varied parameters are defined for multiple tissue compartments. To reduce the amount of data generated in this parameter study, we chose to vary all the tissue compartment values for a single parameter at once. For instance, the DNA binding capacity (T_{DNA}) is defined for all tissue compartments, but in the parameter study we varied all these values as one, using the mean plus/minus standard deviation for all tissue compartment. When the standard deviation was unknown, we used the mean value and a variation

of 20% to define the lower and upper limit.

The parameter study shows that the most important parameters influencing maximum doxorubicin concentration in the scalp skin during scalp cooling are the perfusion of both the scalp skin and the liver, the body mass, the body height and the fraction of doxorubicin bound to the blood F_{B}. Maximum modelled doxorubicin concentration is 0.56 μg ml^{-1}, for an increase in scalp skin perfusion from 0.29 to 0.35 l min^{-1}. A decrease in perfusion to 0.23 l min^{-1} results in a concentration of 0.42 μg ml^{-1}, which is the lowest peak concentration in the parameter study. This influence of perfusion was as expected, since this follows from our analysis of the concentration being flow limited.

The influence of the volume of the scalp is also high, but this result may be regarded as being slightly trivial. The concentration in a compartment is calculated as the ratio of the amount of moles in the compartment to the volume $C_{\mathrm{T}} = \frac{A_{\mathrm{T}}}{V_{\mathrm{T}}}$, and the volume is not directly used in the tissue compartment mass balance (equation 4.33). This means that a smaller volume instantly leads to a higher compartment concentration, and vice versa.

The influence on the maximum concentration is quite large, with the range in concentration being equal to 0.42–0.57 μg ml^{-1}. The influence on average doxorubicin concentration in the scalp skin is a bit lower, however, seeing that results range from 0.34 to 0.40 μg ml^{-1}.

4.6 Conclusion and discussion

In this chapter, we developed a computational model for mass transport of chemotherapy in the human body during scalp cooling. Doxorubicin is used as a chemotherapeutic agent. In the model, we used a lumped–parameter approach with the assumption that doxorubicin exhibits flow–limited characteristics. The validity of these assumptions has been assessed by investigating the mass transfer characteristics in a capillary. From these analyses, it turned out that tissue concentrations are homogeneous for tissues where doxorubicin is not metabolized. Furthermore, doxorubicin transport is almost flow limited. Therefore, a flow–limited, homogeneous approach is a valid first approximation in modelling pharmacokinetics of doxorubicin, especially when parameters for more detailed models are unknown.

Doxorubicin exhibits a strong binding to several proteins in the tissue, such as cardiolipin and DNA. Due to this strong binding, the concentration in the tissue may show inhomogeneities, especially for tissues that are not well perfused. This binding is one of the problems that limits the use of chemotherapy in the treatment of large tumours. Due to presence of large gradients, the drug is unable to reach and kill the centre of a tumour, resulting in ineffective treatment (Lankelma et al., 2000). In normal tissue however, the transport of relatively small molecules is fast. Comparisons of a pharmacological model of doxorubicin to tissue concentration data in

dogs showed that the model was able to predict these concentrations well (Gustafson et al., 2002). Therefore, the pharmacological model developed in this chapter may be used to investigate the effect of scalp cooling, especially the effect of reduced tissue perfusion, on local tissue concentrations.

One limitation of the model is that the only effect of scalp cooling that is modelled is reduced tissue perfusion. Due to cooling, mass transfer characteristics may change. In a study on the temperature dependent dermal absorption of chloroform, a large decrease in skin permeability with decreasing temperature was found (Corley et al., 1953). In our model, the effect of reduced temperature might be modelled using a temperature dependent partition coefficient K_{p} (equation 4.35). For this, however, knowledge of the temperature dependency of these coefficients for doxorubicin is needed. Currently, this data is unavailable. Therefore, any reduced uptake of doxorubicin due to reduced temperature is unaccounted for in the current model. This means that predicted tissue concentrations by the model might be higher than in reality.

The pharmacological model used eight compartments to model the human body. Although a chemotherapeutic agent is modelled, we decided not to include a compartment for a carcinoma. The volume of, and blood flow to the carcinoma is too small to have any effect on the arterial concentration.

The results of the model show that during scalp cooling, maximum tissue concentrations may be reduced by a factor of 3.5 when perfusion is reduced by a factor of 5. The average concentration was reduced by a factor of 1.6. These reductions can have a dramatic influence on cell survival, especially when an additional effect of temperature on metabolism is present. The effects of reduced concentration and reduced temperature on cell survival are studied in chapter 5.

The parameter study showed that important parameters in the model are the perfusion of both the scalp skin and the liver, the body mass and the body height. Other important parameters are the fraction of doxorubicin bound to the blood and the volume of the scalp skin. These parameters and their variability were accounted for in the population based model for scalp cooling, which will be described in chapter 6.

Table 4.6: Effect of changes in I. tissue perfusion (W_{B}) and II. tissue volume (V_{T}) on maximum scalp skin concentration ($C_{\max}$) and average scalp skin concentration $\overline{C}$ during cooling ($T = 19.2^{\circ}$C, $\phi_w = 0.27$). $\bigtriangledown$ and $\bigtriangleup$ correspond to decreasing or increasing a parameter, respectively. Responses of the standard model are $C_{\max} = 0.48\mu$g ml^{-1} and $\overline{C} = 0.38\ \mu$g ml^{-1}

I.	W_{B} $\left(\frac{\mathrm{l}}{\mathrm{min}}\right)$		$C_{\max}$ $\left(\frac{\mu\mathrm{g}}{\mathrm{ml}}\right)$		$\overline{C}$ $\left(\frac{\mu\mathrm{g}}{\mathrm{ml}}\right)$	
	$\bigtriangledown$	$\bigtriangleup$	$\bigtriangledown$	$\bigtriangleup$	$\bigtriangledown$	$\bigtriangleup$
Liver	0.25	0.45	0.52	0.45	0.40	0.35
Heart	0.18	0.34	0.49	0.47	0.38	0.37
Kidney	0.89	1.21	0.50	0.47	0.39	0.36
Bone marrow	0.25	0.33	0.48	0.48	0.38	0.38
Gut	0.95	1.37	0.51	0.46	0.39	0.36
Slowly perfused	1.27	1.87	0.50	0.47	0.37	0.38
Scalp skin	0.23	0.35	0.42	0.56	0.35	0.39

II.	V_{T} $\left(\mathrm{l}\right)$		$C_{\max}$ $\left(\frac{\mu\mathrm{g}}{\mathrm{ml}}\right)$		$\overline{C}$ $\left(\frac{\mu\mathrm{g}}{\mathrm{ml}}\right)$	
	$\bigtriangledown$	$\bigtriangleup$	$\bigtriangledown$	$\bigtriangleup$	$\bigtriangledown$	$\bigtriangleup$
Liver	1.26	2.38	0.48	0.48	0.38	0.38
Heart	0.27	0.43	0.48	0.48	0.38	0.38
Kidney	0.22	0.34	0.48	0.48	0.38	0.38
Bone marrow	1.19	1.75	0.48	0.48	0.38	0.38
Gut	0.93	1.45	0.48	0.48	0.38	0.38
Slowly perfused	41.2	56.2	0.46	0.52	0.37	0.36
Scalp skin	2.33	3.45	0.57	0.43	0.40	0.35

Table 4.7: Effect of changes in assorted parameters on maximum scalp skin concentration ($C_{\max}$) and average scalp skin concentration $\overline{C}$ during cooling ($T = 19.2^{\circ}$C, $\phi_w = 0.27$). $\bigtriangledown$ and $\bigtriangleup$ correspond to decreasing or increasing a parameter, respectively. Responses of the standard model are $C_{\max} = 0.48\ \mu$g ml^{-1} and $\overline{C} = 0.38\ \mu$g ml^{-1}.

varied parameter		limits		$C_{\max}$ $\left(\frac{\mu g}{ml}\right)$		$\overline{C}$ $\left(\frac{\mu g}{ml}\right)$	
		$\bigtriangledown$	$\bigtriangleup$	$\bigtriangledown$	$\bigtriangleup$	$\bigtriangledown$	$\bigtriangleup$
T_{DNA}[1]	(μM)	$\mu_0 - 2SD$	$\mu_0 + 2SD$	0.48	0.48	0.35	0.39
T_{CAL}[1]	(μM)	$\mu_0 - 0.2\mu_0$	$\mu_0 + 0.2\mu_0$	0.48	0.48	0.38	0.38
K_{DNA}	(nM)	100	300	0.49	0.48	0.39	0.37
K_{CAL}	(nM)	300	500	0.48	0.48	0.38	0.38
m_{b}	(kg)	60	80	0.53	0.45	0.40	0.36
h_{b}	(m)	1.49	1.89	0.51	0.46	0.39	0.37
W_{CO}	($\frac{\text{l}}{\text{min}}$)	4.8	6.8	0.49	0.48	0.40	0.36
F_{B}	(-)	0.6	0.8	0.51	0.44	0.40	0.34
F_{f}	(-)	0.05	0.15	0.48	0.48	0.38	0.38
$K_{\text{m},AG}$[1]	($\frac{1}{\text{kg h}}$)	$\mu_0 - 0.2\mu_0$	$\mu_0 + 0.2\mu_0$	0.48	0.48	0.38	0.38
$V_{\text{m},AKR}$[1]	($\frac{\mu\text{mol}}{\text{kg h}}$)	$\mu_0 - 0.2\mu_0$	$\mu_0 + 0.2\mu_0$	0.48	0.48	0.38	0.38
$K_{\text{m},AKR}$[1]	(μM)	$\mu_0 - 0.2\mu_0$	$\mu_0 + 0.2\mu_0$	0.48	0.48	0.38	0.38
$V_{\text{m},PGP}$[1]	($\frac{\mu\text{mol}}{\text{kg h}}$)	$\mu_0 - 0.2\mu_0$	$\mu_0 + 0.2\mu_0$	0.48	0.48	0.38	0.38
$K_{\text{m},PGP}$[1]	(μM)	$\mu_0 - 0.2\mu_0$	$\mu_0 + 0.2\mu_0$	0.48	0.48	0.38	0.38

[1] In the standard PBPK model, this parameter is set for multiple tissue compartments. In the parameter variation, all these tissue parameters were varied at once, using either the mean and standard deviation ($\mu_0 \pm 2SD$) or the mean with a deviation of 20% ($\mu_0 \pm 0.2\mu$) to define the lower and upper limit. Values for μ_0 are shown in table 4.2 and table 4.3.

Chapter 5

Effects of temperature and doxorubicin exposure on keratinocyte damage *in vitro*

5.1 Introduction

Scalp cooling during administration of chemotherapy prevents hair loss (e.g. Ridderheim et al., 2003). The hair preservative effect of scalp cooling is attributed both to reduced blood flow by vasoconstriction and to reduced reaction rates in the body at the level of the hair follicle.

When the scalp is cooled, vasoconstriction is induced and through this, blood flow to the hair follicle is decreased. This reduced blood flow results in a decrease of the total amount of cytotoxic drug available for uptake in the hair follicle. The effect of reduced perfusion was studied in chapter 3, and it was found that cooling the scalp to 20°C reduces local blood flow down to 20% of normal. A further decrease in temperature did not result in a further decrease in local blood flow. Based on this, it might be expected that there is a limit in temperature below which the effectiveness of scalp cooling will not increase anymore. In chapter 4, the effect of this reduction in skin blood flow on local tissue concentration was investigated. It followed that a decrease in perfusion by a factor of 5, reduced this local tissue concentration by a factor of 3.5.

However, the hair preservative effect of scalp cooling is also attributed to reduced cell metabolism. Due to reduced temperatures during scalp cooling, cellular drug uptake and damage are assumed to be lower, and with this hair follicles are thought to be less susceptible to cytotoxic drugs. Decorti et al. (2003) showed that *in vitro* doxorubicin uptake in kidney cells at 37°C was 4.5 times higher than drug uptake at 4°C. In addition, Decorti et al. also showed that doxorubicin uptake is dependent on extracellular concentration. Unfortunately, no studies have been performed to quantify these processes in the human hair follicle.

For a better understanding of the functioning of scalp cooling, it is important to quantify the contribution of reduced drug uptake and drug damage, if any, on the hair preservative effect of scalp cooling. In this chapter, we experimentally investigated the relationship between doxorubicin exposure and cell damage at different temperatures. To do this, we first needed to select a suitable experimental model for the hair follicle, that meets the following criteria. First of all, the model needs to be representative for the effect of scalp cooling on reduced hair follicle damage. Secondly, the model needs to give reproducible results. Finally, the model should allow quick and easy evaluation of a wide range of doxorubicin concentrations and doxorubicin exposure temperatures.

Ideally, one would use an *in vivo* model, since such a model is most representative for the actual situation during scalp cooling. Unfortunately, this representation of the actual situation makes the model less suitable. In an *in vivo* model, one would measure the effect of reduced drug metabolism as well as the effect of reduced perfusion. Therefore, no distinction between the effects of reduced perfusion and reduced metabolism can be made, and it would be nearly impossible to quantify the effect of reduced cell metabolism independently of reduced perfusion.

Since the early 1990's, large steps have been made towards developing an *in vitro* model for the hair follicle (Philpott et al., 1990). Hair follicles, obtained from skin samples removed during cosmetic surgery, are isolated from the skin. In this procedure, the skin samples are cut into small pieces of approximately 1 by 1 cm. Then the dermis is removed by slicing right between the dermis and the hypodermis. In the resultant sample, several hair follicles exist. These hair follicles then need to be carefully removed using tweezers, after which the hair follicle can be grown *in vitro* using special medium.

This *in vitro* hair follicle model offers new possibilities in researching hair follicle related problems (Randall et al., 2003). The *in vitro* grown hair follicle produces the same hair shaft as its *in vivo* grown counterpart (Thibaut et al., 2003), but unfortunately there are some limitations in its use. For one, it does not follow the same cycling–pattern (see chapter 1); *in vitro* hair follicles can be cultured only in an anagen (growing) phase. The time that an *in vitro* grown hair follicle remains in this phase has been extended in the recent years to about 20 days (Thibaut et al., 2003), but still this is substantially less than the 7 years that an *in vivo* hair follicle can stay

in this phase (see chapter 1).

For our experiment, there are some additional drawbacks to the *in vitro* grown hair follicle. At the moment, *in vitro* hair follicles are not commercially available, and the only way of getting these models is by isolating hair follicles from skin samples obtained through hospitals. The described technique for isolating the hair follicles is very delicate. Not all skin samples are suitable for hair follicle isolation, and not all hair follicles obtained are viable. This means that only few hair follicles acquired by this method are suitable for experiments. Therefore, using this *in vitro* model for the hair follicle requires a lot of time and effort, especially in experiments where a large range of boundary conditions need to be investigated.

As described in chapter 1, chemotherapy disrupts the rapidly dividing keratinocytes (the cells that actually produce the hair shaft) in the hair follicle (Cotsarelis and Millar, 2001). Therefore, the use of keratinocytes as an *in vitro* model is indicative for chemotherapy induced damage to the hair follicle. Moreover, human keratinocytes are commercially available and they are easy to cultivate, which means that with this model a wide range of boundary conditions can quickly be investigated. With this, all the selection criteria stated earlier in this section are met. Therefore, we used keratinocytes as an *in vitro* model in our experiments.

The goal of the experiments was to assess the effects of temperature and chemotherapy on keratinocyte survival. In order to establish a final protocol, several pilot experiments were performed.

5.2 Materials and methods

5.2.1 Experimental protocol

To assess the effects of temperature and chemotherapy on cell survival a controlled *in vitro* experiment was conducted using cultured keratinocytes. The effect of chemotherapy was investigated using the chemotherapeutic agent doxorubicin, since it causes hair loss, and this hair loss has been found to be significantly reduced by scalp cooling. We choose an *in vitro* model approach to systematically quantify the influence of temperature and doxorubicin, as well as combinations of temperature and doxorubicin on cell damage. The effects of temperature and doxorubicin on cell damage were determined from cell viability measurements.

A final *in vitro* experiment was optimized using pilot experiments. In the experiments, cells were plated at a particular density in 24–well plates, after which they were incubated for 24 hours to recover from handling. This incubation time was chosen based on experience with these cells. Next, a concentration of doxorubicin was added to each well and the plates were stored at a prescribed temperature. After a specific exposure time, the doxorubicin concentration was removed from each well. Plates were then incubated at 37°C and 5% CO_2 for a certain post–exposure time, to

Table 5.1: Pilot experiments used to determine the optimal variables in the protocol of the final *in vitro* experiment.

	Pilot experiment	Variable obtained
1	Investigate the linearity of the MTT assay.	Range of allowed cell plating densities.
2	Establish a growth curve.	Optimal cell plating density. Post–exposure time
3	Investigate the effect of doxorubicin exposure time.	Doxorubicin exposure time
4	Investigate the effect of doxorubicin exposure temperature.	Range of doxorubicin concentrations and range of doxorubicin exposure temperatures

allow the damage exerted by doxorubicin to be expressed. Finally, this damage was quantified using a viability test.

As stated before, pilot experiments were conducted to determine an optimal toxicity protocol for the final experiment. To this end, a total of 4 pilot experiments were conducted (table 5.1). Of course, both the pilot experiments and the final experiments made use of the same cell line and viability measurement method.

5.2.2 Cell line

Pooled neonatal Normal Human Epidermal Keratinocytes (NHEK) were obtained from Cambrex Bio Science Verviers, Belgium (catalog number CC-2507). These cells have a doubling time of approximately 24 hours. Cells were cultured in T-75 flasks at a seeding density of 3500 cells cm^{-2} under an atmosphere of 95% air and 5% CO_2 at 37°C, using 15 ml of Keratinocyte General Medium (KGM2)(Cambrex Bio Science Verviers, catalog number CC-3107). Medium was refreshed the day after plating, and afterwards every other day until cells reached 70%–80% confluence. Then cells were harvested using 6 ml of trypsin solution and subsequently cryopreserved in liquid nitrogen at a density of $1.2 \cdot 10^6$ cells ml^{-1} using 80% KGM2, 10% FBS and 10% DMSO.

For both the pilot and the final experiments, third passage cells were plated in 24–well plates, after which the plates were incubated at 37°C and 5% CO_2 for a period of time before experiments were performed. The incubation time in the final experiment was obtained from a pilot experiment.

5.2.3 Viability measurement

The damage to the NHEK cells exposed to different temperatures and doxorubicin concentrations was determined by a colorimetric MTT (tetrazolium) viability assay. The assay is based on the observation that viable cells have the ability to metabolize a water–soluble tetrazolium dye 3–(4,5–dimethylthiazol–2–yl)–2,5–diphenyl tetrazolium bromide (MTT), into a product termed purple formazan (Mosmann, 1983; Edmondson et al., 1988; Sgouras and Duncan, 1990). The purple formazan can be solubilized and the optical density of the solute can be determined by using a spectrophotometric technique. The resulting absorbance is directly proportional to the number of cells, and this linearity extends over a wide range of cell numbers (Mosmann, 1983). However, for high cell numbers, the absorbance measurement tends to saturate, meaning that the relationship between cell number and absorption is not linear anymore. The transition point is cell type dependent. Therefore, it is important to investigate what range in cell numbers may be used in the final experiment. To this end, a pilot experiment was conducted that investigated the relationship between NHEK cell seeding number and the resultant absorbance in a viability test.

First, however, the standard viability measurement protocol will be described. This protocol was used in both the pilot experiments and the final experiment and was performed as follows. A standard MTT solution was prepared by dissolving 5 mg ml^{-1} of MTT (MTT formazan, Sigma Aldrich, Zwijndrecht, The Netherlands) in PBS. The standard MTT solution was added to complete medium (KGM2) in a ratio of 1 to 10 to obtain a final solution of 10% MTT solution and 90% KGM2. A volume of 220 μl of this solution was added to all test wells and the plates were left to incubate at 37^{o}C and 5% CO_2 for a period of 45 minutes. After this period, the MTT/medium solution was removed and 200 μl of a solution of 90% DMSO and 10% Triton X was added to extract the purple formazan salt from the cells. Plates were sealed and kept in dark for 30 minutes, after which 100 μl of each well was transferred to a new well of a 96–well plate. The optical density (OD) was measured using an automated spectrophotometric plate reader (Synergy HT, BioTek Instruments Inc, USA) set to 570 nm, and using a reference wavelength of 650 nm. Blanks (100 μl of DMSO/Triton X solution only) were used as an extra control.

For each well the corrected optical density OD(570-650 nm) was provided by the plate reader. Mean optical density and standard error of each temperature and concentration group ($\mathrm{OD}_{T,C} \pm se(\mathrm{OD}_{T,C})$), and their respective control group ($\mathrm{OD}_{T,0} \pm se(\mathrm{OD}_{T,0})$) were calculated. Based on these values, the viability (S) for each temperature and concentration group can be calculated:

$$S_{T,C} = \frac{\mathrm{OD}_{T,C}}{\mathrm{OD}_{T,0}} \tag{5.1}$$

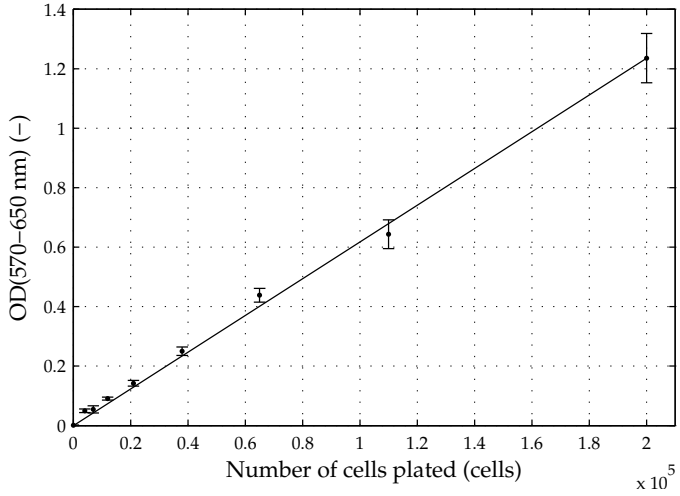

Figure 5.1: Relationship between seeding cell number and MTT absorbance signal (DO 570-650 nm). Data points show the mean value ± standard deviation of eight measurements. The line represents the best linear fit, with the intercept set to zero ($R^2 = 0.997$).

With the standard error of this variable defined as:

$$se(S_{T,C}) = S_{T,C}\sqrt{\frac{se(\mathrm{OD}_{T,0})^2}{\mathrm{OD}_{T,0}^2} + \frac{se(\mathrm{OD}_{T,C})^2}{\mathrm{OD}_{T,C}^2}} \tag{5.2}$$

5.3 Pilot experiments

5.3.1 Linearity of the MTT assay

To check the linearity of the MTT assay in combination with the NHEK cells, and subsequently to determine the optimal cell plating density, the following protocol was used. NHEK cells were plated in 24–well plates at 4000 to $2{\cdot}10^5$ cells per well. A total of 8 different seeding cell numbers were used, with 8 replicates for each number of cells. Wells with no cells were used as a control. Cells were incubated at 37°C and 5% CO_2 for a period of 24 hours to allow the cells to recover from handling. 24 hours after plating, an MTT test was performed. The results of this pilot experiment are shown in figure 5.1. In this figure, it can be seen that a linear relationship exists between the seeding cell number and the MTT absorbance at 570 nm for the entire range of cell seeding number investigated ($R^2 = 0.997$). The control sample, where no cells were plated, shows no signal, as was expected. The standard error for the method is quite low, but it increases with increasing cell number.

The relationship between the seeding cell number and the MTT absorbance is linear, but based on the higher standard deviations at high cell numbers it is preferable to remain in the lower cell seeding portion of the figure. This fact was used to derive an optimal cell plating density.

5.3.2 Optimal cell plating density

The optimal cell plating density can be derived from the linearity of the MTT assay, together with information on expected post–exposure time and cell doubling time.

The effect of doxorubicin on cells is not instantaneous and therefore a certain post–exposure incubation time in our final experiment was needed. Eliaz et al. (2004) showed that there is a large difference in viability between the immediate toxic effect and the delayed toxic effect of doxorubicin, especially for exposure times below 12 hours. When viability was determined immediately after doxorubicin exposure, no damage was visible. A few days after exposure, the effect on cell viability was clearly visible. Therefore, a post–exposure time is needed. Optimal post–exposure time was determined in a pilot–experiment, but the expected post–exposure time was 2 days.

The MTT linearity test shows that the standard deviation of the method increases with increasing cell number. Therefore, we aimed at an optical density of 0.6 (i.e. approximately 100,000 cells, see figure 5.1) for our control group in the final experiment. In this final experiment, we exposed the cells to doxorubicin 24 hours after plating to allow the cells to recover from handling. With an estimated post–exposure time of 2 days and a doubling time of 1 day, we calculated the cell seeding number to be equal to $100,000/2^3 = 12,500$ cells well^{-1}. This cell seeding number corresponds to a cell density of 6000 cells cm^{-2} and was used as a starting point in further experiments.

5.3.3 Optimal post–exposure time

The post–exposure time, which is approximately 2 days, is needed because the effect of doxorubicin on cells is not instantaneous. On the other hand, a post–exposure time that is too long will result in cell numbers that lie outside the linearity of the MTT assay (figure 5.1). Optimal post–exposure incubation time was determined in a pilot experiment. The protocol for this pilot experiment was as follows. Cells were plated in 24–well plates at a cell density of 6000 cells cm^{-2} and incubated at 37^{o}C. An MTT test was performed at day 3, 4 and 6 (8 replicates each).

The results of this test are shown in figure 5.2. Three days after plating, the MTT absorbance is still low (OD = 0.17). After four days the cells show a rapid increase in growth, with an MTT absorbance of OD = 0.62. This rapid increase in cell growth is slowed down after four days, considering a relatively low absorbance signal of OD = 0.79 six days after plating.

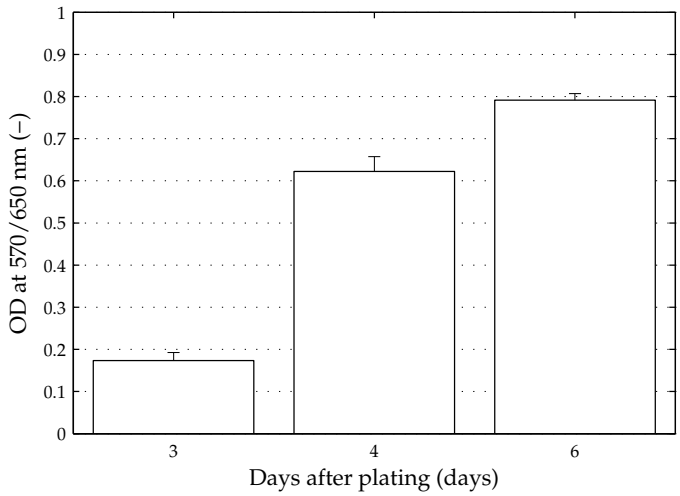

Figure 5.2: Result of a pilot experiment to determine the optimal post–exposure incubation time in the final *in vitro* experiment. An MTT test was performed at day 3, 4 and 6 after cell plating. The bars represent the mean optical density (OD) and standard deviation of 8 replicates.

The MTT absorbance measured 4 days after plating is exactly what we aimed for, based on the linearity of the MTT test and the corresponding standard deviations. Therefore, the viability test in our final experiment was performed 4 days after plating. Since we exposed the cells to doxorubicin 24 hours after plating, this means that a post–exposure time of 3 days was used. The choice of this time indicates that we will obtain a good MTT signal for the control group, and this time is large enough such that the damage exerted by doxorubicin can be measured.

5.3.4 Standard protocol for additional pilot experiments

Now that we had established optimal cell seeding density and post–exposure time, we still needed to determine some variables in the final protocol. These variables are the doxorubicin exposure time and the range in both doxorubicin concentration and doxorubicin exposure temperature. Two pilot experiments were used to establish these parameters. For these pilot experiments, a standard protocol was used as described below.

In this standard protocol, cells were plated in 24–well plates at a cell density of 6000 cells cm^{-2}. Cells were incubated at 37°C for a period of 24 hours to allow the cells to recover from handling. A wide range of concentrations of doxorubicin (Doxorubicin HydroChloride; 2 mg ml^{-1}, obtained from Pharmachemie Haarlem, The Netherlands) in complete medium (KGM2) were prepared. Each well was given a total of 250 μl of a specific doxorubicin concentration. Plates were then incubated for

a chosen exposure time at a specific temperature. For each combination of temperature and doxorubicin concentration, 8 replicates were used. Cells receiving medium without any doxorubicin were used as a control group for each temperature group. At the end of the exposure time, doxorubicin was removed and cells were washed with 500 μl PBS. Fresh medium (250 μl well^{-1}) was added and plates were then incubated at 37°C for a post–exposure time of 72 hours, after which the standard viability measurement was performed.

5.3.5 Doxorubicin exposure time

The influence of doxorubicin exposure time to doxorubicin at two different temperatures was investigated using the standard protocol. For each temperature group, two different doxorubicin exposure times were used. These two exposure times were based on the clinical situation of scalp cooling. In a clinical situation, the arterial concentration is especially high during administration of chemotherapy, and drops immediately after administration ceases (see figure 4.4). We expect that local doxorubicin concentrations in the hair follicle are proportional to the arterial concentrations and therefore we used a doxorubicin exposure time of 4 hours. However, we still needed to investigate whether significant differences exist for deviations in this doxorubicin exposure time.

In a pilot experiment, we used a high and a low doxorubicin exposure temperature. In the high temperature group (T=37°C), we used exposure times of 4 and 7 hours. In the low temperature group (T=20°C) we used exposure times of 2 hours and 6 hours. This difference in exposure times between the low temperature group and the high temperature group is due to the fact that shorter exposure times are more convenient. A standard protocol was used to determine cell viability. A two–tailed t–test was performed to check for significant differences between the exposure times at each doxorubicin concentration (significance level: $\alpha = 0.05$). The results of this pilot experiment are shown in figure 5.3. The upper panel in figure 5.3 shows the influence of a short (2 hour) and long (6 hour) exposure to doxorubicin at 20°C. The lower panel in figure 5.3 shows the effect of a short (4 hour) and long (7 hour) exposure to doxorubicin at 37°C. For both the low and the high temperature group, no significant differences between the two exposure times exist.

In studies on the effect of chemotherapeutic agents, exposure time is normally an important parameter. However, in our study we are focusing on the effect of scalp cooling on metabolism and subsequent hair follicle damage. A relevant doxorubicin exposure time was found to be 4 hours. The pilot experiment on the influence of doxorubicin exposure time did not show any significant differences between various exposure times relevant for scalp cooling. Therefore, we used an exposure time of 4 hours in our final experiment.

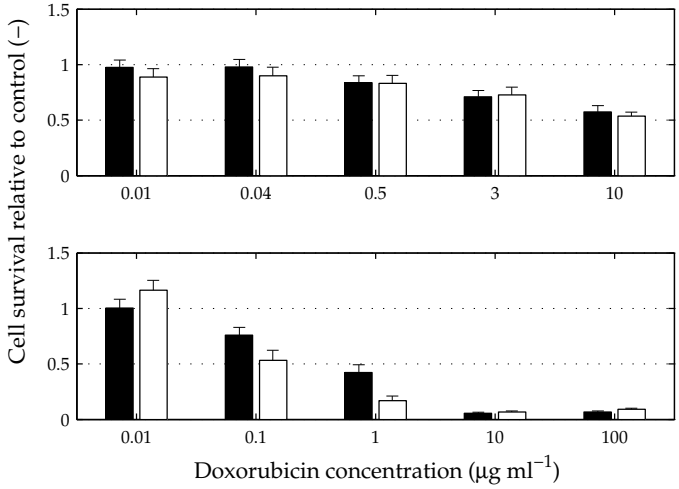

Figure 5.3: Influence of doxorubicin exposure time at 20°C (upper panel) and 37°C (lower panel) for short (■) and long (□) exposure times. The used exposure times at 20°C were 2 and 6 hours, respectively. At 37°C, these exposure times were 4 and 7 hours, respectively. Values represent the mean and standard error of 8 samples.

5.3.6 Doxorubicin exposure temperature

The influence of doxorubicin exposure temperature was investigated using the standard protocol with five different temperature groups. Cells were exposed to various doxorubicin concentrations for 4 hours at a temperature of either 14, 18, 22, 26 or 37°C. In this pilot experiment, we slightly deviated from the standard protocol. For each temperature and concentration, we now used a sample size of 6 replicates (instead of 8) in order to carry out this experiment in one go. The results of this pilot experiment are shown in figure 5.4. For each doxorubicin concentration, viability of NHEK cells is lowest in the 37°C temperature group. Between the various other temperature groups, no obvious relationship is visible. Also, the standard deviation of the experiment is high. The small number of samples is insufficient to find an accurate mean.

Based on the results of this pilot experiment, we tried to increase the statistical power in our final experiment. To do this, we used a sample size of 8 again. Furthermore, we extended the range of temperatures investigated. Moreover, we used only three temperature groups in our final experiment: a low temperature (10°C), a medium temperature (22°C) and a high temperature (37°C). We chose to use a medium temperature of 22°C, since Gregory et al. (1982) showed that in order for scalp cooling to be effective, temperatures had to be reduced below this value (see also chapter 1).

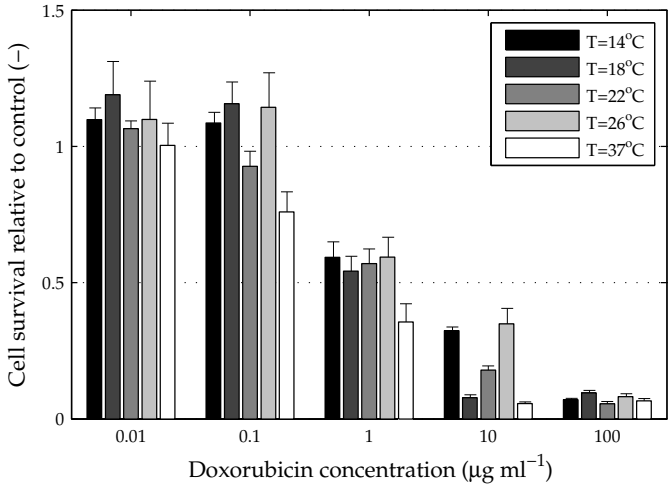

Figure 5.4: Influence of doxorubicin exposure temperature on keratinocyte damage. Bars represent the mean and standard deviation of 6 replicates each.

5.3.7 Doxorubicin concentration

Based on previous pilot experiments, we were able to define a good range in doxorubicin concentrations that should be used in our final *in vitro* experiment. From figure 5.4 we can see that the viability of NHEK cells at a concentration of 100 μg ml^{-1} is close to zero for all temperature groups. At 10 μg ml^{-1}, some deviations from the zero viability are visible for temperature groups 26°C and 14°C. At 0.01 μg ml^{-1}, the viability for all temperature groups is close to one, meaning that this concentration is too low to have a significant effect on cell viability.

We investigated a total of 7 doxorubicin concentrations. To gain insight into the effect of a wide range of doxorubicin concentrations, we used a minimum concentration of 0.01 μg ml^{-1} and a maximum concentration of 10 μg ml^{-1}. The range was covered by using concentrations of 0.04, 0.1, 0.5, 1.0 and 3.0 μg ml^{-1}.

5.4 Final *in vitro* experiment

5.4.1 Experimental protocol

Based on the results of several pilot experiments, a final protocol was developed. This final protocol is depicted in table 5.2 and table 5.3 and will be described in more detail below.

Cells were plated in 24–well plates at a cell density of 6000 cells cm^{-2}. Cells were incubated at 37°C for a period of 24 hours to allow the cells to recover from

Table 5.2: Protocol for the final *in vitro* experiment to determine the effect of temperature, doxorubicin and combinations of temperature and doxorubicin on keratinocyte cell damage.

Step	Description
1	Plate cells in 24–well plates at 6000 cells cm^{-2}.
2	Incubate cells at 37°C and 5% CO_2 for 24 hours to recover from handling.
3	Add specific concentration of doxorubicin and place cells at specific temperature.
4	Maintain temperature and doxorubicin concentration for a total exposure time of 4 hours.
5	Remove doxorubicin, add fresh medium and place cells at 37°C and 5% CO_2 for 72 hours.
6	Measure viability using MTT test

Table 5.3: Schematic overview of the doxorubicin concentrations and temperature groups used and their replicate values in the final *in vitro* experiment to determine the effect of temperature, doxorubicin and combinations of temperature and doxorubicin on keratinocyte cell damage.

	Doxorubicin concentration (μg ml^{-1})							
Temperature	Control	0.01	0.04	0.1	0.5	1.0	3.0	10
$T_L = 10$°C	n=8	n=8	n=8	n=8	n=8	n=8	n=8	n=8
$T_M = 22$°C	n=8	n=8	n=8	n=8	n=8	n=8	n=8	n=8
$T_H = 37$°C	n=8	n=8	n=8	n=8	n=8	n=8	n=8	n=8

handling. Concentrations of doxorubicin in KGM2 (0.01, 0.04, 0.1, 0.5, 1.0, 3.0 or 10.0 μg ml^{-1}) were prepared. Cells were then exposed to 250 μl of a specific doxorubicin concentration. Plates were incubated for 4 hours at either a low temperature ($T_L = 10$°C), a medium temperature ($T_M = 22$°C) or a high temperature ($T_H = 37$°C). For each combination of temperature and doxorubicin concentration, a sample size of 8 was used. Cells receiving medium without any doxorubicin were used as a control group for each specific temperature. At the end of the exposure time, doxorubicin was removed and cells were washed with 500 μl PBS. Fresh medium (250 μl $well^{-1}$) was added to each well and plates were then incubated at 37°C for a post–exposure time of 72 hours after which the standard viability measurement was performed (see section 5.2.3).

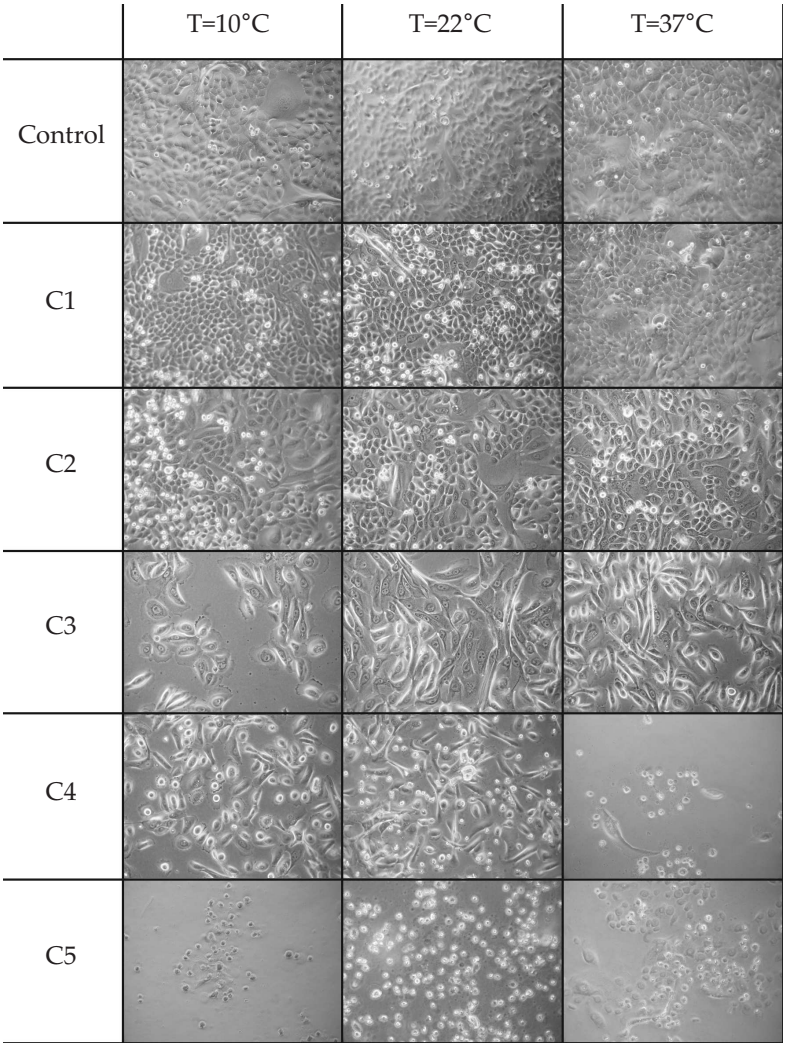

Figure 5.5: Microscopic photographs of cells exposed to selected doxorubicin concentrations. Photographs are taken at a magnification of 10x. C1 = 0.01 μg ml^{-1}, C2 = 0.04 μg ml^{-1}, C3 = 0.5 μg ml^{-1}, C4 = 3.0 μg ml^{-1}, C5 = 10 μg ml^{-1}.

5.4.2 Data analysis

The final experiment investigated the effect of 7 different doxorubicin concentrations and 3 different exposure temperatures, with a sample size of 8 for each concentration and each temperature.

An analysis of variance (ANOVA) was performed using statistical software (SPSS version 15.0, SPSS inc.), using a general linear model. The viability is statistically

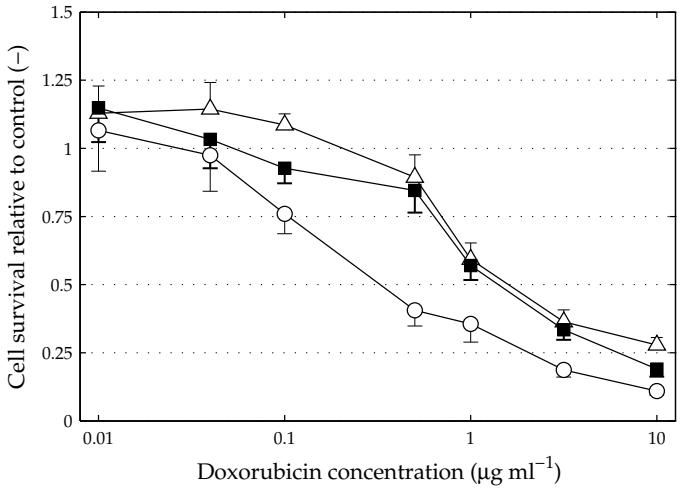

Figure 5.6: Cell viability as a function of doxorubicin concentration at different temperatures. △= T_{L} (10°C), ■ = T_{M} (22°C) and ○ = T_{H} (37°C). Data points show the mean and standard error of 8 replicates. The results of a significance test are shown in table 5.4

modelled as:

$$S_{T,C} = \mu + \alpha T + \beta C + \gamma(T \cdot C) + \epsilon \tag{5.3}$$

This means that we will investigate whether temperature, concentration and an interaction term are significantly relevant for describing our data. Where appropriate, a post–hoc analysis was used using Tamhane's T2 criterium (based on unequal variances) to test for differences between various doxorubicin concentrations and various exposure temperatures. A significance level of $p < 0.05$ was used in these statistical tests.

5.4.3 Results

Microscopic photographs of cells at selected concentrations are shown in figure 5.5 on page 89. Here we can see that the control groups of all temperatures show similar cell counts. With increasing concentration, the number of cells decrease. At 5 μg ml^{-1} (C4), a clear difference is visible between the high temperature group and both the medium and low temperature group. The difference between these groups at other concentrations is less well defined. The results of the viability determination are shown in figure 5.6. This figure shows the cell viability as a function of doxorubicin concentration, for different doxorubicin exposure temperatures. In this figure, we can see that the viability of keratinocytes as a function of doxorubicin concentration shows a decreasing s–curve with increasing concentrations. Viability levels are

slightly above 1 for low concentrations (0.01 μg ml^{-1}) and with increasing concentrations viability gradually drops towards zero for high concentrations (10 μg ml^{-1}). For different temperature groups, cell viability at a specific concentration is always lowest for the high temperature group. In the mid–section of the concentration range (i.e. 0.1 – 1 μg ml^{-1}) the differences between the high temperature group (T_{H}) and the two lower temperature groups (T_{L} and T_{M}) are more pronounced. Cell viability for these lower temperature groups decreases more slowly than for the high temperature group, until at a concentration of 1 μg ml^{-1} a rapid drop in cell viability is visible. The difference between the individual temperature groups at low and high concentrations is therefore small.

From an ANOVA analysis, we found that the effect of doxorubicin concentration on NHEK viability was highly significant [F(6,161) = 165.213, p < 0.001] as was the effect of temperature on NHEK viability [F(6,161) = 37.054, p < 0.001]. The effect size of doxorubicin (η_{p}^2, see equation 3.10) was higher than the effect size of temperature ($\eta_{\mathrm{p}}^2 = 0.882$ compared to $\eta_{\mathrm{p}}^2 = 0.358$).

For all temperature groups, increased doxorubicin concentration has a significant decreasing effect on cell viability. This effect was highly significant for the high temperature group [F(6,49) = 119.400, p < 0.001], the intermediate temperature group [F(6,49) = 33.166, p < 0.001] and the lowest temperature group [F(6,49) = 68.225, p < 0.001] Based on these results, a post–hoc analysis was performed for each temperature group to check where a significant transition in cell viability as function of doxorubicin concentration occurs. This transition point may be viewed as the inflection point of the S–curve. For the low and medium temperature group, we found a transition point between 1.0 and 3.0 μg ml^{-1}. The highest temperature group has a transition point slightly below 0.5 μg ml^{-1}.

The ANOVA analysis also revealed a significant interaction between doxorubicin and temperature on cell viability [F(6,161) = 2.754, p = 0.002], although the effect is smaller than that of temperature and doxorubicin ($\eta^2 = 0.199$). This significant interaction term shows that the effect of temperature on cell viability is not the same at the levels of different doxorubicin concentrations. For low and high doxorubicin concentrations, there is hardly any influence of a lower temperature on cell survival. In the mid–section of the graph this influence is far more substantial.

From table 5.4 it can be seen that significant differences exist between T_{L} and T_{H} for concentrations of 0.1 μg ml^{-1} and up, except for a concentration of 1 μg ml^{-1}. At this concentration, the significance level is not high enough, but still a trend is visible (p < 0.1). Between T_{M} and T_{H} significant differences exist for concentrations of 0.5 μg ml^{-1} and up, except for a concentration of 1 μg ml^{-1} where no significant difference is visible. The only significant difference between T_{L} and T_{M} exist at a concentrations of 10 μg ml^{-1}, although a trend is visible at a concentration of 0.1 μg ml^{-1}.

Table 5.4: Significance between different temperature groups at a specific doxorubicin concentration for results of the final *in vitro* experiment (figure 5.6). p–Values are shown with their respective significance level. Trends ($p < 0.1$) are marked with an asterisk.

DOX (μg ml^{-1})	F–value	p–value	T_L vs T_H	T_M vs T_H	T_L vs T_M
0.01	F(2,21) = 0.315	(p = 0.733)			
0.04	F(2,21) = 1.958	(p = 0.166)			
0.1	F(2,21) = 15.187	(p < 0.001)	p < 0.01		p < 0.1*
0.5	F(2,21) = 31.605	(p < 0.001)	p < 0.001	p < 0.001	
1	F(2,21) = 4.380	(p < 0.05)	p < 0.1*		
3	F(2,21) = 12.908	(p < 0.001)	p < 0.01	p < 0.01	
10	F(2,21) = 22.587	(p < 0.001)	p < 0.001	p < 0.05	p < 0.05

5.5 Conclusion and discussion

In this chapter, we examined the role reduced metabolism has on the hair preservative effect of scalp cooling. For this, a controlled *in vitro* experiment was conducted to assess the damage exerted by doxorubicin on human epidermal keratinocytes for a range of chemotherapy concentrations and exposure temperatures. The effects of temperature and doxorubicin on cell damage were determined from cell viability measurements (MTT assay). Several pilot experiments were used to establish a final protocol. In the final experiment, a total of 7 doxorubicin concentrations and 3 different exposure temperatures were used, and in each group a sample size of 8 wells was used.

We found that increased doxorubicin concentrations have a significant decreasing effect on keratinocyte cell viability. Viability was close to 1 for low concentrations, and close to 0 for high concentrations. In between, the relationship between doxorubicin concentration and cell viability shows an S–curve.

We also found that reduced temperature has a significant increasing effect on keratinocyte cell viability. The two cooled temperature groups (10°C and 22°C) show a higher cell viability for each doxorubicin concentration than the 37°C group. At the mid–range of doxorubicin concentrations (0.04–1 μg ml^{-1}), the effect of reduced temperature is more pronounced than in the extreme values of doxorubicin concentration. This observation is confirmed by the fact that an interaction term of doxorubicin concentration and exposure temperature was significant. The increased effect of reduced temperature was significant for doxorubicin concentrations of 0.1 μg ml^{-1} and higher. We found no significant differences between the low (10°C) and medium (22°C) group.

The results of the experiment are in line with the hypothesis of scalp cooling (see chapter 1). In this hypothesis, the reduced temperature due to scalp cooling will result in lower perfusion and a lower cellular metabolism. With this, the supply, uptake and damage of a chemotherapeutic agent will be diminished.

However, some results of the experiment were not as expected. For one, it is remarkable to see that there is no significant difference between the medium and low temperature group. Thus, it seems that there is a limit in effect of reduced temperature. In a pilot study to determine optimal doxorubicin exposure temperature (figure 5.4) we found that an exposure temperature of 26°C also showed increased cell viability, and this increase did not differ from other temperature groups. During scalp cooling, a skin temperature of approximately 20°C is reached. Based on the results of our experiment, one might expect that the limit in effect of reduced temperature during scalp cooling may be reached for a temperature as high as 26°C. This means that during scalp cooling, the effect of reduced metabolism is already at its maximum. However, care has to be taken when the results of an *in vitro* experiment are generalized. Therefore, further studies on the effect of reduced temperature on cell damage are needed to exactly define this limit. Ideally, an *in vitro* hair follicle model is used in these studies. Our current study confines the boundary conditions in doxorubicin concentration and exposure temperature that can be used in further studies.

Another unexpected result can be found for low doxorubicin concentrations (0.01 and 0.04 μg ml^{-1}). At these concentrations, the MTT assay for each temperature group showed a higher viability than the respective control group. Due to the fact that each specific temperature group has its own control group, it is unlikely that this effect is due to a measurement error. This means that apparently, cells are metabolically more active when exposed to a small amount of doxorubicin. It is possible that cells in the control group are close to reaching confluence at the time that viability is determined. As cells reach confluence, there is not enough room for new cells. Therefore, the rate at which cells divide will become lower and hence their metabolic activity will decrease. Another possibility is that a small amount of doxorubicin will stimulate cells to repair damage exerted to the cells. Hence, it may actually result in larger cell growth compared to a control group receiving no doxorubicin. At this point however, we have no indication for which explanation may be true.

The effect of scalp cooling on hair cell damage can be evaluated using our experiments on the relationship between temperature and perfusion (chapter 3), our numerical model for pharmacokinetics (chapter 4) and the results of the experiment in this chapter. During scalp cooling, perfusion is reduced to 20% of its original value. With this, our pharmacological model shows that the maximum concentration in the scalp skin reduces from 1.66 μg ml^{-1} without cooling to 0.56 μg ml^{-1} with cooling. The *in vitro* experiments (figure 5.6) indicate that this reduction in both temperature and concentration may increase cell survival from approximately 25% to 85%. Probably, a cell survival of 85% is large enough for the hair follicle to remain in an anagen

stage. When the effect of reduced perfusion is not taken into account in this evaluation, the cell survival at a concentration of 1.66 μg ml^{-1} at a lower temperature would be equal to only 50%. Most likely, this 50% damage to the hair follicle is not enough to prevent hair loss. Based on this, we expect that both reduced perfusion and reduced metabolism are important for the hair preservative effect of scalp cooling. In the next chapter, a complete model of scalp cooling will be derived. There, the results of the *in vitro* cell experiments will be used to establish a likely value for critical viability.

Chapter 6

Computational evaluation of scalp cooling protocols*

6.1 Introduction

For the computational evaluation of scalp cooling protocols, a numerical model for scalp cooling was developed. This model is based on models for heat transfer (chapter 2) and mass transfer (chapter 4). Relationships obtained between temperature and perfusion (chapter 3) are incorporated in the model, as is knowledge of variability and uncertainty in parameters. Before each simulation, parameters of the model are randomly assigned. Hence, each simulation simulates a fictional patient, taken from a population.

The computational model for scalp cooling is used to model the response of a large set of individuals to scalp cooling. The general procedure for each individual is as follows (see figure 6.1). Based on the known mean values and standard deviations of relevant parameters, a possible member of the population is modelled. The heat transfer model is used to calculate the skin temperature and subsequent perfusion during scalp cooling. Next, the pharmacological model is used to determine the response of this person to chemotherapy with and without scalp cooling. To deter-

*Parts of this chapter, together with parts of chapter 4 have been submitted for publication as:
Janssen, F.E.M., Van Leeuwen, G.M.J. and Van Steenhoven, A.A. A computational model for scalp cooling to prevent chemotherapy induced hair loss incorporating modelling of variability. *Physics in Medicine and Biology.*

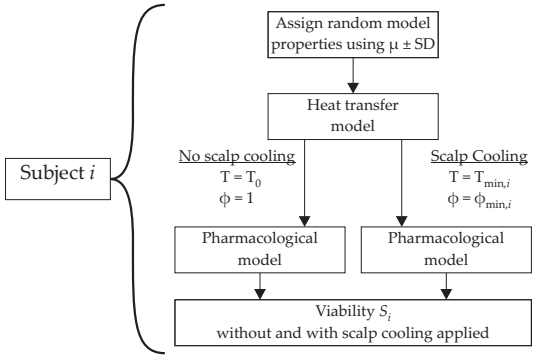

Figure 6.1: Flow chart of the computational model for scalp cooling to simulate the response of multiple individuals to scalp cooling. In the model a total of n persons are simulated. For each subject i the procedure consists of assigning random variables. Then the heat transfer model is used to calculate T_{skin} and ϕ_{min}. Finally, the pharmacological model calculates the tissue concentration with and without scalp cooling. With this, the resulting viability can be calculated.

mine the response to scalp cooling, the value of relative perfusion obtained with the heat transfer model is used. When this procedure is used for a large set of individuals, the parameters obtained give an indication of the response of a population to a certain treatment.

In this chapter we will describe the population based model for scalp cooling. Using the model, parameter studies were performed, and scalp cooling protocols were evaluated. At the end of this chapter, an optimized protocol for scalp cooling is described.

6.2 Modelling of uncertainty and variability

6.2.1 Input parameters

The known variability in physiological parameters may be used to determine a scalp cooling response of a population. Three of the most important physiological parameters determining the response of a human being to an administered drug are (Nestorov, 1999):

1. Body mass;
2. Cardiac output;
3. Tissue mass and blood flow fractions.

These three parameters, as well as parameters that can be related to these three parameters will be defined in the population model for scalp cooling.

In the Netherlands, the biggest group of patients that is being offered scalp cooling during chemotherapy is a female group being treated for breast cancer. Therefore, we will only consider female individuals in our numerical model. Variability in body mass (m_b) is modelled using the average body height (h_b) and body mass index (BMI $= m_\mathrm{b}/h_\mathrm{b}^2$). According to Statistics Netherlands (CBS), the Dutch female population has an average body height of $h_\mathrm{b} = 1.69 \pm 0.1$ (mean $\pm$ standard deviation), and an average body mass index of BMI $= 24.5 \pm 2$. In the complete model for scalp cooling, both BMI and body height are randomly selected, using the known mean and standard deviation. With these two values, the body mass is readily defined.

The body height is then used to scale the thicknesses of the brain and skull tissue layer in the heat transfer model. For this, a scaling variable is used. The scaling variable is defined as

$$\lambda_1 = \frac{h_\mathrm{b}}{h_{\mathrm{b},0}} \tag{6.1}$$

since it is expected that the size of the head in adults scales linearly with the body length. The thickness of the brain and skull are multiplied with this scaling parameter to obtain a mean value for this person. Subsequently, to allow for modelling of variability, a random thickness that lies within the known variation of the two layers is added (or subtracted for a negative value) to the thickness of both the brain and skull layer.

Other tissue layers are treated differently. The thickness of the hair layer is determined using a mean value and a standard deviation, without applying a scaling parameter. The thickness of the skin is not varied, since the thickness of the skin is relatively constant in a population. The thickness of the fat layer is adjusted using the scaling parameter (λ_1) and another scaling parameter, that is based on the fat percentage (f_F) of the current subject regarded:

$$\lambda_2 = \frac{f_\mathrm{F}}{f_{\mathrm{F},0}} \tag{6.2}$$

in which $f_{\mathrm{F},0}$ is the fat percentage of the standard subject. The fat percentage for an adult female human being can be estimated using (Deurenberg et al., 1991):

$$f_\mathrm{F} = (1.20\,\mathrm{BMI}) + (0.23\,\mathrm{age}) - 5.4 \tag{6.3}$$

In our model, we used an average age of 50 years, and with a BMI of 24.5, the fat percentage for the standard model is equal to $f_{\mathrm{F},0} = 35.5\%$. The thickness of the fat layer (d_f) is now calculated using the scaling parameter for height and the scaling parameter for fat:

$$d_\mathrm{f} = d_{\mathrm{f},0}\lambda_1\lambda_2 \tag{6.4}$$

In chemotherapy, doses are usually calculated in milligrams per body surface area. The body surface area is calculated using the DuBois relation (DuBois and

DuBois, 1916), which relates the surface area A_b to the easily measurable body mass m_b in kg and body height h_b in cm:

$$A_\mathrm{b} = 0.007184\Big(m_\mathrm{b}^{0.425} h_\mathrm{b}^{0.725}\Big) \tag{6.5}$$

Another important parameter defining the response to any administered drug is the cardiac output (Q_CO). An empirical relationship has been found that relates cardiac output to body mass in kg(Calder, 1984):

$$Q_\mathrm{CO} = (0.187) m_\mathrm{b}^{0.81} \tag{6.6}$$

Here, the cardiac output is defined in l min^{-1}. The variability in cardiac output can be modelled using the coefficient of variation, defined as the ratio of the standard deviation to the mean value, $c_\mathrm{v} = \sigma/\mu$. For the empirical relationship for cardiac output, coefficients of variation are reported of $c_\mathrm{v} = 31\%$ on the coefficient and $c_\mathrm{v} = 1.3\%$ on the exponent (Nestorov, 1999).

The available information on tissue mass and blood flow fraction is also used in the variability simulations. For each tissue compartment – except the rapidly perfused tissue compartment – both tissue mass fraction and blood flow fraction are randomly assigned using the mean value and standard deviations from the standard model. The values for the rapidly perfused tissue compartment are obtained by subtracting the sum of the other tissue fractions from unity, such that both total body mass and blood flow for the individual model are correct. For the scalp skin, the same perfusion value is used in both the heat transfer model and the pharmacological model.

6.2.2 Determination of critical viability

To determine the viability, we used the results of the cell experiments in chapter 5. The dependence of viability on drug concentration has been modelled by (Ribba et al., 2005):

$$S = a + \frac{1}{b + k_\mathrm{d} C} \tag{6.7}$$

For each temperature group, parameters a, b and k_d were fitted. This resulted in different parameters for each temperature group (see figure 6.2). For each parameter, a temperature dependent function was postulated and fitted. The resulting equations for a, b and k_d are:

$$a = 0.1 + 0.059 \exp\left(\frac{10 - T}{2}\right) \tag{6.8a}$$

$$b = 1.011 - 0.001\big(37 - T\big) \tag{6.8b}$$

$$k_\mathrm{d} = 1.0 + 3.65 \exp\left(-\frac{37 - T}{5}\right) \tag{6.8c}$$

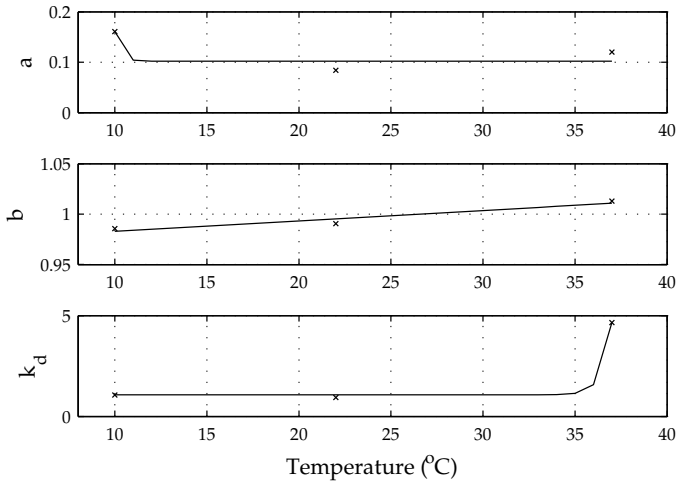

Figure 6.2: Result of the parameter fit to equation 6.7. Best fits for parameters a, b and k_{d} for each temperature are shown. Based on results, temperature dependent functions were postulated. The solid lines represent the best fits (see equation 6.8).

The result of the fit is shown in figure 6.3. Although only three temperature data points are used, the fit obtained makes sense. Some deviations with individual points exist, but these deviations are always smaller than the standard error at that point. The fit obtained has, of course, to be used with care due to the limited amount of data points. Future research is needed to provide more detailed information about the temperature dependency.

To determine critical viability, we used two different studies that evaluated the success of scalp cooling. The first study (Anderson et al., 1981) investigated the effect of scalp cooling during a 10 minute intravenous administration of 40 mg of doxorubicin. Scalp cooling was applied 15 minutes before administration, during administration and 20 minutes after administration. Before scalp cooling was applied, the hair of the patient was wetted. The success rate in this study was 100% (for patients with normal liver function). The second study (Gregory et al., 1982) investigated the effect of scalp cooling during administration of 40 mg m^{-2} of doxorubicin. Scalp cooling was applied, without wetting the hair first, 20 minutes before administration, during administration and for a period of 30–40 minutes after administration. All patients showed normal liver function. The success rate in this second study was 42%. Of these 42% patients, all showed slight hair loss, but not sufficient for them to require a wig. The average skin temperature during scalp cooling in this study was 21°C.

We simulated these two different studies. The obvious differences between the two studies are the higher dose in the second study, and the wetting of the hair in the first study. To model the last difference, we conservatively doubled the conductivity

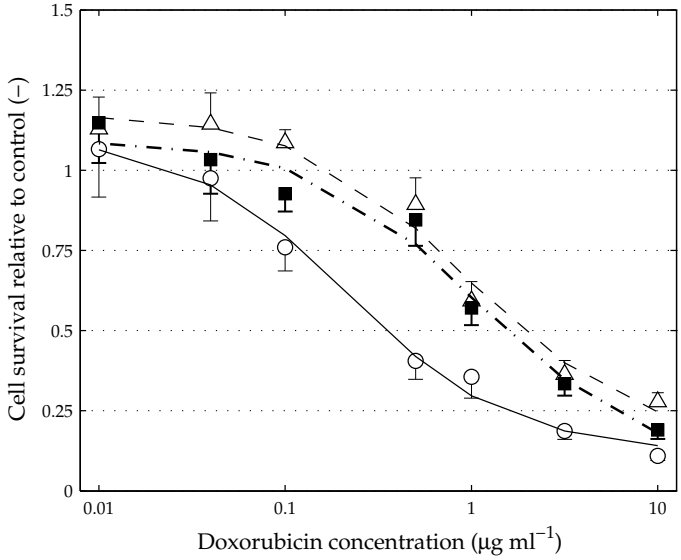

Figure 6.3: Cell viability as a function of doxorubicin concentration and exposure temperature (equation 6.7). △= T_{L} (10°C), ■ = T_{M} (22°C) and ○ = T_{H} (37°C). Data points show the mean and standard error of 8 replicates. The fits are shown for 37°C (—), 22°C (-·-) and 10°C (- -)

of the hair layer to 0.08 W m^{-1} K^{-1}. Each study was then simulated using a sample size of 100 patients. For each patient, the temperature during scalp cooling and the maximum concentration in the scalp skin was used to determine the viability. The resulting distribution in viability of the second study was then used to calculate the critical viability for which holds:

$$p(S > S_{\mathrm{crit}}) = 0.42 \tag{6.9}$$

The results of the first study were used as a control, to check whether all patients received a successful treatment. To match the average skin temperature of the computational model to the values of the second study, we iteratively varied the thickness of the hair layer. This resulted in a hair layer thickness of 4.6 mm, and this value is used as a standard value in the model.

Histograms of the viability obtained during cooling are shown in figure 6.4. In the top panel, the results of the control study are shown (success rate of 100%), the bottom panel shows the results of the study with a success rate of 42%.

We checked whether these histograms show normal distribution using a Lilliefors hypothesis test of composite normality. This test indicated that both viability results are not normally distributed ($p < 0.05$).

Therefore, we used a cumulative histogram to find out what critical viability belongs to a scalp cooling effectiveness of 42%. This critical viability is equal to

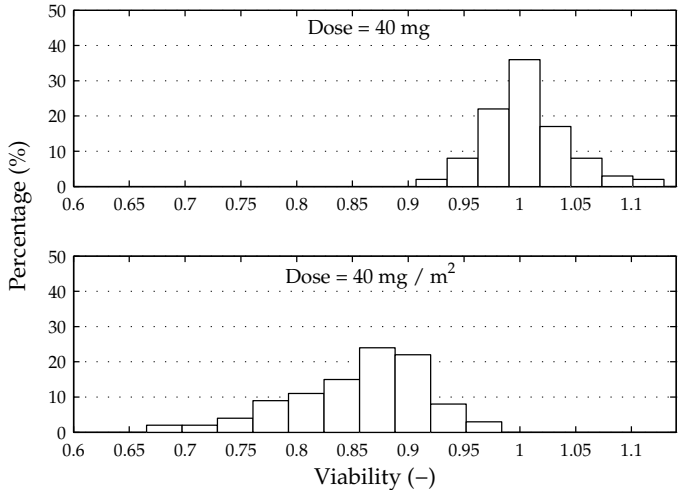

Figure 6.4: Calculated viability histograms using simulations of a population. The top panel shows the viability distribution for a doxorubicin dose of 40 mg; the bottom panel shows the effect of a doxorubicin dose of 40 mg m^{-2}.

$S_{\text{crit}} = 0.88$. The viability response of the control study indicates that 100% of the observations are above this critical value.

Equation 6.7 may now be used to calculate iso–viability lines in a temperature, concentration graph. Each iso–viability line satisfies:

$$C = \frac{1}{k_{\text{d}}}\Big(\frac{1}{S-a} - b\Big) \tag{6.10}$$

with a, b and k_{d} given by equation 6.8a–c.

A temperature, concentration graph of the two studies is shown in figure 6.5. In this figure we can see that iso–viability lines run from a high concentration at low temperatures to a low concentration at higher temperatures. With increasing temperatures, the iso–viability lines show an S–curve. Care must be taken when interpreting results that lie outside the range of temperatures for which the graph was fitted (10°C < T < 37°C). For instance, the rapid increase in iso–viability lines at temperatures below 10°C has not been validated experimentally. It is expected that the iso–viability lines show an increase when temperatures are below 10°C, but to what extent this increase occurs is not certain.

The black line in figure 6.5 denotes the critical viability ($S_{\text{crit}} = 0.88$). The critical viability may differ from patient to patient. Also, the transition from satisfactory hair preservation to complete hair loss probably occurs at a wide range of viability levels. However, in our study we assume that the transition between acceptable hair preservation and unsatisfactory hair loss occurs at the critical viability value. Therefore, we assume that patients that lie below the black line in the temperature–

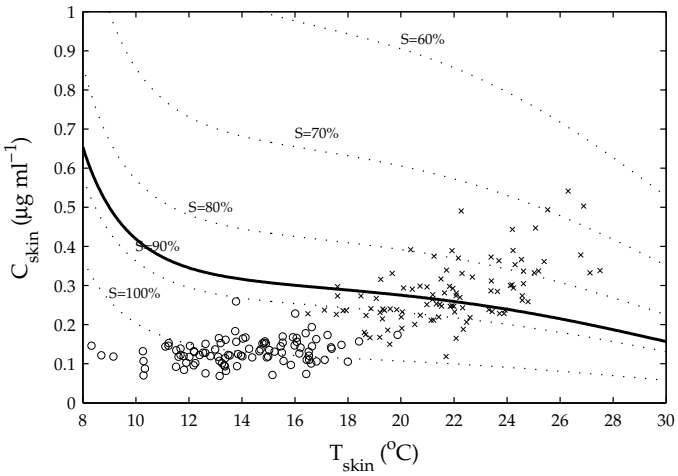

Figure 6.5: Temperature–concentration diagram for the determination of the critical viability. (○) 40 mg; (×) 40 mg m^{-2}. The solid black line denotes the critical viability value, determined to be $S_{\text{crit}} = 0.88$.

concentration graph show acceptable hair preservation. Patients that are above this line are considered to show unacceptable hair loss.

The temperature–concentration graph of the simulation indeed shows that all patients from the control study have viabilities higher then the critical viability value. For the study where 42% showed good hair preservation, we can see that patients that are slightly above the line show either too high concentration (i.e. too high perfusion) or too high temperature (i.e. too high metabolism). These patients may be helped by more extensive cooling. For patients above the 80% viability line, further cooling might not result in a better chance of hair preservation.

6.2.3 Optimal skin temperature and drug dose

The relationship obtained for cell viability as a function of doxorubicin concentration and exposure temperature, in combination with the value obtained for critical viability, was used to determine the optimal scalp cooling temperature at different doses of doxorubicin. The results indicated what temperatures should be reached during scalp cooling given the treatment dose.

Simulations were used to see the effect of skin temperature on viability for different doses. For this, the pharmacological model from chapter 4 was used with prescribed skin temperature. The relationship between temperature and perfusion was modelled according to the results of chapter 3 (equation 3.11). Variability was not taken into account in these simulations. A total of 5 doses were evaluated, ranging from 20 mg to 120 mg. The resulting temperature and concentration are used to

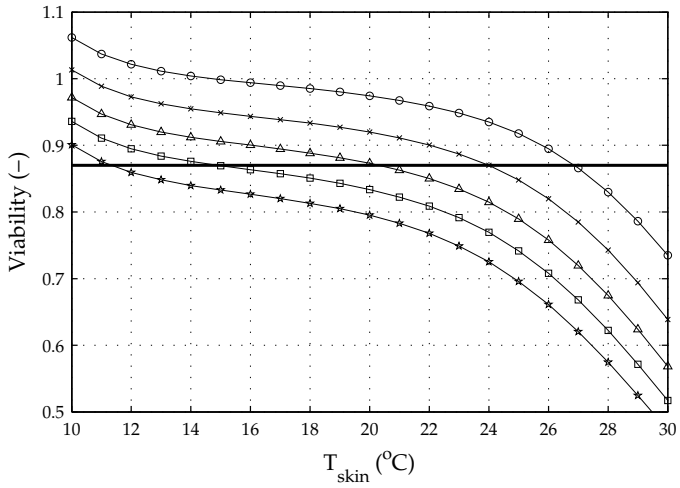

Figure 6.6: Influence of skin temperature on tissue concentration and subsequent viability of hair follicles after a dose of 40 mg (○), 60 mg (×), 80 mg (△), 100 mg (□) or 120 mg (⋆). The critical viability ($S_{\text{crit}} = 0.88$) is denoted by the black line.

calculate the viability, using equation 6.7. The results of these simulations are shown in figure 6.6.

In this figure, the critical viability ($S_{\text{crit}} = 0.88$) is denoted by the black line. All values that are above this line are considered to be cases where hair loss is prevented; values below the line show unacceptable hair loss. For a dose of 40 mg, this means that the scalp has to be cooled to approximately 27°C in order to prevent hair loss. With increasing doxorubicin concentration this temperature decreases until for a dose of 120 mg, a temperature of 11°C is necessary. An important aspect in this figure is that it shows the result of the standard model, and any variability that might occur is not considered in the graph. This is something that has to be accounted for in the evaluation of scalp cooling protocols.

The critical temperature for each dose was determined. This temperature is defined as the temperature at which viability is larger than the critical value. The results are shown in table 6.1.

The critical temperature is equal to 27°C for a dose of 40 mg and decreases linearly to 11°C for a dose of 120 mg. During scalp cooling, the average skin temperature is equal to 20°C (see chapter 2). With some modifications to the protocol, it is possible to lower this temperature. However, in chapter 3 we found that large differences exists between subjects in the degree to which the scalp skin temperature is reduced during cooling. In addition, at some point a limit in temperature is reached where further cooling is uncomfortable for the patient (see chapter 1). Therefore, we think that scalp cooling should aim to reduce the skin temperature not further than 16°C. Based on this, and the fact that variability in viability will occur, we think that

Table 6.1: Critical skin temperature needed during scalp cooling at different doxorubicin concentrations.

Dose (mg)	$T_{\text{skin,crit}}$ (°C)
40	27
60	24
80	20
100	15
120	11

scalp cooling should not be applied for doses that are higher than 60–70 mg (approximately 40 mg m^{-2}). With this in mind, we evaluated some important scalp cooling protocol parameters.

6.3 Evaluation of scalp cooling protocol parameters

The scalp cooling protocol parameters that can be influenced in scalp cooling are the following:

- the temperature of the cap;
- the time that scalp cooling is applied;
- the doxorubicin infusion time;
- the thermal conductivity of the hair;
- the thickness of the hair layer.

The influence of the above parameters was investigated using the model for scalp cooling that incorporates modelling of variability. For each variation, a total of 50 fictional patients were modelled. Each patient received a dose of 40 mg m^{-2}. The effectiveness (ε) of the scalp cooling protocol is defined as:

$$\varepsilon = \frac{n(S > S_{\text{crit}})}{n_{\text{totaal}}} \times 100\% \tag{6.11}$$

6.3.1 Cap temperature

The first parameter that we investigated was the temperature of the cold cap. In most present day scalp cooling devices this temperature can be set beforehand, although

Table 6.2: Influence of cap temperature on scalp cooling effectiveness (ε). Without scalp cooling, the average maximum skin concentration and average viability are $C_{\text{skin}} = 0.97 \pm 0.09$ μg ml^{-1} and $S = 0.36$ (-), respectively.

T_{cap} (°C)	T_{skin} (°C)	ϕ_w (-)	C_{skin} ($\frac{\mu g}{ml}$)	S (-)	ε (%)
-12	20.2 ± 3.1	0.23 ± 0.08	0.27 ± 0.07	0.87 ± 0.06	54
- 8	21.6 ± 2.8	0.25 ± 0.07	0.28 ± 0.06	0.86 ± 0.05	36
- 4	22.9 ± 2.9	0.27 ± 0.1	0.30 ± 0.1	0.83 ± 0.09	34
0	23.8 ± 2.2	0.28 ± 0.09	0.31 ± 0.1	0.83 ± 0.08	26

it is quite normal to use a standard setting for each patient. This standard setting is a cap temperature of -8°C.

A total of four population based simulations were used, in which the temperature of the cap was varied from -12°C to 0 °C. In each simulation a total of 50 people were used. The results of the variations in cap temperature can be found in table 6.2. The standard response of the model is for a cap temperature of -8°C. With this cap temperature the temperature of the skin is reduced to 21.6°C and the matching relative perfusion is 0.25. This reduction in perfusion yields a skin concentration of 0.28 μg ml^{-1}, resulting in a viability of 0.86. This average viability is slightly below the critical viability value of 0.88, which means that small changes in temperature and perfusion can have a large impact on the success of scalp cooling. The effectiveness of the procedure is $\varepsilon = 36\%$. Without scalp cooling, the mean viability is approximately 0.36, resulting in an effectiveness of $\varepsilon = 0\%$. This means that without scalp cooling, hair loss will occur, as was expected for doxorubicin.

Increasing the cap temperature to 0°C results in significant increases in skin temperature, relative perfusion and skin concentration, and a decrease in viability. Viability is considerably lower than the value required for hair preservation.

The differences between the standard cap temperature setting and the remaining cap temperatures are less pronounced. Increasing the cap temperature to -4°C results in slightly higher temperature, relative perfusion and tissue concentration. The average viability is just below the critical viability. Although the difference in S is small, the effectiveness drops to only 42%. Decreasing the cap temperature to -12°C results in lower skin temperature, perfusion and skin concentration. The average viability is slightly increased and with this the effectiveness is $\varepsilon = 54\%$. The difference between the response at -12°C and the response at -8°C is not significant. However, the temperature of the cap may be used to fine tune the skin temperature during cooling.

Based on the above, the optimal scalp cooling protocol will use a cap temperature

Table 6.3: Influence of duration of scalp cooling on scalp cooling effectiveness (ε).

t_{cool} (hr)	T_{skin} $(^{\circ}\text{C})$	ϕ_w $(-)$	C_{skin} $\left(\frac{\mu\text{g}}{\text{ml}}\right)$	S $(-)$	ε $(\%)$
2	21.4 ± 3.3	0.24 ± 0.08	0.31 ± 0.09	0.84 ± 0.07	28
4	21.7 ± 3.2	0.24 ± 0.08	0.27 ± 0.06	0.86 ± 0.05	34
6	21.5 ± 3.0	0.24 ± 0.08	0.27 ± 0.08	0.86 ± 0.07	46
8	22.0 ± 3.1	0.23 ± 0.09	0.26 ± 0.08	0.87 ± 0.07	46

of -8°C or lower. The setting of the cap temperature may be used to tweak the skin temperature towards a lower value.

6.3.2 Duration of scalp cooling

Next we evaluated the effect of different scalp cooling times. In the standard model, the duration of scalp cooling is 4 hours with an infusion time of 2 hours. We evaluated the effect of scalp cooling with cooling times of 2, 4, 6 and 8 hours. The results are shown in figure 6.3.

For all simulations, skin temperature and perfusion during cooling are similar. However, there is some variation in the maximum concentration and the resulting viability.

A cooling time of 2 hours is equal to the administration time, and therefore gives a slightly higher value for skin concentration than the other cooling times. Within the other cooling times, no differences exist. The temperature and concentration obtained are close to the critical value of 0.88. A cooling time of 6 or 8 hours shows no increase in viability, compared to a cooling time of 4 hours. This indicates that a cooling time that is slightly larger than the administration time is sufficient for the hair preservative effect of scalp cooling. Based on this, the cooling time in the optimal scalp cooling protocol is slightly longer than the infusion time. A cooling time of 1 hour in addition to the infusion time is sufficient.

6.3.3 Infusion time of doxorubicin

The next parameter that was evaluated was the infusion time of doxorubicin. Based on the standard cooling time of 4 hours, we evaluated the effect of 4 different infusion times. These times are 1, 2, 3 and 4 hours, with 2 hours being the infusion time in the standard model. The results are shown in table 6.4.

The results show that the short infusion time has the highest effectiveness, and effectiveness decreases with increasing infusion time. This result is not as expected. The rate of infusion is equal to the ratio of the dose to the infusion time. Since all

Table 6.4: Influence of doxorubicin infusion time on scalp cooling effectiveness (ε).

t_{inf} (hr)	T_{skin} (°C)	ϕ_w (-)	C_{skin} ($\frac{\mu g}{ml}$)	S (-)	ε (%)
1	21.4 ± 2.8	0.23 ± 0.07	0.27 ± 0.07	0.87 ± 0.06	48
2	21.6 ± 2.7	0.25 ± 0.08	0.29 ± 0.08	0.85 ± 0.06	40
3	21.9 ± 2.7	0.24 ± 0.07	0.28 ± 0.07	0.86 ± 0.06	30
4	21.7 ± 2.7	0.26 ± 0.07	0.30 ± 0.07	0.84 ± 0.06	28

Table 6.5: Influence of use of conditioner on scalp cooling effectiveness (ε).

k_{hair} ($\frac{W}{m\,K}$)	T_{skin} (°C)	ϕ_w (-)	C_{skin} ($\frac{\mu g}{ml}$)	S (-)	ε (%)
0.04	21.4 ± 3.0	0.23 ± 0.08	0.27 ± 0.08	0.86 ± 0.07	46
0.08	13.6 ± 2.4	0.18 ± 0.06	0.22 ± 0.05	0.95 ± 0.05	92

patients receive the same dose, the rate of infusion is higher for shorter infusion times. Therefore, a higher tissue concentration is expected for shorter infusion times.

However, the differences between the various infusion times are small and the results of the viability are close to the critical viability. This means that small differences can have a large effect on effectiveness. The current results show no indication that infusion time has an effect on the resulting viability. Therefore, infusion times need not to be adjusted in the optimal scalp cooling protocol.

6.3.4 Use of conditioner

In the clinic, conditioner is often applied to the hair to improve the thermal contact between the cold cap and the head. We evaluated the effect of this conditioner on the hair preservative effect of scalp cooling. The use of conditioner is modelled by increasing the mean thermal conductivity of the hair layer from 0.04 to 0.08 W m^{-1} K^{-1}. The results of these simulations are shown in table 6.5.

Due to the increased thermal contact between the cap and the skin when conditioner is applied, the skin temperature during cooling is significantly lower than the skin temperature without applying conditioner. The value of the perfusion is also lower when conditioner is used. The mean value for perfusion is 0.18, meaning that relative perfusion has reached its minimum value. The mean doxorubicin concentration in the skin is equal to 0.22 μg ml^{-1} and with this the mean viability is equal to 0.95. The effectiveness with this method increases from 46% to 92%.

Table 6.6: Influence of hair layer thickness on scalp cooling effectiveness (ε).

d_{hair} (mm)	T_{skin} (°C)	ϕ_w (–)	C_{skin} ($\frac{\mu g}{ml}$)	S (–)	ε (%)
4.6	21.3 ± 3.4	0.24 ± 0.08	0.29 ± 0.09	0.85 ± 0.07	44
3.5	18.5 ± 3.0	0.19 ± 0.07	0.24 ± 0.06	0.90 ± 0.05	72

Increasing the thermal conductivity of the hair layer is successful for increasing the effectiveness of scalp cooling. However, the skin temperature obtained is below the temperature that is thought to be necessary in order for scalp cooling to work. In a previous section, we determined the minimum skin temperature to be approximately 16°C. One important aspect of the use of conditioner is its controllability, which is not high for a fluid. This may lead to some areas on the scalp (i.e. ears, front of the head) that are also affected. Due to the increased thermal conductivity and the resulting low skin temperatures, it is expected that many patients will consider the scalp cooling treatment with use of conditioner to be unpleasant. This might cause patients to abandon scalp cooling.

In these simulations, a dose of 40 mg m^{-2} was used. The results of the simulation with conditioner applied show that the effectiveness is 92%, even though a low temperature is reached. This indicates that the dose for some patients is too high for scalp cooling to have an effect. Only for patients receiving a lower dose, an effectiveness close to 100% may be reached.

The use of conditioner causes lower temperatures, causing in turn more discomfort. In some cases, the use of conditioner may be justified (i.e. in patients where scalp temperature cannot be decreased effectively), but in general the use results in skin temperatures that are too low. The additional hypothermia induced only has a small effect on viability.

6.3.5 Thickness of the hair layer

A piece of advice that is given to patients in a clinical setting is to get a haircut – a short one– before chemotherapy treatment. Preferably, the hair layer is reduced by thinning the hair, so that when the hairs are flattened by the cap, the resulting hair layer is less thick than normal. In this way, the thermal contact between the cap and the skin is improved, resulting in lower skin temperatures and an increased effectiveness of scalp cooling. The effect of this advice to thin out the hair and to get a shorter haircut is evaluated using a hair layer size that is 75% of the normal value. The results are shown in table 6.6.

Reducing the thickness of the hair layer reduces the skin temperature during

Table 6.7: Effect of different doxorubicin doses on scalp cooling effectiveness (ε) using the optimal scalp cooling protocol.

Dose $\left(\frac{\text{mg}}{\text{m}^2}\right)$	T_{skin} $\left(^{\circ}\text{C}\right)$	ϕ_w $\left(-\right)$	C_{skin} $\left(\frac{\mu\text{g}}{\text{ml}}\right)$	S $\left(-\right)$	ε $\left(\%\right)$
20	16.9 $\pm$ 3.5	0.20 $\pm$ 0.06	0.12 $\pm$ 0.02	1.00 $\pm$ 0.05	100
30	17.6 $\pm$ 3.3	0.21 $\pm$ 0.08	0.19 $\pm$ 0.05	0.94 $\pm$ 0.05	90
40	17.2 $\pm$ 3.5	0.19 $\pm$ 0.07	0.24 $\pm$ 0.06	0.91 $\pm$ 0.05	70

cooling to 18.5°C, with an accompanying perfusion value of 0.19. The reduction in perfusion and temperature is enough to increase the viability from 0.85 to 0.90. This results in an effectiveness equal to 72%. Compared to the effectiveness of 42% in the standard situation, the effect of a reduced hair layer on effectiveness is considerable. This effect is reached with only a small amount of extra cooling. The success rate with use of conditioner (table 6.5) is 92%, but for this a substantial amount of extra cooling is necessary ($T_{\text{skin}} = 13.6^{\circ}\text{C}$). Because of the associated discomfort with these low temperatures, it is very likely that patients will stop the use of scalp cooling (Katsimbri et al., 2000). In the optimal scalp cooling protocol, everyone should be advised to get a short haircut including thinning out the hair.

6.4 Optimal scalp cooling protocol

Based on the previous simulations, an optimal scalp cooling protocol was formulated. In the optimal scalp cooling protocol, people are advised to get a haircut including thinning out the hair, effectively reducing the hair layer thickness to an average of 3.5 mm. The infusion time is taken according to standard protocols and we used a value of 2 hours in our simulations. The scalp cooling time was set to 3 hours, which is slightly longer than the infusion time. To ensure that each patient reaches a low skin temperature, the cap temperature was set to -10°C. With this protocol, we expect good hair preservation and comfort for patients receiving scalp cooling.

The results of the new protocol were evaluated using the scalp cooling model with modelling of variability. Three different doses were used: 20, 30 and 40 mg m^{-2}. For each dose, a total of 50 persons were simulated. The results of the simulations are shown in table 6.7.

With the optimized scalp cooling protocol skin temperatures are reduced to approximately 17°C, and the average relative perfusion is 0.20. The combination of tissue concentration and skin temperature results in viability values ranging from 1.0 for the lowest concentration to 0.91 for the highest concentration. The corre-

sponding effectiveness ranges from 100% to 70%. The results show that especially for low doses (20–30 mg m^{-2}) the effectiveness of scalp cooling is high. For a dose of 40 mg m^{-2}, a strong decrease in effectiveness is visible. Apparently, skin concentration is too high in some patients for scalp cooling to be successful for every patient. This is due to the fact that for this dosage regime, the actual amount of doxorubicin administered is over 60–70 mg, a value that was earlier derived to be the maximum value for scalp cooling. Therefore, individuals that receive a dose that is higher than 60–70 mg are unlikely to benefit from scalp cooling. In a clinical setting, this is something that needs to be accounted for when offering scalp cooling to patients, or when patients ask for scalp cooling.

6.5 Conclusion and discussion

In this chapter, we developed a computational model for scalp cooling that incorporates modelling of variability. The model for scalp cooling was based on the earlier heat transfer model (chapter 2) and pharmacological model (chapter 4). Several physiological relationships, as well as known standard deviations for parameters in the model were used to model variability. The relationship between temperature and perfusion, obtained in chapter 3, was incorporated into the model.

The dependence of viability on temperature and concentration was investigated in chapter 5, and the results were used to establish a function for viability, with temperature and concentration as independent variables. It should be noted that the function for viability obtained describes an *in vitro* situation, and therefore care has to be taken when the results are translated to an *in vivo* situation. However, the experiments that were performed in chapter 5 made use of a representative cell type for the hair follicle. Therefore, we expect that the relationship obtained is able to describe the trends that will be visible in a real life situation. Another drawback of the fitted equation is that its temperature dependency is only based on three different temperatures. This induces a lot of uncertainty in the equation obtained. However, our *in vitro* experiments showed that there were only small differences in viability between 22°C and 10°C, which is exactly the range of temperatures at which scalp cooling is aimed. These small differences are correctly described by the equation obtained. Therefore, we expect that the relationship obtained for viability as a function of temperature and concentration is able to predict a measure of hair loss during scalp cooling.

The resulting equation was used to establish a value for the critical viability, defined as the viability above which hair loss is prevented. For this, two independent studies were used and critical viability was determined as $S_{\text{crit}} = 0.88$. We used a discrete value for critical viability. However, in reality a range in critical viability may exist, and most probably, the critical value will also show inter–subject variability. On the other hand, we tried to determine a value that is representative for

acceptable hair preservation. Although this criterium may be subjective, its values are discrete: the result of scalp cooling is either acceptable hair preservation or unacceptable hair loss.

Ideally, the critical viability obtained will be validated using other studies where hair loss occurs. Recent studies evaluated the effect of scalp cooling (e.g. Ridderheim et al. 2003), but here most patients were given a combination of drugs making evaluation difficult. The amount of patients that received doxorubicin only, was too small to be able to obtain good validation. Therefore, validation with independent data is necessary to gain confidence in the model and the determined critical value. However, the validation with available data of two independent studies showed no inconsistencies. Hence, we are confident that the model is able to predict trends in scalp cooling.

The value for critical viability was used to determine the critical skin temperature at different doses. We found that especially for high doses (80–120 mg), skin temperatures need to be uncomfortably low ($T_{\text{skin}} < 12^{\circ}\text{C}$). For doses below 80 mg, skin temperatures need to be reduced to approximately 16°C. Therefore, we concluded that scalp cooling can be applied for doses as high as 60–70 mg.

We evaluated the effect of several scalp cooling protocol parameters on scalp cooling effectiveness using our scalp cooling model with variability. The parameters investigated were the temperature of the cap, scalp cooling time, doxorubicin infusion time, application of conditioner during cooling and the advice of getting a haircut. We found that the cap temperature should be below -4°C. Fine tuning in skin temperature may be obtained by setting the temperature of the cap. A scalp cooling time that is slightly longer than the infusion time is sufficient for the hair preservative effect of scalp cooling. Longer durations did not show a significant improvement on viability. The infusion time did not have a large effect on viability. The use of conditioner resulted in skin temperatures that are uncomfortably low. Reducing the thickness of the hair layer to 75% resulted in a large decrease in mean skin temperature.

Given the above, an optimized scalp cooling protocol was developed, with a cap temperature of $T_{\text{cap}} = -10^{\circ}\text{C}$, infusion time of 2 hours, a cooling time equal to infusion time plus one hour and the advice of getting a haircut. Conditioner is not recommended in the optimal protocol, although it may be used in patients where skin temperatures during cooling remain high. Used doxorubicin doses may not exceed 60–70 mg, and the skin temperature should be reduced to approximately 17–18°C. Ideally, skin temperatures should be monitored during scalp cooling. If skin temperatures are too high, the cap temperature may be adjusted to lower the temperature of the skin to the desired temperature. With this protocol, the scalp cooling model shows that hair prevention is most effective for doses below 60–70 mg.

Chapter 7

Conclusions and recommendations for future work

7.1 Conclusions

A distressing side effect of cancer chemotherapy treatment is hair loss. This hair loss may be prevented by cooling the scalp during administration of chemotherapeutic agents. The effect of scalp cooling is attributed to two mechanisms. The first mechanism is vasoconstriction due to reduced skin temperature, leading to reduced supply of drugs to the hair follicle. The second mechanism is reduced reaction rates at lower temperatures, affecting drug uptake and damage in the hair follicle. A lack of knowledge of the mechanisms of scalp cooling and consequently a lack in uniformity in cooling protocol results in varying success rates of scalp cooling. The goal of this thesis was to quantify the contributions of the putative mechanisms by which scalp cooling prevents hair loss, and hereby investigate possible options for improving efficacy of current day scalp cooling protocols.

A heat transfer model for the head during scalp cooling has been developed. Parameter studies using this model show that the parameters that have the largest influence on skin temperature during scalp cooling are the thermal resistances of both the fat layer and the hair layer. The scalp skin may be viewed as a point of interest, connected through an insulating fat layer to a hot source (the brain) on the one side, and connected through an insulating hair layer to a cold source (the cold cap) on the other side. Increasing the thermal resistance of the fat layer (by either in-

creasing the thickness of the layer or reducing the thermal conductivity) will result in lower skin temperatures. Our model showed that in this case skin temperatures may be 8°C lower compared to the standard model. Decreases in thermal resistance resulted in skin temperatures that were approximately 3°C higher. Increasing the thermal resistance of the hair layer resulted in 6°C higher skin temperatures during cooling, compared to the standard model. Decreasing the thermal resistance yielded skin temperatures that are 10°C lower. Without perfusion in the skin, skin temperatures were less than 1°C lower compared to the standard model. This shows that the thermal contribution of the blood flow in the skin is small.

Reduction in blood flow is important in the hypothesis of scalp cooling. Experiments were performed to quantify the relationship between skin temperature and perfusion during scalp cooling. The results show that during scalp cooling, blood flow reaches a plateau. This plateau is reached at a skin temperature reduction of approximately 12°C. Here, skin perfusion is about 20% of normal and further cooling does not result in a reduction in perfusion. Experiments also showed that there is a large inter–subject variability in skin temperatures reached during cooling and minimum perfusion values. Bülow et al. (1985) found a similar plateau in perfusion during scalp cooling, although they found that this plateau was reached at a temperature reduction of approximately 6°C.

The effect of reduced blood flow on doxorubicin concentrations in the skin was analysed using a physiologically based pharmacological model. A simulation of a scalp cooling procedure using the standard model showed that reducing perfusion to 20%, reduces maximum doxorubicin concentrations in the skin by a factor of 3.5. A parameter study identified important parameters. These important parameters are the perfusion of both the skin and the liver, body mass, body height and the fraction of doxorubicin bound to the blood. Decreasing liver perfusion resulted in higher doxorubicin concentrations, whereas decreasing skin perfusion resulted in lower doxorubicin concentrations. Decreases in body mass and body height resulted in doxorubicin concentrations that were higher. Finally, a reduction in the fraction of doxorubicin that is bound to the blood resulted in higher doxorubicin concentrations in the skin. The range in doxorubicin concentrations for changes in these parameters was 0.42–0.57 μg ml^{-1}, with doxorubicin concentration in the standard model being equal to 0.48 μg ml^{-1}. The results of the parameter study are as expected, since the most influential parameters in a pharmacological model are the body mass, cardiac output and both tissue mass and blood flow fractions (Nestorov, 1999).

In an *in vitro* study, the effect of both reduced doxorubicin concentrations and reduced temperature on keratinocyte damage was studied. Cell survival significantly increased with decreasing doxorubicin concentrations. When compared to an exposure temperature of 37°C, a decrease in temperature also has a significant increasing effect on cell survival. However, no significant differences were found between exposure temperatures of 22°C and 10°C. At a concentration of 0.5 μg ml^{-1}, cell sur-

Table 7.1: Optimal scalp cooling protocol.

Parameter		Setting
Skin temperature	T_{skin}	17–18°C
Cap temperature	T_{cap}	-10°C
Infusion time	t_{inf}	2 hours
Cooling time	t_{cool}	3 hours
Hair cut		yes
Conditioner		no
Doxorubicin dose		$<$ 60–70 mg

vival increased from 41% (37°C) to 85% and 89% by reducing temperature to 22°C and 10°C, respectively. The results of the experiments at 37°C show similarities with *in vitro* experiments with doxorubicin on a different cell type (Eliaz et al., 2004). The increased cell survival at lower exposure temperature is in line with another study, which showed that doxorubicin uptake in kidney cells was significantly higher at 37°C than at 4°C (Decorti et al., 2003).

A relationship between cell survival and both exposure temperature and doxorubicin concentration was incorporated into an integrated model of scalp cooling which has been used for population studies. A value for critical cell survival was established by comparing results of the model to two independent studies on the effectiveness of scalp cooling. The critical value for cell survival (viability) is defined as the value above which patients do not show hair loss. This value is determined to be $S_{\text{crit}} = 0.88$.

Results of the population based model for scalp cooling show that both reduced perfusion and reduced metabolism are required for the hair preservative effect of scalp cooling. A plot of viability isolines in a temperature, concentration graph shows that the effect of reduced perfusion is more important than the effect of reduced temperature. This is in direct conflict with statements made by Bülow et al. (1985), who concluded that the reduction in blood flow is not the most significant factor in the hair preservative effect of scalp cooling.

An optimal scalp cooling protocol was developed, based on parameter studies. The optimal scalp cooling protocol (table 7.1) aims to reduce skin temperatures to 17–18°C by setting the cap temperature to -10°C. Infusion time of doxorubicin may be used as stated in standard protocols (approximately 2 hours), and scalp cooling time should be equal to infusion time plus 1 hour. Parameter studies show that maintaining scalp cooling for a long period of time does not increase the effectiveness of scalp cooling. Patients should be advised to get a hair cut before starting chemotherapy treatment with scalp cooling. This hair cut should be used to reduce the thickness of the hair layer by thinning the hair, such that the insulating layer between the cap

and the skin is reduced. The use of conditioner is not advised, since it cools the head to uncomfortable levels. A maximum doxorubicin dose exists, above which scalp cooling most likely will not be effective. With the optimized protocol, scalp cooling may be effective for doses up to 60–70 mg.

7.2 Recommendations for further research

Heat transfer in the human head during scalp cooling was modelled using a 1-D approach. This allowed for quick and easy identification of important parameters. However, a more detailed description of heat transfer in the human head is necessary to address the problem of an irregular-fit cap. A 3-D model seems most suitable for this, and allows the study of the effect of regional differences in parameters on local temperature and blood flow during scalp cooling.

In our pharmacological model, scalp cooling was accounted for by reducing local blood flow to the skin compartment. Other effects of temperature are not included in the current model. It is expected, however, that drug transport over the capillary membrane is also temperature dependent. Currently, data on temperature dependent doxorubicin uptake into tissues is unavailable. However, Corley et al. (1953) developed a model for temperature dependent uptake of chloroform in human skin, based on experimental data. A similar procedure might be used to improve our current pharmacological model.

To relate drug concentration and exposure temperature to cell survival, *in vitro* experiments were performed on normal human epidermal keratinocytes. In our experiments, we used three temperatures that are representative for scalp cooling. For the cooled group, no significant differences in cell survival were found, compared to a non–cooled group. The transition point in the protective effect of temperature lies between 22°C and 37°C. Preliminary results indicate that at 26°C, there might also be an increased effect on viability. More experiments are needed to define this transition point exactly.

Although the cells used in our *in vitro* experiment are representative of the cells that produce the hair shaft, *in vitro* experiments are not able to simulate the complex interaction that these cells have in an *in vitro* situation. For a better understanding of the effect of scalp cooling on a hair follicle, *in vitro* experiments on a complete hair follicle is required as a next step. In these experiments, the distribution of doxorubicin in the hair follicle and subsequent cell damage need to be studied. Eventually, *in vivo* evaluation of the effect of exposure temperature and doxorubicin concentration on hair follicle damage is needed.

We developed a population–based model for scalp cooling, which includes a measure for critical cell survival that is needed to prevent chemotherapy induced hair loss. In our model, critical cell survival largely depends on local skin temperature, local perfusion and local tissue concentrations. Evaluation of current day scalp

cooling protocols, and validation of our model, requires data on skin temperature, perfusion and tissue concentrations during scalp cooling. Therefore, these variables need to be measured in clinical studies on the hair preservative effect of scalp cooling.

References

Aaron, L. (2005). Physiologically based pharmacokinetic modelling: A sound mechanistic basis is needed. *British Journal of Clinical Pharmacology*, 60(6):581–583.

Andersen, A., Holte, H., and Slørdal, L. (1999). Pharmacokinetics and metabolism of doxorubicin after short–term infusions in lymphoma patients. *Cancer Chemotherapy and Pharmacology*, 44:422–426.

Anderson, J. E., Hunt, J. M., and Smith, I. E. (1981). Prevention of doxorubicin–induced alopecia by scalp cooling in patients with advanced breast cancer. *Clinical Research*, 282:423–424.

Arkin, H., Xu, L., and Holmes, K. (1994). Recent development in modelling heat transfer in blood perfused tissues. *IEEE Transactions on Biomedical Engineering*, 41(2):97–107.

Bejan, A. (1993). *Heat Transfer*. New York: John Wiley & Sons Inc.

Bonner, R. and Nossal, R. (1981). Model for laser doppler measurements of blood flow in tissue. *Applied Optics*, 20(12):2097–2107.

Botchkarev, V. A., Komarova, E. A., Siebenhaar, F., Botchkareva, N. V., Komarov, P. G., Maurer, M., Gilchrest, B. A., and Gudkov, A. V. (2000). P53 is essential for chemotherapy-induced hair loss. *Cancer Research*, 60:5002–5006.

Breasted, J. (1930). *The Edwin Smith Surgical Papyrus*. Chicago: University of Chicago Press. Translation from original.

Breed, W. P. (2004). What is wrong with the 30-year-old practice of scalp cooling for the prevention of chemotherapy-induced hair loss? *Support Care Cancer*, 12:3–5.

Brown, R., Delp, M., Lindstedt, S., Rhomberg, L., and Beliles, R. (1997). Physiological parameter values for physiologically based pharmacokinetic models. *Toxicology and Industrial Health*, 13:407–484.

Bülow, J., Friberg, L., Gaardsting, O., and Hansen, M. (1985). Frontal subcutaneous blood flow, and epi- and subcutaneous temperatures during scalp cooling in normal man. *Scandinavian Journal of Clinical and Laboratory Investigations*, 45(6):505–508.

Calder, W. (1984). *Size, Function, and Life History*. Harvard University Press, London.

Cash, T. (2001). The psychology of hair loss and its implications for patient care. *Clinics in Dermatology*, 19(2):161–166.

Chan, K., Cohen, J., Gross, J., Himmelstein, K., Bateman, J., Tsu-Lee, Y., and Marlis, A. (1975). Prediction of adriamycin disposition in cancer patients using a physiologic pharmacokinetic model. *Cancer Treatment Report*, 62:1161–1171.

Chen, H.-S. G. and Gross, J. (1979). Physiologically based pharmacokinetic models for anticancer drugs. *Cancer Chemotherapy and Pharmacology*, 2:85–94.

Chen, M. and Holmes, K. (1980). Microvascular contributions in tissue heat transfer. *Annals of the New York academy of Sciences*, 335:137–150.

Corley, R., Gordon, S., and Wallace, L. (1953). Physiologically based pharmacokinetic modelling of the temperature–dependent dermal absorption of chloroform by humans following bath water exposures. *Toxicological Sciences*, (13–23).

Cotsarelis, G. and Millar, S. (2001). Towards a molecular understanding of hair loss and its treatment. *Trends in Molecular Medicine*, 7(7):293–301.

Daniels, P. S. and Hyslop, S. G. (2003). *Almanac of World History*. Washington: the National Geographic Society.

Davis, S., Benson, B., and Bramson, H. (2001). Prevention of chemotherapy–induced alopecia in rats by CDK inhibitors. *Science*, 291:134–137.

Decorti, G., Peloso, I., Favarin, D., Klugmann, F., Candussio, L., Crivellato, E., Mallardi, F., and Baldini, L. (2003). Handling of doxorubicin by the (l)(l)(c)-(p)(k)1 kidney epithelial cell line. *The Journal of Pharmacology and Experimental Therapeutics*, 125(1):832–840.

Dennis, B., Eberhart, R., Dulikravich, G., and Radons, S. (2003). Finite-element simulation of cooling of realistic 3-d human head and neck. *Journal of Biomechanical Engineering*, 125(6):832–840.

Deurenberg, P., Weststrate, J., and Seidell, J. (1991). Body mass index as a measure of body fatness: Age- and sex-specific prediction formulas. *British Journal of Nutrition*, 65(2):105–114.

Diao, C., Zhu, L., and Wang, H. (2002). Cooling and rewarming for brain ischemia or injury: Theoretical analysis. *Annals of Biomedical Engineering*, 31(3):346–353.

DuBois, D. and DuBois, E. (1916). A formula to estimate the approximate surface area if height and weight be known. *Archives of Internal Medicine*, 17:863–871.

Edmondson, J. M., Armstron, L. S., and Martinez, A. O. (1988). A rapid and simple (m)(t)(t)-based spectrophotometric assay for determining drug sensitivity in monolayer cultures. *Journal of Tissue Culture Methods*, 11(1):15–17.

Eliaz, R. E., Nir, S., Marty, C., and Szoka Jr., F. C. (2004). Determination and modeling of kinetics of cancer cell killing by doxorubicin and doxorubicin encapsulated in targeted liposomes. *Cancer Research*, 64:711–718.

Fiala, D., Lomas, K., and Stohre, M. (1999). A computer model of human thermoregulation for a wide range of environmental conditions: The passive system. *Journal of Applied Physiology*, 87(5):1957–1972.

Fournier, R. L. (1999). *Basic Transport Phenomena In Biomedical Engineering*. Taylor & Francis.

Gregory, R., Cooke, T., Middleton, J., Buchanan, R., and Williams, C. (1982). Prevention of doxorubicin–induced alopecia by scalp hypothermia: Relation to degree of cooling. *British Medical Journal*, 284:1674.

Grevelman, E. and Breed, W. (2005). Prevention of chemotherapy-induced hair loss by scalp cooling. *Annals of Oncology*, 16(3):352–358.

Gustafson, D., Rastatter, J., Colombo, T., and Long, M. (2002). Doxorubicin pharmacokinetics: Macromolecule binding, metabolism, and excretion in the context of a physiologic model. *Journal of Pharmaceutical Sciences*, 91(6):1488–1501.

Hardy, M. H. (1992). The secret life of the hair follicle. *Trend In Genetics: TIG*, 8(2):55–61.

Harris, P. and Gross, J. (1975). Preliminary pharmacokinetic model for adriamycin. *Cancer Chemotherapy Report*, 59:819–825.

Hoang, K.-C. T. (1995). Physiologically based pharmacokinetic models: Mathematical fundamentals and simulation implementations. *Toxicology Letters*, 79:99–106.

Hsieh, P. C., Davis, M. E., Lisowski, L. K., and Lee, R. T. (2006). Endothelial-cardiomyocyte interactions in cardiac development and repair. *Annual Review of Physiology*, 68:51–66.

Jacquet, J.-M., Bressolle, F., Galtier, M., Bourrier, M., Donadio, D., Jourdan, J., and Rossi, J.-F. (1990). Doxorubicin and doxorubicinol: Intra- and inter-individual variations of pharmacokinetic parameters. *Cancer Chemotherapy and Pharmacology*, 27:219–225.

Janssen, F., Van Leeuwen, G., and Van Steenhoven, A. (2004). Numerical simulation of scalp cooling to prevent chemotherapy-induced alopecia. *Proceedings of the ASME-ZSIS International Thermal Science Seminar II*, pages 357–361.

Janssen, F., Van Leeuwen, G., and Van Steenhoven, A. (2005a). Biological and physiological mechanisms of scalp cooling to prevent chemotherapy induced alopecia. *Abiomed/Ercoftac Workshop on Blood Flow Modelling and Diagnostics*, LN 6:405–414.

Janssen, F., Van Leeuwen, G., and Van Steenhoven, A. (2005b). Modelling of temperature and perfusion during scalp cooling. *Physics in Medicine and Biology*, 50:4065–4073.

Janssen, F., Van Leeuwen, G., and Van Steenhoven, A. (2005c). Numerical simulation of scalp cooling to prevent chemotherapy-induced alopecia. *Strojniški Vestnik – Journal of Mechanical Engineering*, 51:386–390.

Johnson, J. M., Yen, T. C., Zhao, K., and Kosiba, W. A. (2005). Sympathetic, sensory, and nonneuronal contributions to the cutaneous vasoconstrictor response to local cooling. *American Journal of Physiology*, 288:H1573–H1579.

Jones, L. and Steinert, P. (1996). Hair keratinization in health and disease. *Dermatologic Clinics*, 14(4):633–650.

Katsimbri, P., Bamias, A., and Pavlidis, N. (2000). Prevention of chemotherapy-induced alopecia using an effective scalp cooling system. *European Journal of Cancer*, 36(6):766–771.

Kernick, D. P., Tooke, J. E., and Shore, A. C. (1999). The biological zero signal in laser doppler fluximetry - origins and practical implications. *Pflügers Archiv European Journal of Physiology*, 437(4):624–631.

Kotte, A. N. (1998). *Design of a numerical model for describing the heat transfer due to vascular trees*. PhD thesis, Utrecht University.

Lagendijk, J. (1982). The influence of bloodflow in large vessels on the temperature distribution in hyperthermia. *Physics in Medicine and Biology*, 27(1):17–23.

Lankelma, J., Luque, R. F., Dekker, H., Schinkel, W., and Pinedo, H. M. (2000). A mathematical model of drug transport in human breast cancer. *Microvascular Research*, 59:149–161.

Leung, H., Paustenbach, D., Murray, F., and Andersen, M. (1990). A physiological pharmacokinetic description of the tissue distribution and enzyme-inducing properties of 2,3,7,8-tetrachlorodibenzo-p-dioxin in the rat. *Toxicology and Applied Pharmacology*, 103(3):399–410.

Massey, C. S. (2004). A multicentre study to determine the efficacy and patient acceptability of the paxman scalp cooler to prevent hair loss in patients receiving chemotherapy. *European Journal of Oncology Nursing*, 8:121–130.

Messenger, A. G. (1993). Control of hair growth: An overview. *The Journal of Investigative Dermatology*, 101(1):4S–9S. Supplement.

Mosmann, T. (1983). Rapid colorimetric assay for cellular growth and survival: Application to proliferation and cytotoxicity assays. *Journal of Immunological Methods*, 65:55–63.

Nelson, D. and Nunneley, S. (1998). Brain temperature and limits on transcranial cooling in humans: Quantitative modeling results. *European Journal of Applied Physiology and Occupational Physiology*, 78(4):353–359.

Nestorov, I. A. (1999). Sensitivity analysis of pharmacokinetic and pharmacodynamic systems: I. a structural approach to sensitivity analysis of physiologically based pharmacokinetic models. *Journal of Pharmacokinetics and Biopharmaceutics*, 27(6):577–596.

Olsen, E. (2003). *Disorders of Hair Growth*. London: McGraw-Hill. p 284.

Paus, R. and Cotsarelis, G. (1999). The biology of hair follicles. *The New England Journal of Medicine*, 341(7):491–497.

Pennes, H. (1948). Analysis of tissue and arterial blood temperatures in the resting human forearm. *Journal of Applied Physiology*, 1(1):93–122.

Pérgola, P. E., Kellog, D. L., Johnson, J. M., Kosiba, W. A., and Solomon, D. E. (1993). Role of sympathetic nerves in the vascular effects of local temperature in human forearm skin. *American Journal of Physiology*, 265:H785–H792.

Philpott, M., Green, M., and Kealey, T. (1990). Human hair growth in vitro. *Journal of Cell Science*, 97(part 3):463–471.

Protière, C., Evans, K., Camerlo, J., d'Ingrado, M., Macquart-Moulin, G., Viens, P., Maraninchi, D., and Genre, D. (2002). Efficacy and tolerance of a scalp-cooling system for prevention of hair loss and the experience of breast cancer patients treated by adjuvant chemotherapy. *Support Care Cancer*, 10(7):529–537.

Randall, V. A., Sundberg, J. P., and Philpott, M. P. (2003). Animal and in vitro models for the study of hair follicles. *Journal of Investigative Dermatology Symposium Proceedings*, pages 39–45.

Renkin, E. (1954). Filtration, diffusion, and molecular sieving through porous cellulose membranes. *The Journal of General Physiology*, 38:225–243.

Ribba, B., Marron, K., Agur, Z., Alarcón, T., and Maini, P. (2005). A mathematical model of doxorubicin treatment efficacy for non-hodgkin's lymphoma: Investigation of the current protocol through theoretical modelling results. *Bulletin of Mathematical Biology*, 67:79–99.

Ridderheim, M., Bjurberg, M., and Gustavsson, A. (2003). Scalp hypothermia to prevent chemotherapy-induced alopecia is effective and safe: A pilot study of a new digitized scalp-cooling system used in 74 patients. *Support Care Cancer*, 11(6):371–377.

Rogers, G. E. (2004). Hair follicle differentiation and regulation. *The International Journal of Developmental Biology*, 48(2–3):163–170.

Schuh, H. (1957). Differenzenverfahren zum Berechnen von Temperatur-Ausgleichsvorgängen bei Eindimensionaler Wärmeströmung in Einfachen und Zusammengesetzten Körpern. *VDI-Forschungsheft*, 459:1–37.

Sgouras, D. and Duncan, R. (1990). Methods for the evaluation of biocompatibility of soluble synthetic polymers which have potential for biomedical use: 1 - use of the tetrazolium–based colorimetric assay (MTT) as a preliminary screen for evaluation of *in vitro* cytotoxicity. *Journal of Materials Science: Materials in Medicine 1*, 1:61–68.

Stańczyk, M., Van Leeuwen, G., and Van Steenhoven, A. (2007). Discrete vessel heat transfer in perfused tissue - model comparison. *Physics in Medicine and Biology*, 52:1–13.

Stenn, K. and Paus, R. (2001). Control of hair follicle cycling. *Physiological Reviews*, 81(1):449–494.

Stern, M. (1975). *In Vivo* evaluation of microcirculation by coherent light scattering. *Nature*, 254:56–58.

Stiefel, M., Shaner, A. M., and Schaefer, S. D. (2006). The edwin smith papyrus: The birth of analytical thinking in medicine and otolaryngology. *Laryngoscope*, 116(2):182–188.

Terasaki, T., Iga, T., Sugiyama, Y., and Hanano, M. (1982). Experimental evidence of characteristic tissue distribution of adriamycin: Tissue dna concentration as a determinant. *Journal Of Pharmaceutical Pharmacology*, 34:597–600.

Theil, F., Guentert, T., Haddad, S., and Poulin, P. (2003). Utility of physiologically based pharmacokinetic models to drug development and rational drug discovery candidate selection. *Toxicology Letters*, 138(1-2):29–49.

Thibaut, S., Collin, C., Langbein, L., Schweizer, J., Gautier, B., and Bernard, B. (2003). Hair keratin pattern in human hair follicles grown in vitro. *Experimental Dermatology*, 12(2):160–164.

Thompson, C. S., Holowatz, L. A., and Kenney, W. L. (2005). Attenuated noradrenergic sensitivity during local cooling in aged human skin. *Journal of Physiology*, 564(1):313–319.

Turk, J. (1993). Rudolf virchow–father of cellular pathology. *Journal of the Royal Society of Medicine*, 86(12):688–689.

Van Leeuwen, G. (1998). *Numerical Modelling Of Heat Transfer In Hypothermia*. PhD thesis, Utrecht University.

Van Leeuwen, G., Hand, J., Lagendijk, J., Azzopardi, D., and Edwards, A. (2000). Numerical modeling of temperature distributions within the neonatal head. *Pediatric Research*, 48(3):351–356.

Van Steenhoven, A. (1993). *The Physics of Heart and Circulation*, chapter 15 - Velocity Profiles in Large Arteries, pages 295–320. Institute of Physics Publishing, Bristol U.K.

Van Steensel, M., Happle, R., and Steijlen, P. (1999). Molecular genetics of the hair follicle: State of the art. *Proceedings of the Society for Experimental Biology and Medicine*, 223:1–7.

Weinbaum, S. and Jiji, L. (1985). A new simplified equation for the effect of blood flow on local average tissue temperature. *ASME Journal of Biomechanical Engineering*, 107(2):131–139.

Weinbaum, S., Jiji, L., and Lemons, D. (1984). Theory and experiment for the effect of vascular microstructure on surface tissue heat transfer–part i: Anatomical foundation and model conceptualization. *ASME Journal of Biomechanical Engineering*, 106(4):321–330.

Wissler, E. H. (1998). Pennes' 1948 paper revisited. *Journal of Applied Physiology*, 85(1):35–41.

Wulff, W. (1974). The energy conservation equation for living tissue. *IEEE Transactions on Biomedical Engineering*, 21:494–495.

Xu, X., Tikuisis, P., and Giesbrecht, G. (1999). A mathematical model for human brain cooling during cold-water near-drowning. *Journal of Applied Physiology*, 86(1):265–272.

Appendix A

Validation of the numerical heat transfer model

A.1 Introduction

In this chapter, the numerical model will be validated to known analytical solutions. These analytical solutions include solutions for time dependent heat conduction, stationary heat production and stationary heat production with a perfusion term.

The standard properties that are used in the model are shown in table A.1. Properties are chosen such that these resemble the properties that are used in biological situations. The results of the numerical model will be compared to the analytical solution for each specific case. The difference between the two is defined as:

$$\epsilon = T_{\text{num}} - T_{\text{ana}} \tag{A.1}$$

This difference can be used to establish a case specific measure of error.

Table A.1: Standard properties used to validate the heat transfer model.

parameter	symbol	value
Initial temperature	T_{i}	40°C
Ambient temperature	T_{a}	20°C
Radius of the sphere	r	0.1m
Density	ρ	1000 kg m^{-3}
Heat capacity	c	3800 kg m^{-3}
Nodes	N	50

Table A.2: Properties used to validate the heat transfer model for $\mathrm{Bi} \ll 1$. Standard model properties are given in table A.1

parameter	symbol	value
Thermal conductivity	k	500 W m^{-1} K^{-1}
Heat transfer coefficient	h	5 W m^{-2} K^{-1}

A.2 Time dependent conduction

In this section we will validate the numerical model for time dependent conduction. Two different cases are regarded, based on different values for the Biot number, which is defined as the ratio of the heat transfer resistance inside the body to the heat transfer resistance outside the body:

$$\mathrm{Bi} = \frac{hr}{k} \tag{A.2}$$

Two different heat transfer regimes exist, namely $\mathrm{Bi} \ll 1$ and $\mathrm{Bi} \gg 1$, and these two regimes will be used to validate the numerical model.

A specific measure of error can be defined using the imposed temperature difference $\Delta T = T_\mathrm{i} - T_\mathrm{a}$. With this the specific error is equal to:

$$\xi = \frac{\epsilon}{\Delta T} \tag{A.3}$$

The validity of the model for time dependent heat conduction will be defined using this measure.

A.2.1 Low Biot number

In the case that the Biot number is much smaller than 1, the heat transfer resistance in the body is much smaller than the heat transfer resistance outside the body. In this case, the temperature inside the body may be viewed as being homogeneous. The analytical solution for the temperature at the centerline of the body is then given by (Bejan, 1993):

$$T = T_\mathrm{a} + (T_\mathrm{i} - T_\mathrm{a}) \exp\Big(-\frac{hA}{\rho c V} t\Big) \tag{A.4}$$

Properties for the sphere that are used in this validation are shown in table A.2. With these properties, the Biot number is equal to $\mathrm{Bi} = 1 \cdot 10^{-3}$ and therefore the temperature inside the sphere is homogeneous. The results of the simulations with the model with these properties are shown in figure A.1. The top figure shows the temperature of the centerline of the sphere as a function of time for both the model and the analytical solution. The difference between the results of the model and the

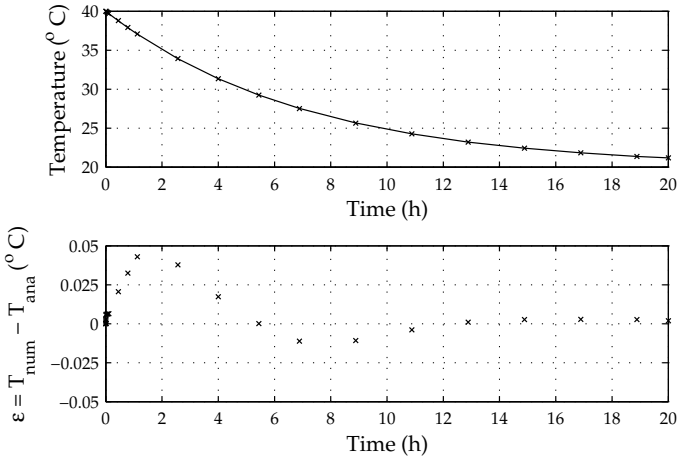

Figure A.1: Validation of the numerical model for heat transfer in case of a low Biot number ($\mathrm{Bi} = 1 \cdot 10^{-3}$). Top: Results of the model (x) compared to the analytical solution (–). Bottom: Difference between the numerical solution and the analytical solution.

analytical solution is shown in the bottom figure. From this bottom figure, we can see that this difference in time is less than $\epsilon = 0.05$°C. With an imposed temperature difference of $\Delta T = 20$°C, this means that the error is less than $\xi = 0.25\%$.

We can conclude that the model produces accurate results for low Biot numbers. Next, the validity for high Biot numbers will be investigated.

A.2.2 High Biot number

For high Biot numbers, the resistance inside the body is higher than the resistance of heat transfer outside the body. This means that the temperature inside the body is not homogeneous.

For $\mathrm{Bi} \gg 1$ the analytical solution is dependent on the Fourier and Biot number: (Bejan, 1993):

$$\frac{T(r,t) - T_\mathrm{a}}{(T_\mathrm{i} - T_\mathrm{a})} = \sum_{n=1}^{\infty} K_n \frac{\sin(s_n r/r_0)}{s_n r/r_0} \exp(-s_n^2 \mathrm{Fo}) \tag{A.5}$$

In which the K_n coefficients are given by

$$K_n = 2\frac{\sin(s_n) - s_n \cos(s_n)}{s_n - \sin(s_n)\cos(s_n)} \tag{A.6}$$

and where the characteristic values s_n are the roots of the equation

$$s_n \cot(s_n) = 1 - \mathrm{Bi} \tag{A.7}$$

Table A.3: Properties used to validate the heat transfer model for $\mathrm{Bi} \gg 1$. Standard model properties are given in table A.1

parameter	symbol	value
Thermal conductivity	k	0.5 W m^{-1} K^{-1}
Heat transfer coefficient	h	50 W m^{-2} K^{-1}

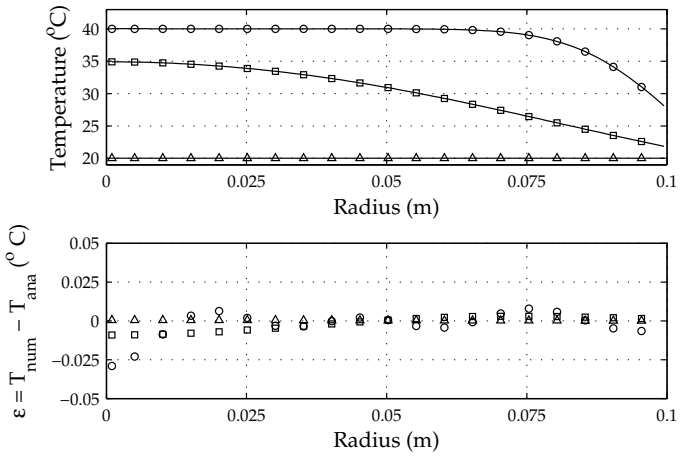

Figure A.2: Validation of the numerical model for heat transfer in case of a high Biot number ($\mathrm{Bi} = 10$). Top: Results of the model for $\mathrm{Fo} = 0.01$ (○), $\mathrm{Fo} = 0.1$ (□) and $\mathrm{Fo} = 1.0$ (△), compared to the analytical solution (–). Bottom: Difference between the numerical solution and the analytical solution.

Specific properties for this validation can be found in table A.3. With these properties, the Biot number is equal to $\mathrm{Bi} = 10$ and therefore the temperature inside the sphere is homogeneous. The results of the simulations with the model with these properties are shown in figure A.2. The top figure shows the temperature of the centerline of the sphere as a function of time for both the model and the analytical solution. The difference between the results of the model and the analytical solution is shown in the bottom figure.

The temperature difference between the numerical model and the analytical solution is less than $\epsilon = 0.025$°C. Once again, the relevant temperature difference is equal to $\Delta T = 20$°C, and with this the error is less than $\xi = 0.125\%$. Based on these simulations, we may conclude that the model produces accurate results for time dependent conduction for both low and high Biot numbers.

In the next section, we will validate the model when there is heat generation in the tissue.

Table A.4: Properties used to validate the heat transfer model with heat production. Standard model properties are given in table A.1

parameter	symbol	value
Thermal conductivity	k	0.5 W m^{-1} K^{-1}
Heat transfer coefficient	h	50 W m^{-2} K^{-1}
Heat production	q_{m}	8000 W m^{-2} K^{-1}

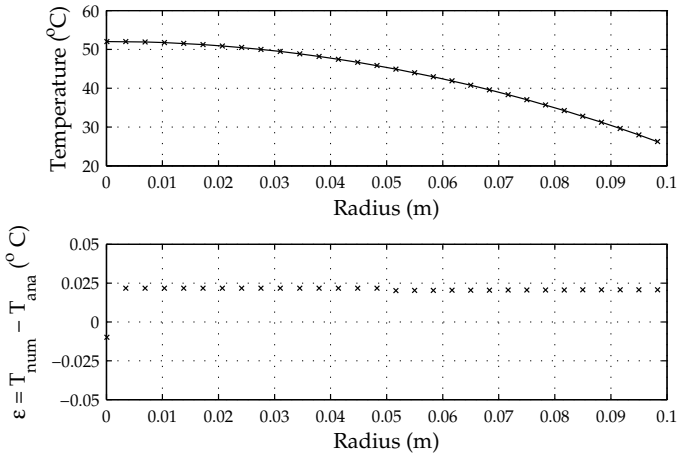

Figure A.3: Validation of the numerical model for heat transfer with heat production. Top: Results of the model (x) compared to the analytical solution (–). Bottom: Difference between the numerical solution and the analytical solution.

A.3 Heat generation

The next validation considers the heat generation term in the bio–heat equation for spherical coordinates. Consider a sphere with radius r_o, a uniform heat source q_{m} and convective heat loss at the surface. In a stationary situation, the temperature distribution in the sphere can be written as (Bejan, 1993):

$$T(r) = T_{\mathrm{a}} + \frac{q_{\mathrm{m}} r_0^2}{6k}\left(1 - \left(\frac{r}{r_0}\right)^2\right) + \frac{q_{\mathrm{m}} r_0}{3h} \tag{A.8}$$

We will use this analytical solution to validate the model in case the Biot number is high. Specific properties for this validation can be found in table A.4. The results of the simulations with the model with these properties are shown in figure A.3. In the top figure, the numerical solution and analytical solution in steady–state are shown and we can see that these two solutions provide a good match. The differ-

Table A.5: Properties used to validate the heat transfer model.

parameter	symbol	value
Thermal conductivity	k	0.5 W m^{-1} K^{-1}
Heat Production	q_m	8000 W m^{-3}
Perfusion	w_b	5 kg m^{-3} s^{-1}
Density of blood	ρ_b	1000 kg m^{-3}
Specific heat of blood	c_b	3800 J kg^{-1} K^{-1}
Heat transfer coefficient	h	50 W m^{-2} K^{-1}

ence between the two is shown in the bottom figure, from which it is clear that the temperature difference between the numerical solution and the analytical solution is equal to $\epsilon = 0.025$°C. A relevant temperature difference is now defined using the maximum and minimum temperature in the sphere, being 52°C and 26°C. With this, the relevant temperature difference is $\Delta T = 26$°C, and the error is equal to $\xi = 0.1\%$. Therefore we may consider the model to be valid, at least in stationary situations, when heat production in the tissue plays a role.

Next, we will investigate the validity of the model when heat production and perfusion play a role in the model.

A.4 Bio–heat transfer

An analytical solution for the bio–heat transfer equation in steady–state is given by (Fiala et al., 1999):

$$T(r) = T_a + \frac{q_m}{\rho_b c_b w_b} - \frac{\frac{hr_0^2}{kr}\left(-T_a + T_b + \frac{q_m}{\rho_b c_b w_b}\right)\sinh\left(r\sqrt{\frac{\rho_b c_b w_b}{k}}\right)}{r_0\sqrt{\left(\frac{\rho_b c_b w_b}{k}\right)}\cosh\left(r_0\sqrt{\frac{\rho_b c_b w_b}{k}}\right) + \left(\frac{hr_0}{k} - 1\right)\sinh\left(r_0\sqrt{\frac{\rho_b c_b w_b}{k}}\right)} \tag{A.9}$$

We used this equation to validate the numerical model, using parameters defined in table A.5. The results of the simulation are shown in figure A.4. The top figure shows the temperature profile of the sphere in steady–state, whilst the bottom figure shows the temperature difference between the numerical solution and the analytical solution. From this figure we can see that the error is equal to zero for most part of the sphere. At the outer part of the sphere the solution is less exact, resulting in a temperature difference of $\epsilon = 0.025$°C. A relevant temperature difference is now based on the maximum and minimum temperature in the tissue, being 37°C and 33°C, respectively. With this, $\Delta T = 4$°C and the error is equal to $\xi = 0.6\%$. With this, we can conclude that the model produces accurate results for steady–state heat transfer with perfusion.

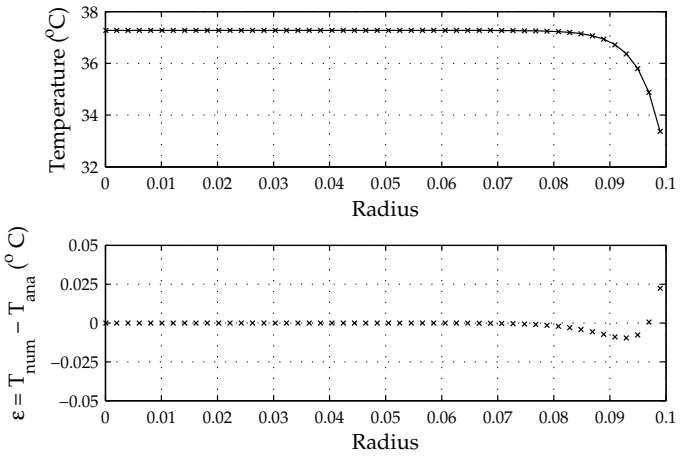

Figure A.4: Validation of the numerical model for heat transfer with heat production and perfusion in steady–state. Top: Results of the model (x) compared to the analytical solution (–). Bottom: Difference between the numerical solution and the analytical solution.

Curriculum Vitae

Francis–Paul Janssen was born in Geleen on November 25, 1978. From 1991 till 1997 he attended pre–university education (VWO) at the S.G. Groenewald in Stein. In 1997 he started his Mechanical Engineering studies at the Eindhoven University of Technology. In his second and third year, he followed a side track within the Mechanical Engineering department that focused on the use of mechanical engineering for medical purposes.

Francis–Paul continued in this field of work in his master's study. He did an internship at the Maastricht University, in the Department of Human Biology. There, he worked on a computational model for heat transfer in the human body. He started his graduation project in 2002 in the Energy Technology group of prof. dr. ir. Van Steenhoven at the Eindhoven University of Technology. The project focused on the development of a computational model that can be used to monitor heat transfer and heat content of a patient undergoing (cardiac) surgery.

After graduating in March 2003, Francis–Paul started to work on his Ph.D. project in the same group. The aim of the project was to gain more insight in the underlying biological and physiological mechanisms of scalp cooling to prevent chemotherapy induced hair loss. For this, computational work was combined with experimental results. The results of this work are described in this thesis.

Dankwoord

Met dit proefschrift komt er een einde aan een hele interessante tijd aan de Technische Universiteit Eindhoven. Met veel plezier kijk ik terug op de afgelopen vier jaar, waarin ik op zowel professioneel als persoonlijk vlak veel geleerd heb. Veel mensen hebben mij (bewust of onbewust) hierbij geholpen. Graag zou ik hen op deze plek willen bedanken.

Allereerst gaat mijn dank uit naar Wim Breed, zonder wiens inzet dit bijzondere en uitdagende project in deze vorm nooit tot stand zou zijn gekomen. Daarnaast wil ik in het bijzonder mijn eerste promotor professor Anton van Steenhoven en copromotor Gerard van Leeuwen bedanken voor hun (dagelijkse) begeleiding. De discussies die ik met hen voerde, leidden vaak tot nieuwe inzichten. Ook gaven ze mij het duwtje in de rug dat ik nodig had wanneer het soms wat tegenzat bij mijn experimenten.

Het onderzoek naar de relatie tussen hoofdhuidtemperatuur en –doorbloeding is grotendeels uitgevoerd aan de Universiteit Twente, waar Wiendelt Steenbergen en Vinay Rajan vol enthousiasme het idee voor het onderzoek oppikten en constructief meedachten aan de uitwerking ervan. Zij leverden de benodigde Laser Doppler apparatuur waarmee het experiment uitgevoerd is. Marcel van den Wildenberg van Incomed International wil ik bedanken voor het belangeloos beschikbaar stellen van een Paxman koelsysteem. De thermokoppels die gebruikt zijn tijdens deze experimenten, zijn van de deskundige hand van Peter Ewalts.

Bijzonder trots ben ik op het afronden van de cel–experimenten, aangezien dit soort experimenteel werk totaal nieuw voor mij was. In het begin hebben Carlijn Bouten van BMT en Guido Roosen van Philips mij de mogelijkheden (maar vooral ook onmogelijkheden) van het *in vitro* experimenteren duidelijk gemaakt. Met name praktische vaardigheden werden mij in eerste instantie bijgebracht door Birgit Faber. Later hebben Debbie Bronneberg en vooral Jolet Sonsma mij enorm geholpen om gestalte te geven aan mijn onderzoek. Anita Mol, Anita van de Loo en Rolf Pullens stonden altijd klaar voor het beantwoorden van praktische vragen die ik had tijdens mijn werk in het lab. Carlijn Bouten wil ik extra bedanken, omdat ze ondanks haar drukke schema toch de tijd vond om de resultaten van de experimenten, en het uiteindelijke verslag daarover, met een kritisch oog te bekijken. Elaine Farndale van de Universiteit van Tilburg ben ik dankbaar voor het aanscherpen van het Engels.

In het begin van mijn promotie waren Jeroen en Milenko mijn kamergenoten. De gesprekken die we hadden tijdens ons werk werden al snel voortgezet buiten werktijd, waarbij onze partners Roos, Brankica en Audrey ook aanwezig waren. Daarbij ging het vaak over de verschillen tussen de Nederlandse en Servische cultuur, meestal geïllustreerd aan de hand van traditionele spijs en drank.

Later werd Natascha mijn kamergenoot. Het onderwerp van haar promotie is gelijk aan het onderwerp van mijn afstuderen, waardoor we elkaar dan ook vaak hebben kunnen helpen. Met veel plezier kijk ik terug op onze gezamenlijke bezoeken aan congressen in Warschau en Egmond aan Zee. De wetenschappelijke discussies die ik met haar had hebben een nuttige bijdrage geleverd aan mijn proefschrift. Daarnaast kon ik bij haar ook altijd terecht voor de minder wetenschappelijke discussies.

Goede wetenschap kan alleen bedreven worden wanneer je af en toe achterover leunt. Ontspanning dus, die ik veelal gevonden heb in de dagelijkse koffiepauzes met Natascha, Gerard, Arjan, Henk, Sylvia, Pieter, Rudy, Frank en soms ook Dorus en Svetlana. Maar zeker ook in de wekelijkse zaalvoetbal wedstrijden van het dQ–team waarbij ik in het doel stond. Met o.a. Jeroen Mans, Jeroen van Oijen, Martin, Marcel, Bart, Bogdan, Ties en Maosheng hebben we onder leiding van Koen Schreel veel spannende en leuke wedstrijden gespeeld. Opvallend is overigens dat bijna het gehele voetbalteam, wanneer er niet gevoetbald moest worden, zich bezighield met Bridge. Ook Stanley, Joost en Rob speelden dan mee. Ik heb altijd erg uitgekeken naar de gezellige gesprekken en het fanatieke spel tijdens deze lunchpauzes. Verdere ontspanning kwam ook van de vele evenementen en groepsuitjes, vaak georganiseerd door Martin en Marjan, waarbij iedereen elkaar op een andere manier leerde kennen. Voor een gezellig of serieus gesprek, zowel privé als zakelijk, kon ik ook altijd terecht bij Linda of Mechline.

Verder wil ik mijn vrienden en familie bedanken voor hun steun. In het bijzonder wil ik mijn ouders Adèle en Jacques bedanken voor hun onvoorwaardelijke steun in mijn keuzes. Het is fijn om te weten dat ik altijd bij hen terecht kan voor een luisterend oor en advies.

Tot slot een speciaal woord van dank aan mijn vrouw Audrey. Met haar intelligentie, praktisch inzicht, statistische kennis, maar bovenal haar liefde heeft ze een onzichtbare, maar toch grote bijdrage geleverd aan dit proefschrift. Bij haar kon ik altijd terecht, ook voor problemen die te maken hadden met mijn onderzoek. Ze zocht dan samen met mij naar oplossingen, en vaak vonden we die. Wanneer dat onverhoopt niet lukte, wist ze me toch op te vrolijken, veelal gebruik makend van onze poezen Jules en Snow. Op het laatst, toen mijn proefschrift meer en meer tijd opslokte, gaf ze me de ruimte om daar aan te werken. Meis, ik heb je lief!

Francis-Paul Janssen
Waalre, april 2007

Het dak van de wereld
Wacht op mij tot ik er ben
Tot ik ontdekt heb
Dat het is verdwenen
Ik kan verder dan ik denk

Bløf ∼ Vrij
Blauwe Ruis (2002)